ADVANCED ENERGY MATERIALS
www.advenergymat.de

Graphene-Containing Nanomaterials for Lithium-Ion Batteries

Songping Wu, Rui Xu, Mingjia Lu, Rongyun Ge, James Iocozzia, Cuiping Han, Beibei Jiang, and Zhiqun Lin**

Graphene-containing nanomaterials have emerged as important candidates for electrode materials in lithium-ion batteries (LIBs) due to their unique physical properties. In this review, a brief introduction to recent developments in graphene-containing nanocomposite electrodes and their derivatives is provided. Subsequently, synthetic routes to nanoparticle/graphene composites and their electrochemical performance in LIBs are highlighted, and the current state-of-the-art and most recent advances in the area of graphene-containing nanocomposite electrode materials are summarized. The limitations of graphene-containing materials for energy storage applications are also discussed, with an emphasis on anode and cathode materials. Potential research directions for the future development of graphene-containing nanocomposites are also presented, with an emphasis placed on practicality and scale-up considerations for taking such materials from benchtop curiosities to commercial products.

1. Introduction

In the ongoing battle to raise the profile of sustainable development from a mere buzzword and mild curiosity to a new, globally competitive industry, rechargeable batteries are a prospective game changer. With increased investment into bio-energy, solar energy, and various other alternative fuel technologies, high performance energy storage devices have become more attractive and have achieved encouraging development in recent years. This combination of economic interest and scientific development creates a unique opportunity to redress certain aspects of the increasing energy crisis and associated environmental issues.[1–5] Indeed, the notion of tackling such a grand challenge as advanced energy storage devices may seem impractical. It is only natural to justify advancing such energy devices particularly when available effort and funding might be far better spent in solving other problems. Here the challenge is posed: why should one care about energy storage?

It is clear that global per capita energy usage is constantly on the increase. Portable electronic devices, vehicles and other mobile, untethered technologies must take all of their energy with them for their effective time of use. The effectiveness of such technologies is thus limited primarily by the ability to store energy, rather than either generation or delivery. Among the current candidates, rechargeable lithium-ion batteries (LIBs) are establishing their dominant position as small, universal power sources for portable energy storage. Furthermore, they are widely considered to be one of the best choices for small electronic equipment.[6] Of particular note is that electrical vehicles are now being commercialized using such a technology. The presence of commercially available battery-powered vehicles is indicative of a fundamental paradigm shift in the automobile industry for the first time since its inception more than a century ago. Therefore, rechargeable ultra-high energy storage devices, as the core elements in the electrical vehicles, have understandably attracted great attention.[6] LIBs possess a large energy density of 120 Wh kg^{-1}.[1,2] However, the theoretical capacity of commercial anode materials (i.e., graphite) is only 372 mAh g^{-1}, thus severely limiting the improvement in overall energy storage capacity.[7] It is clear that novel high performance electrode materials are highly desirable due to the requirements for high-power applications, such as electrical vehicles, stationary electricity storage and portable devices in communication (smartphones, tablets, laptops) and medical sectors (orthotics, prosthetics, pacemakers, biointerfacial devices) among others. Recently, significant research efforts have focused on developing alternatives (i.e., transition metal oxides, Si, Sn, etc.) to current anode materials.[2,8–10]

Due to its large specific surface area (2630 m^2 g^{-1}),[11] excellent conductivity (≈15,000 cm^2 $V^{-1}s^{-1}$ at 300 K and ≈60,000 cm^2 V^{-1} s^{-1} at 4 K),[12] high thermal conductivity (≈3,000 W mK^{-1} near room temperature)[13] and planar sp^2-hybridized carbon framework,[14] graphene is often selected as a matrix to support metal anode materials.[15–20] Graphene possesses some intriguing characteristics, including various

Dr. S. Wu, R. Xu, M. Lu, R. Ge
School of Chemistry and Chemical Engineering
South China University of Technology
Guangzhou 510641, P.R. China
E-mail: chwsp@scut.edu.cn
Dr. J. Iocozzia, Dr. C. Han, Dr. B. Jiang, Prof. Z. Lin
School of Materials Science and Engineering
Georgia Institute of Technology
Atlanta, GA 30332, USA
E-mail: zhiqun.lin@mse.gatech.edu

DOI: 10.1002/aenm.201500400

interactions due to the delocalized π electrons, and susceptibility to chemical modification.[21] It is worth noting that graphene itself possessed a much higher capacity,[22–24] with initial discharge and charge capacities of 1059 mAh g^{-1} and 732 mAh g^{-1} at 50 mA g^{-1}, respectively.[25] Recently, high reversible capacity (1331 mAh g^{-1} at 50 mA g^{-1} after 100 cycles), excellent rate-performance (328 mAh g^{-1} at 5 A g^{-1}), and good cycling stability up to 1000 cycles and high current density were observed for the scIPA-reduced GO_2 electrode.[26] The remarkable electrochemical performance of scIPA-reduced GO_2 can be attributed to the presence of a large amount of hydrogen-terminated groups, numerous defect sites, and large interlayer spacing. As was the case for the development of semiconducting materials over the last 50 years, many mixed components (i.e. doping) and mixed morphology structures derived from graphene have been investigated. More recently, few-layered graphene (FLG)[27] with a reversible capacity of 400 mAh g^{-1} at 0.1 C, few-layer reduced graphene oxide (rGO) possessing 346 mAh g^{-1} capacity at 1 C after 60 cycles,[28] morphology-controlled graphene nanosheets[29] and ultrathin-shell graphene hollow spheres[30] (a reversible specific capacity of 249.3 mAh g^{-1} at 5 A g^{-1}) were also reported. Graphene has been doped with many elements and mixed elements, including sulfur,[31] boron,[32] nitrogen,[33] phosphorus-nitrogen,[34] and nitrogen-sulfur.[35] More complex multi-component graphene materials have also been investigated as well, including N-doped aligned CNT/graphene sandwiches,[36] amine functionalized graphene nanoflakes (AFGs),[37] polypyrrole anthraquinone sulfonate/graphene,[38] polymer functionalized graphene,[39,40] 9,10-Anthraquinone (AQ) and its derivatives,[41] and carboxylic group functionalized graphene.[42] Clearly, there are many combinations of different materials with graphene that are being investigated as electrodes in lithium-ion batteries. The materials mentioned so far can be classified as 2D materials in that they are essentially modified graphene planes. Interestingly, modified graphene has recently been reported as a high performance cathode material for LIBs. When employed as a cathode in LIBs, the two-dimensional porous graphene nanosheets exhibited an outstanding cycle stability of 395 mAh g^{-1} at 5 A g^{-1} for more than 5100 cycles and excellent rate capability of 135 mAh g^{-1} at a high current density of 15 A g^{-1}.[43]

Recently, 3D graphene-containing materials have also been developed.[44] Some of the major groups seen so far include graphene–carbon nanochain webs,[45] graphene oxide–graphite–carbon layers,[46] amorphous carbon–graphene,[47] unique cross-linked graphene architectures,[48] MWCNTs–graphene nanostructures,[49] and self-adaptive graphene.[50] **Figure 1** shows the structure and performance characteristics of a 3D graphene-containing battery material.

With so many combinations of inexpensive and readily available battery materials, it is easy to forget that the heat generation properties of these materials may be vastly different. Thermal management in LIBs is also very important as it is related to the safety of the technology. Since LIBs have unfairly garnered some reputation for catching fire, addressing heat removal concerns are more prominent than ever. Thus, this issue is just as important as any performance measures when looking to develop consumer products. Fortunately, researchers understand this point and much work has been invested into thermal conductivity improvement in graphene-enhanced hybrid phase change materials, as noted by Goli et al.[51] Though, more work in this area is essential as current densities are increased and cycle times increased. Moreover, the long term effects of such currents, and point-of-failure studies, are lacking. Development in battery research has expanded to include new materials and better performance characteristics. With flexible and light weight display technology becoming more established, even the form of what constitutes a battery is changing. Traditional hard cell batteries are no longer the only form being investigated as efforts turn to flexible battery technologies.

As a promising flexible battery, graphene paper with promising performance characteristics has been recently reported. Performance characteristic including a discharge capacity of 450 mAh g^{-1} at 300 mA g^{-1},[52] a stabilized capacity of 1300 mAh g^{-1} at 60 mA g^{-1},[53] a capacity of 576 mAh g^{-1} with good cycling stability,[54] and a remarkably high power density of 6450 W kg^{-1} are observed for flexible LIB electrodes.[55] Research into multifunctionality and control of the crumpling

Dr. Songping Wu obtained his Ph.D. at South China University of Technology, China in 2002. Having previously worked as a visiting scholar at The Hong Kong Polytechnic University (2006–2007) and Georgia Institute of Technology (2013–2014), he has held the position of Associate Professor at South China University of Technology since 2004. He has been working on advanced functional ceramic materials and Li-ion battery materials. His current research interests are focused on graphene-based materials for lithium ion batteries.

Prof. Zhiqun Lin is a Professor in the School of Materials Science and Engineering at Georgia Institute of Technology. He received his Ph.D. in Polymer Science and Engineering from University of Massachusetts Amherst, MA, USA in 2002. His research interests include perovskite, polymer, and dye-sensitzed solar cells, semiconductor organic–inorganic nanocomposites, photocatalysis, hydrogen generation, lithium-ion batteries, quantum dots, conjugated polymers, block copolymers, polymer blends, hierarchical structures, surface and interfacial properties, multifunctional nanocrystals, and Janus nanostructures.

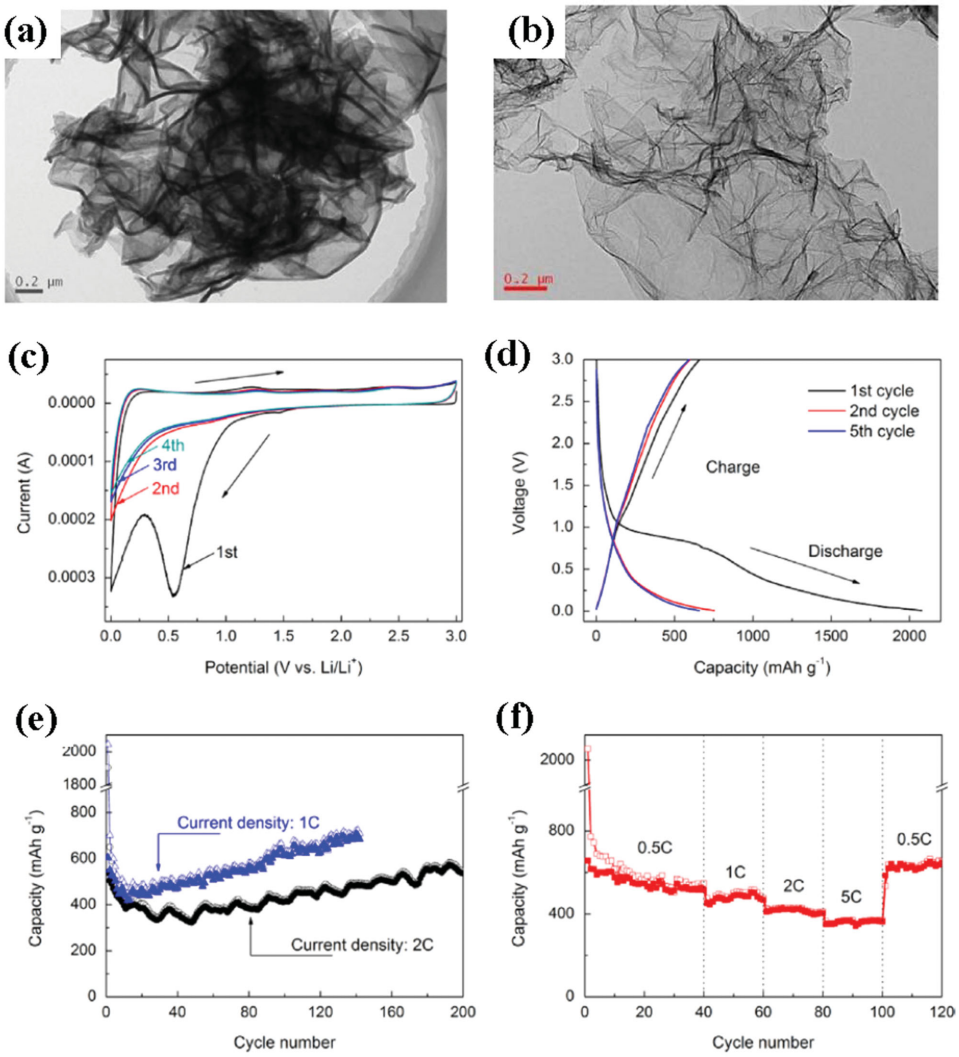

Figure 1. FETEM images of a) GO/SiO_2 and b) 3D-G. c) First to fourth current–voltage curves of 3D-G at a scan rate of 0.5 mV s^{-1}. d) The first, second and fifth charge/discharge curves of 3D-G at a current density of 0.5 C, 1 C = 372 mA g^{-1}; e) cycling performances of 3D-G at 1 C and 2 C; and f) rate performance of 3D-G. Reproduced with permission.[48] Copyright 2014, Elsevier.

and unfolding of large-area graphene is also very important for energy storage applications.[56]

Despite promising developments in graphene and graphene/carbon composites, composites containing nanoparticles with large theoretical capacity and graphene may prove to be even more attractive due to the variety of inorganic nanoparticles, various structural configurations of nanoparticles and graphene, enhanced Li-storage performance, high volumetric energy density, and low cost. On one hand, inorganic nanomaterials have shown great potential as electrodes in LIBs; on the other hand, scalable production of large quantities of defect-free few-layer graphene[57–59] allows it to enter commercialization more easily. The combination of these two developments may provide an opportunity to profoundly influence the next generation of battery development and commercialization.

When considering all the aforementioned advantages in performance, processability, scalability and safety, it is clear that graphene-containing composite materials have the ability and variety for applications as electrode materials in LIBs. A diversity of structures reported can be classified into six different models, as summarized by Raccichini et al. (**Figure 2**).[20] In general, graphene acts as a support for electroactive nanomaterials, and prevents them from re-stacking by lowering the van der Waals interactions among the layers. Moreover, the elastic and highly conductive graphene improves the electrical conductivity of composites and buffers the volume expansion of electrode materials during cycling.[20]

We note that there are several recent reviews on graphene-containing materials for energy storage and conversion.[60–62] However, a critical review that concentrates exclusively on graphene-containing materials for applications in LIBs is lacking. This review aims to provide an up-to-date and comprehensive summary of recent advances in the rational design of graphene-containing composite anodes and cathodes. Detail will be given specifically to established and generalizable synthetic

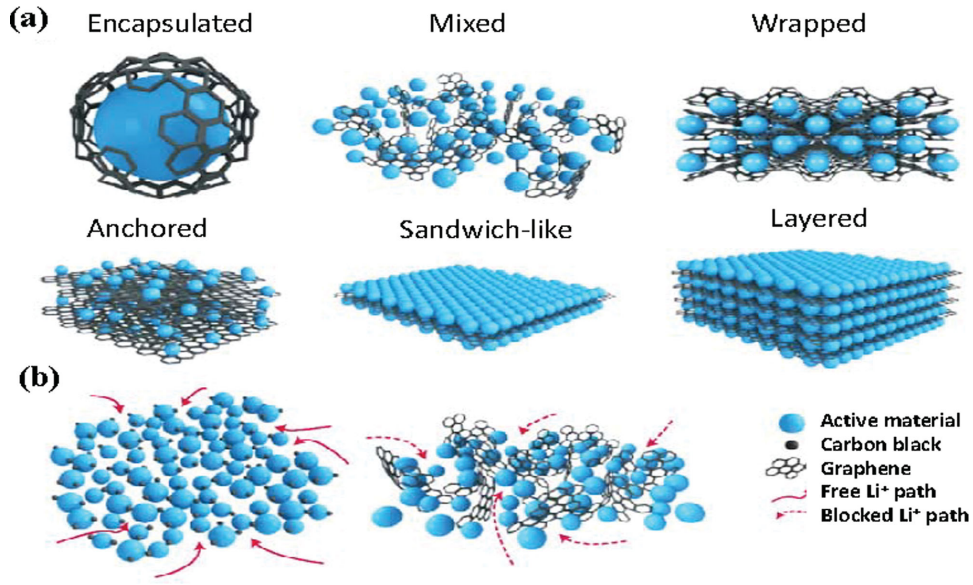

Figure 2. Structural models and a possible drawback of graphene composites. a) All models (except where specifically indicated) refer to composites in which graphene and the active material are synthesized through one-pot processes. Encapsulated: Single active-material particles are encapsulated by graphene. Mixed: Graphene and active materials are synthesized separately and mixed mechanically during the electrode preparation. Wrapped: The active-material particles are wrapped by multiple graphene sheets. This structure represents pseudocapacitor electrodes. Anchored: This is the most common structure for graphene composites, in which electroactive nanoparticles are anchored to the graphene surface. Sandwich-like: Graphene is used as a template to generate active material/graphene sandwich structures. Layered: Active-material nanoparticles are alternated with graphene sheets to form a composite layered structure, which has been proposed for use in metal-ion battery anodes and cathodes. b) Li^+ paths in (left) carbon black- and (right) graphene-based electrodes in the mixed structural model. The figure highlights a possible drawback of graphene in terms of Li^+ mobility. Reproduced with permission.[20] Copyright 2014, Macmillan Publishers Ltd. Nature.

routes, structural configurations spanning several dimensions, electrochemical performance, and Li-cycling mechanisms present in each specific instance. This review primarily emphasizes commercially available or readily synthesizable inorganic materials for use in graphene electrodes and battery design, with the express intention of reviewing approaches with scale-up and/or commercialization potential.

2. Anode Materials

As discussed by Reddy et al.,[61] there exist three basic electrochemical reactions that can occur during the charge/discharge process; that is, intercalation/deintercalation, alloying/dealloying, and conversion (redox) reactions. In some situations, they act synergistically to offer large and stable capacities (**Figure 3**). It is believed that the active materials in graphene-containing composites follow the same reaction mechanisms during the complete lithium cycling.

2.1. Anode Based on Li Intercalation–Deintercalation Reaction: Titanate

Three important conditions need to be satisfied for the so-called "topotactic reaction" involving lithium. First, the compound must be crystalline and there must be empty sites in the host crystal lattice. However, this was recently contested in recent works.[63] Second, the host compound must contain a transition metal or rare earth metal. Lastly, metal oxides with 2D or 3D structures are the most suitable for Li cycling (Figure 3).

TiO_2 is a promising candidate as an anode for LIBs due to its low cost, availability, and environmental friendliness. TiO_2 experiences the following Li-ion intercalation/deintercalation reaction during charging and discharging:[64,65]

$$TiO_2 + xLi^+ + xe^- \leftrightarrow Li_xTiO_2. \quad (1)$$

Figure 3 provides a more complete description of this reaction as well as other lithium cycling mechanisms in different material systems.

Earlier studies on TiO_2/graphene hybrid nanostructures mainly concentrated on Li cyclability under low current density. A representative group of research in this area includes TiO_2-graphene hybrid nanostructures by Wang et al.,[66] anatase TiO_2/graphene composite anodes by Choi et al.,[67] a sandwich-like graphene-containing mesoporous anatase titania material (≈5 nm) (G–TiO_2) by Yang et al.,[68] and photocatalytically reduced TiO_2 nanoparticle/graphene materials by Qiu et al.[69] For the last one, TiO_2–rGO composites offered reversible discharge and charge capacities of 310 mAh g^{-1} and 270 mAh g^{-1}, and retained 200 mAh g^{-1} up to 100 cycles. Similar results were also confirmed by Zhen et al.,[70] showing that rutile TiO_2 nanobundle–rGO composites afforded a reversible capacity of 300 mA h g^{-1} at 0.6 C after 500 cycles.

More recently there has been interest in Li cycling performance under large current density for TiO_2–graphene anode materials. This is an important distinction for taking new energy

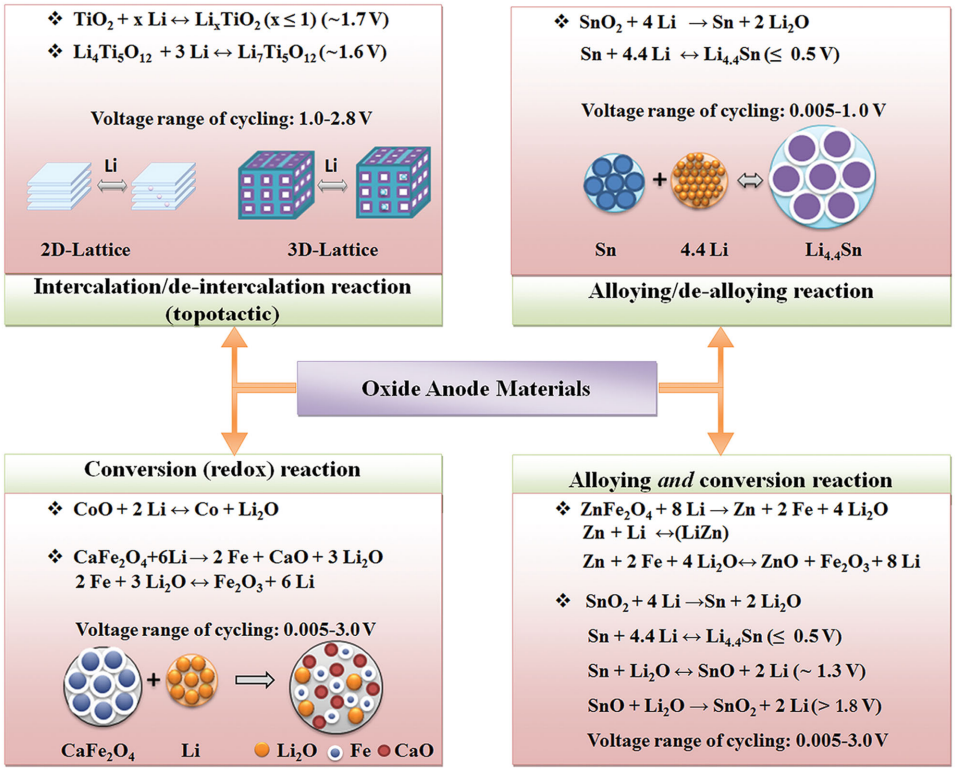

Figure 3. Classification of oxide anode materials based on reversible Li insertion and extraction processes: intercalation/deintercalation, alloying/dealloying, and conversion (redox) reactions. The latter two processes can act synergistically to afford large and stable capacities. Some selected examples and schematic diagrams of the processes are given. The voltages shown are vs. Li metal. Reproduced with permission.[61] Copyright 2013, American Chemical Society.

storage materials from a benchtop curiosity to a practical material. In 2013, Ban et al.[71] reported that TiO_2 (≈10 nm) deposited rGO sheets by atomic layer deposition (ALD) showed stable capacities of ≈120 mAh g^{-1} at 1 A g^{-1}. Jiang et al.[72] showed a 3D foam architecture of ultrafine TiO_2 nanoparticles embedded in N-doped graphene networks, exhibiting reversible capacities of 165 mAh g^{-1} and 143 mAh g^{-1} at 1 C and 5 C rate after 200 cycles. Wang et al.[73] proposed that the reversible capacity of TiO_2/N–rGO via hydrothermal method up to 126.8 mAh g^{-1} at 10 C and still remained at 118.4 mAh g^{-1} after 100 cycles. A reversible capacity of 166.3 mAh g^{-1} at 5 C for TiO_2–rGO nanocomposites was another performance improvement recently reported.[74] It is important to note that an impressive discharge capacity of 141.7 mAh g^{-1} after 100 cycles at 5 A g^{-1} was realized by using mesoporous TiO_2/graphene composites.[75] It is encouraging to see improved performance of such devices not only at larger current densities but cycle times as well.

Additional recent investigations have looked into multi-component materials, including different phases and morphologies of titania, metal oxides, and their spatial arrangement. Materials recently developed include N-doped TiO_2 nanotube/N-doped graphene composites,[76] graphene–TiO_2 nanotubes (Gr–TNTs),[77] anatase TiO_2/graphene nanosheets (**Figure 4**),[78] graphene nanoscroll encapsulated TiO_2 nanowires,[79] and graphene-wrapped TiO_2@Co_3O_4 coaxial nanobelt arrays.[80] These materials provided more information on how the Li cycling properties and reaction mechanism varies for vastly different graphene–TiO_2 composites. Furthermore, it underscores how robust lithium cycling truly is in order for it not only to be observed but also be successful across many different device formulations.

Among several lithium host materials under consideration, $Li_4Ti_5O_{12}$ is a unique zero strain material, and logically considered to possess stable discharge voltage, good cycle performance and excellent safety. The lithium cyclability of $Li_4Ti_5O_{12}$ can be described by:

$$Li_4Ti_5O_{12} + 3Li^+ + 3e^- \leftrightarrow Li_7Ti_5O_{12} \quad (2)$$

Currently, several novel routes have been developed to produce graphene-containing $Li_4Ti_5O_{12}$. Zhu et al.[81] adopted an electrospinning/heating treatment process to obtain composites of 1 wt% graphene and high specific capacity $Li_4Ti_5O_{12}$ (LTO). At a discharging and charging rate of 22 C, the specific capacity of the graphene–LTO nanocomposite was maintained at 110 mAh g^{-1}. It was also interesting to note a 91% retention of the initial capacity of the composite after 1300 cycles. As reported by Shi et al.,[82] mixtures of micro-sized LTO and graphene were heat treated to produce LTO/graphene composites, which had a discharge capacity of 132.2 mAh g^{-1} in the first cycle, remaining at 124.0 mAh g^{-1} after 300 charge/discharge cycles. Very recently, the investigation on Li cycling properties of graphene-wrapped $Li_4Ti_5O_{12}$ (LTO) prepared by Oh and co-workers[83] exhibited an outstanding specific capacity of 147 mAh g^{-1} at 10 C over 100 cycles. Similar results were

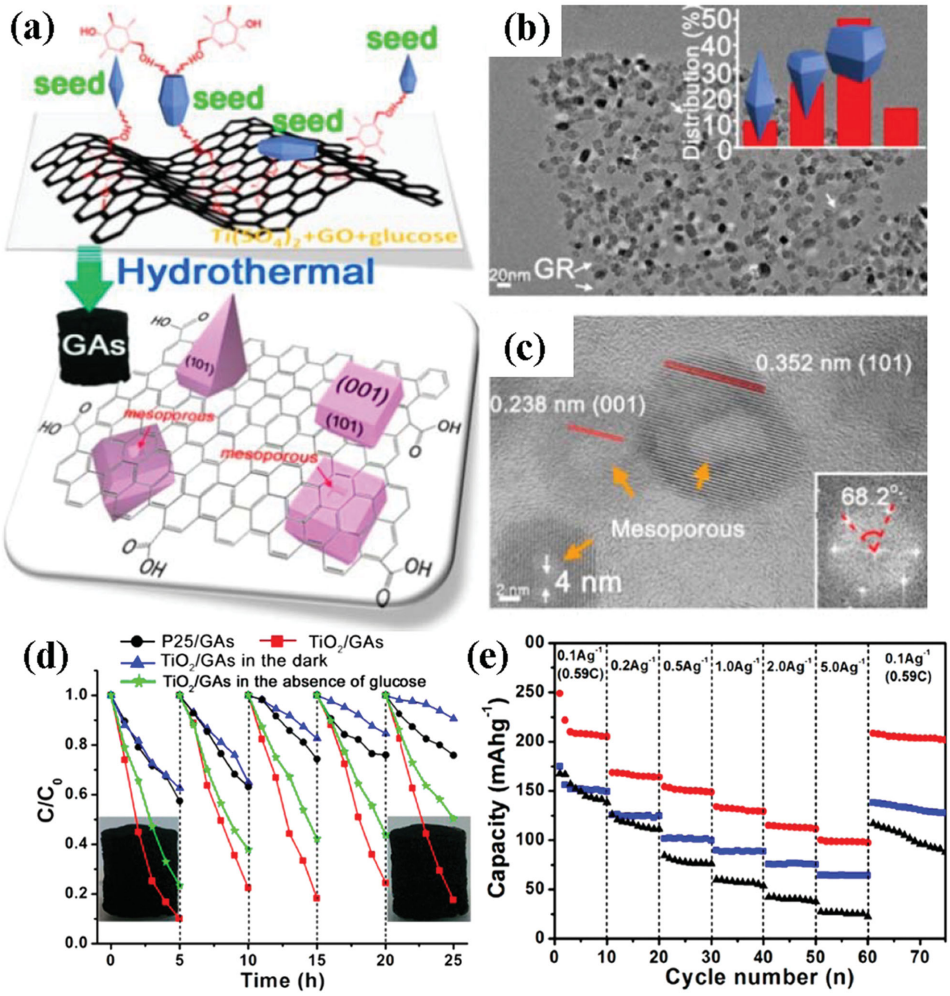

Figure 4. a) Glucose-linked transformation pathway for the in situ growth of TiO_2 nanocrystals with (001) facets on the GAs surface. b) Transmission electron miscroscope (TEM) image for TiO_2/GAs (67 wt% of TiO_2 in TiO_2/GAs). Inset shows the corresponding morphology distribution of the TiO_2 nanocrystals derived from 100 the of TiO_2 crystals in image (b). c) HRTEM image for TiO_2/GAs (67 wt%). Inset shows the corresponding fast Fourier transform (FFT) pattern. d) Cycling photodegradation of MO under simulated solar light irradiation (with an AM (air mass) 1.5 air mass filter). e) Cycling performance of TiO_2/GAs (red), TiO_2/GAs in the absence of glucose (blue), and pure TiO_2 (black) electrodes at different current densities from 0.1 to 5.0 A g^{-1}. Reproduced with permission.[78] Copyright 2014, American Chemical Society.

also reported by Ni et al.[84] and Li et al.[85] with heat treated $Li_4Ti_5O_{12}$/rGO sheet composites achieving a specific capacity of 154 mAh g^{-1} (at 10 C) and 149 mAh g^{-1} (at 20 C).[84]

Beyond the active materials in such anode materials, the packaging and coating of these materials are also important. Dual protection for $Li_4Ti_5O_{12}$ with graphene/CNTs via a rheological phase reaction offered an initial discharge capacity of 172 mAh g^{-1}, which levelled off at 150 mAh g^{-1} and 144 mAh g^{-1}, respectively, even at 5.0 C and 10.0 C.[85] Yang et al.[86] showed that cathodically induced graphene (CIG)/$Li_4Ti_5O_{12}$(LTO) anode materials displayed a specific energy of 272 Wh kg^{-1} at the power of 136 W kg^{-1}. Intriguingly, the percolation threshold of graphene nanosheets as conductive additives in $Li_4Ti_5O_{12}$ anodes was also taken into consideration.[87]

Despite the presence of graphene conferring several advantages, including the improvement of conductivity, the prevention of particles from aggregation during preparation, and the increase of rate properties of graphene–titanate hybrids, the graphene seems to exert a limited influence on improving the specific capacity of the hybrids, owing to the inherently low specific capacity of titanate, especially for $Li_4Ti_5O_{12}$ which has a limited theoretical capacity of 175 mAh g^{-1}.[88]

2.2. Anode Based on Alloying–Dealloying Reaction

As pointed out by Reddy,[61] elements like Si,[89] Sb, Sn, In, Cd and Mg[90] can facilitate lithium storage and cycling behaviour via alloying–dealloying reactions at potentials less than 1 V vs. Li metal. Therefore, such elements are prospective anode materials for LIBs. The Li cycling mechanism of metal in LIBs is given in Equation (3).

$$\text{Alloying reaction}: M + nLi^+ + ne^- \leftrightarrow Li_nM \quad (3)$$

However, repeated investigations have explicitly demonstrated the very unreliable Li cyclability of Sn, Si, Sb, etc. via alloying–dealloying reactions as they experience large volume changes during discharge and charge, in some cases as high as 300%, inevitably giving rise to "electrochemical pulverization" of the active material on the electrode. Ultimately, this leads to electrode disintegration and capacity fading under long-term cycling. Graphene can effectively accommodate the volume expansion of inorganic nanomaterials, leading to markedly improved Li-cycling performance.

Recent investigation into sheet-like Sb/graphene hybrids[91] and Ni@graphene yolk–shell structures[92] has demonstrated that graphene/metal composites could offer good lithium cycling properties. For example, a first discharge (Li-uptake) capacity of 1034 mAh g^{-1} for Sb/graphene,[91] and a stable cycling capacity of 800 mAh g^{-1} at 0.1 A g^{-1} for Ni@graphene and 490 mAh g^{-1} at 1 A g^{-1}, lasting for more than 100 cycles without any decay.[92] In 2014, Yuan et al.[93] reported that a practical capacity of Ge (1332 mAh g^{-1}; calculated according to the mass fraction of Ge nanoparticles in the Ge/rGO/C nanocomposite electrode) as cycled at a 0.2 C rate was achieved. Qin et al.[94] showed a similar result, i.e., a capacity of 1258 mAh g^{-1}, even after 50 charge/discharge cycles for germanium quantum dots embedded in a N-doped graphene matrix with a sponge-like architecture (Ge/GN sponge).

As an important study,[95] large mesoporous Si sponge (MSS) anodes have demonstrated excellent performance in lithium batteries. MSS anodes possessed a capacity of up to ≈750 mAh g^{-1} based on the total electrode weight with >80% capacity retention over 1,000 cycles. Lithium–silicide transformations from amorphous to crystalline[96] and the dynamics of electrochemical lithiation/delithiation of graphene-encapsulated silicon nanoparticles[97] were studied to further understand the lithium cycling mechanism during charging and discharging. Sponge-like materials offer one promising route to addressing the volume expansion problems associated with such materials, by essentially accommodating the volume expansion internally into void space. In fact, graphene-containing tin and silicon are a popular research area owing to the large theoretical specific capacity of Sn (993 mAh g^{-1}) and Si (4200 mAh g^{-1}). Owing to this, the following sections will be dedicated to a close look at these particular metal/graphene anode materials and the sourcing considerations for the metals.

2.2.1. Sn/Graphene

Among group IV elements, Sn, less toxic and less expensive than other candidates, is of importance as a promising alternative material for advanced anode materials in LIBs. The bulk phase is known to have a higher theoretical capacity owing to the Li alloy formation (i.e., $Li_{4.4}Sn$). However, the practical application of Sn-based anodes is hampered by its poor cyclability because of a large volume change of 259%.[98] The incorporation of graphene can effectively accommodate the volume change of Sn anode and thus improve its cycling performance.

Recently, Lian et al.[99] covered porous nano-sized Sn@C/graphene with a 3D carbon network. This material delivered a reversible specific capacity of 600 mAh g^{-1} after the fiftieth cycle. Similar performance in Li-cyclability of hydrothermal Sn/graphene structures has been reported by Zhou et al. with improved capacities up to 838.4 mAh g^{-1} at 0.1 A g^{-1} after 100 cycles.[100]

Various synthesis approaches were also explored. Microwave reduction followed by annealing was applied by Beck et al. to yield Sn/graphene composites,[101] which afforded a Li cycling performance of 790–850 mAh g^{-1}, depending on the composition, and a stable reversible capacity of 500 mAh g^{-1}. Besides the hydrothermal route, solvothermal synthesis followed by thermal treatment has been demonstrated to be a viable route to Sn–In/GNS composites,[102] which possessed a storage capacity of 865.6 mAh g^{-1} at 100 mA g^{-1} rate and rate capability of 493.2 mAh g^{-1} at 600 mA g^{-1} after 25 cycles. Qin et al.[103] investigated core–shell Sn@G via a chemical vapour deposition (CVD) technique. Sn@G showed high rate performance (1022 mAh g^{-1} at 0.2 C and 270 mAh g^{-1} at 10 C, respectively) and an extremely high cycling capacity of 682 mAh g^{-1} at 2 A g^{-1} and 96.3% capacity retention after 1000 cycles (**Figure 5**). A 3D hollow Sn@C–graphene hybrid material produced via an assembly method was also reported by Zheng et al. with similar high performance characteristics.[104] Such materials are highly promising for both their performance stability and use of established and readily scalable synthesis techniques.

Recently, graphene encapsulated Sn nanoparticles (Sn-NPs) synthesized via microwave plasma irradiation of SnO_2 exhibited larger-than-theoretical reversible capacities of 1037 mAh g^{-1} even after prolonged cycling. The cycling ability exceeds 5000 times in half-cells at a 6 C rate while retaining 400 mAh g^{-1} reversible capacities.[105] While larger-than-theoretical performance is indeed interesting, it is more suggestive of a lack of complete understanding of what theoretic limits are rather than indicative of some super materials. Nonetheless, the high performance characteristics of such materials are encouraging.

As discussed above, the Li cycling performance of graphene-containing tin anodes are highly stable when mixed with graphene due to compensating for the volume expansion during Li cycling.

2.2.2. Si/Graphene

Silicon is an attractive material for anodes in energy storage devices.[106] The main challenges associated with silicon anodes are structural degradation and instability of the solid–electrolyte interphase caused by the large volume change (≈300%) during cycling. As a consequence, various strategies have been adopted to address the issue. We will discuss the role of graphene for accommodating the volume expansion during Li cycling in the following sections.

Commercially available Si nanoparticles: a) Si: Commercially available Si nanoparticles are frequently used materials in Si–graphene (SG) paper composites via self-assembly approaches.[107] Silicon–graphene composites possessing a ≈1100 mAh g^{-1} under a low current density of 50 mA g^{-1}[108,109] have been reported by Tang et al.[108] They utilized a previously reported "breath figure" method to prepare a self-assembled Si/honeycomb–rGO composite film (Si/H–rGO)

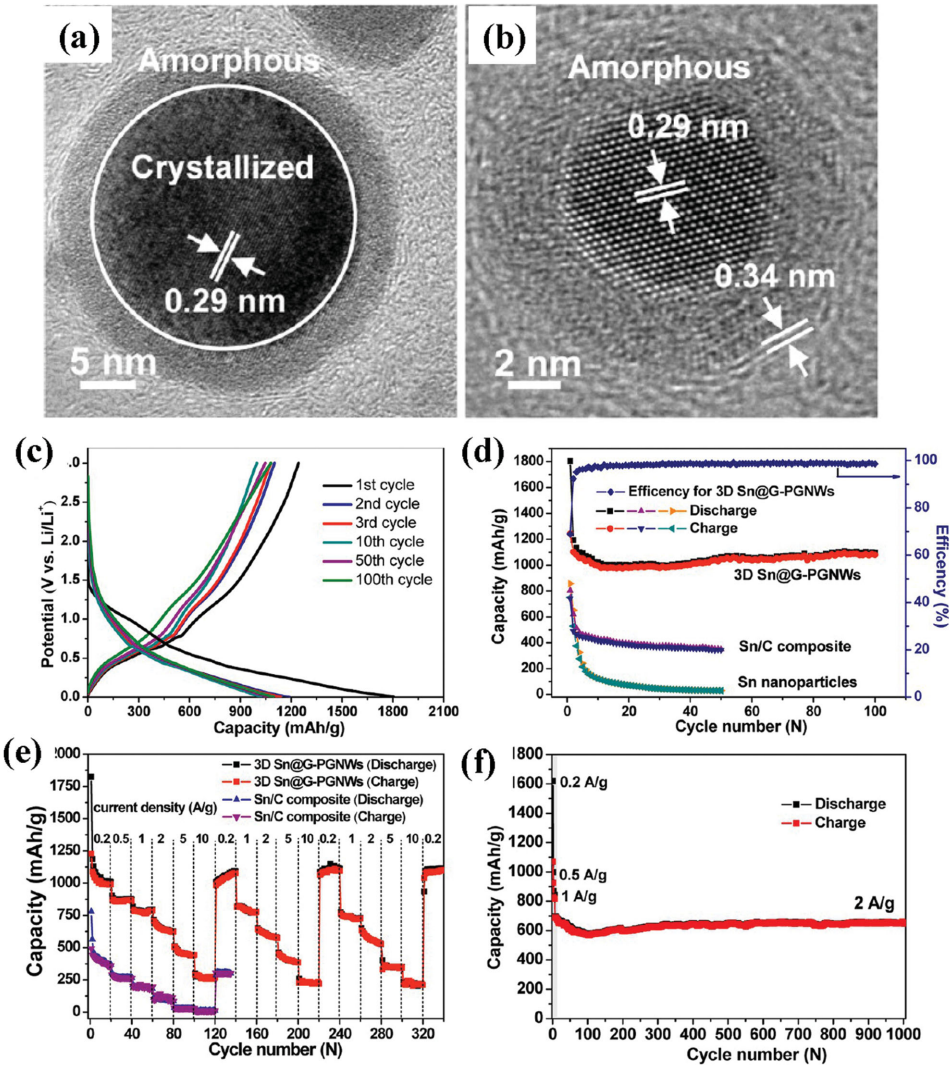

Figure 5. a, b) High resolution transmission electron microscopy (HRTEM) images of Sn@G nanoparticles. c) Voltage profiles of the 3D Sn@G–PGNW (porous graphene networks) electrode at a current density of 0.2 A g^{-1}. d) Cycle performance of the 3D Sn@G–PGNWs, Sn/C composite, and commercial Sn nanoparticles at a current density of 0.2 A g^{-1}. e) Rate cycle performance of the electrodes of 3D Sn@G–PGNWs and Sn/C composite at charge/discharge rates from 0.2 to 10 C (1 C = 1 A g^{-1}) for 340 cycles. f) Cycle performance of the 3D Sn@G–PGNW electrode at current densities of 0.2, 0.5, and 1 A g^{-1} for the initial six cycles and then 2 A g^{-1} for the subsequent 1000 cycles. Reproduced with permission.[103] Copyright 2014, American Chemical Society.

using commercial silicon. Of particular interest is a high specific capacity and good cycling stability of 1118 mAh g^{-1} after 50 cycles at 50 mA g^{-1} for the honeycomb rGO structure. Recently, Li et al.[109] successfully synthesized graphene-encapsulated pyrolyzed polyaniline-grafted Si composites via π–π interaction and electrostatic attraction. The resulting composite exhibited a reversible capacity of ≈1500 mAh g^{-1} at 50 mA g^{-1} and above 900 mAh g^{-1} at 2 A g^{-1}, respectively and retained a specific capacity of about 70% of the initial capacity even after 300 cycles (**Figure 6**). Again, the complexity of different forms that can be realized is truly unlimited even when using a relatively small number of simple materials. An important point to take away from this review is the wealth of materials, combinations and spatial arrangements that can be investigated.

We note that high capacity of ≈1450 mAh g^{-1} can be obtained at 500 mA g^{-1}. Lithium cyclability properties of Si/rGO architecture, in which commercial Si nanoparticles were entrapped in the rGO nanosheets via a self-assembly process,[110] produced a first discharge capacity of 2438 mAh g^{-1} at 500 mA g^{-1} which remained as high as 1481 mAh g^{-1} after 50 cycles (**Figure 7**). In a related work, Si@C/G[111,112] possessed an excellent cycling stability with a capacity of 1431 mAh g^{-1} after 100 cycles at a current density of 500 mA g^{-1}.[112] In sharp contrast, a commercially available Si–graphene composite (XG-SiG) offered a specific capacity of 1000 mAh g^{-1} at 0.5 C after 50 cycles.[113] It is clear then that laboratory-scale materials can offer improved cycle stability with higher capacities at higher current densities. There is still room for major improvement across all materials and combinations.

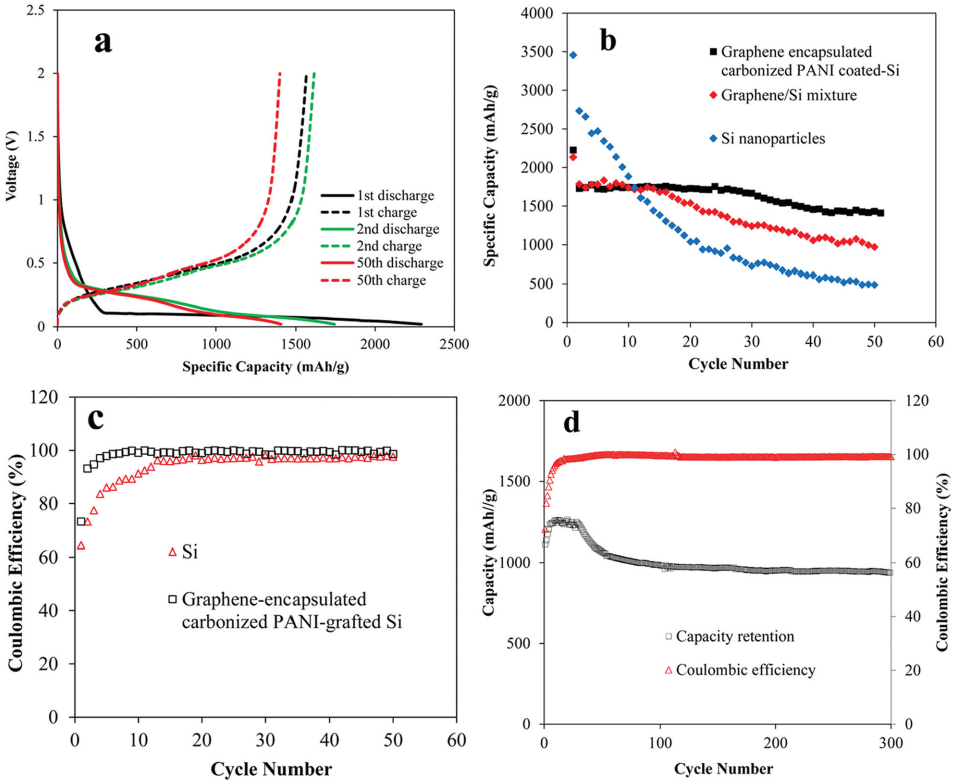

Figure 6. a) Charge/discharge curves of the graphene-encapsulated pyrolyzed PANI (polyaniline)-grafted Si. b) Capacity retention and c) Coulombic efficiency of the Si, the graphene/Si mixture, and the graphene-encapsulated pyrolyzed PANI-grafted Si at a constant current density of 100 mA g^{-1}. d) Capacity retention of the graphene-encapsulated pyrolyzed PANI-grafted Si at 2 A g^{-1}. Reproduced with permission.[109] Copyright 2014, American Chemical Society.

Recently, high capacity and excellent rate performance have been achieved. Multi-layered commercial Si NPs/rGO anode nanostructures by Chang et al.,[114] made via assembly of alternating Si/rGO layers on porous Ni foams, possessed a reversible capacity up to 1500 mAh g^{-1} at 2400 mA g^{-1} (1 C) after 100 cycles, and 630 mAh g^{-1} at 10 C after 152 cycles.

A combination of commercial Si-NP with graphene by means of a wet chemical method (including filtration[115,116] was also taken into consideration. In 2009, Tung et al. reported a versatile solution-based process for the large-scale production of single-layer chemically converted graphene over the entire area of a silicon/SiO_2 wafer.[117] In 2010, Lee et al.[116] reported Si–graphene (SG) paper composites (via filtration), consisting of commercial Si nanoparticles well distributed between graphene sheets, that offered a high storage capacity of more than 2200 mAh g^{-1} after 50 cycles at 1000–50 mA g^{-1} during discharge/charge, which decreased to 1500 mAh g^{-1} after 200 cycles, only a 0.5% loss per cycle. Recently, Li et al.[118] reported an elastic composite of wrinkled graphene sheets and Si nanoparticles, manufactured in the colloidal state, exhibited good cycling stability of 1044 mAh g^{-1} at a current density of 200 mA g^{-1} after 100 cycles.

Other synthesis routes have also been reported. In 2008, Chan et al.[89] utilized the vapour–liquid–solid and vapour–solid template-free growth methods to produce silicon nanowires directly on a stainless steel current collector. Lithium cyclability of silicon NWs achieves a charge capacity of 3541 mAh g^{-1} at C/20. Another study[119] demonstrated that a 50/50 wt% commercial Si/graphene composite, produced by discharge-plasma-assisted milling (P-milling), delivered a discharge capacity of 866 mAh g^{-1} after 200 cycles under 0.4 mA cm^{-2}. N-doped graphene-like nanosheets via milling followed by carbonization, possessed discharge capacities of 819 mAh g^{-1} after 50 cycles at 200 mA g^{-1}.[120] Su et al.[121] took note of Si/graphite@graphene composites by a spray-drying method followed by a heat treatment. The composites showed a high initial charge capacity of 820.7 mAh g^{-1} at 50 mA g^{-1}, and still delivered high initial charge capacities of 766.2 mAh g^{-1} at 500 mA g^{-1}. A facile freeze-drying method was utilized by Chen et al.[122] and Chabot et al.[123] Si/graphene nanocomposites, exhibiting capacities of above 850 mAh g^{-1} after 100 cycles at a rate of 100 mA g^{-1}[122] and specific capacity of 786.3 mAh g^{-1} after 200 cycles,[123] were readily observed. Carbon nanofibers encapsulating Si nanoparticles (CNFs/SiNPs) via an electrospinning method afforded 1048 mAh g^{-1} at a high current density of 890 mA g^{-1} after 200 cycles.[124]

Obviously, the electrochemical performance of commercial Si NPs/graphene composites generally stabilizes above a reversible capacity of 750 mAh g^{-1}, depending on the nature of the silicon, including morphology, size, defects, and the status of the graphene, i.e. simple mixing, encapsulating or anchoring (see Figure 2). It is clear that the way materials are arranged in anode composites is just as important as the types of materials of which it is composed.

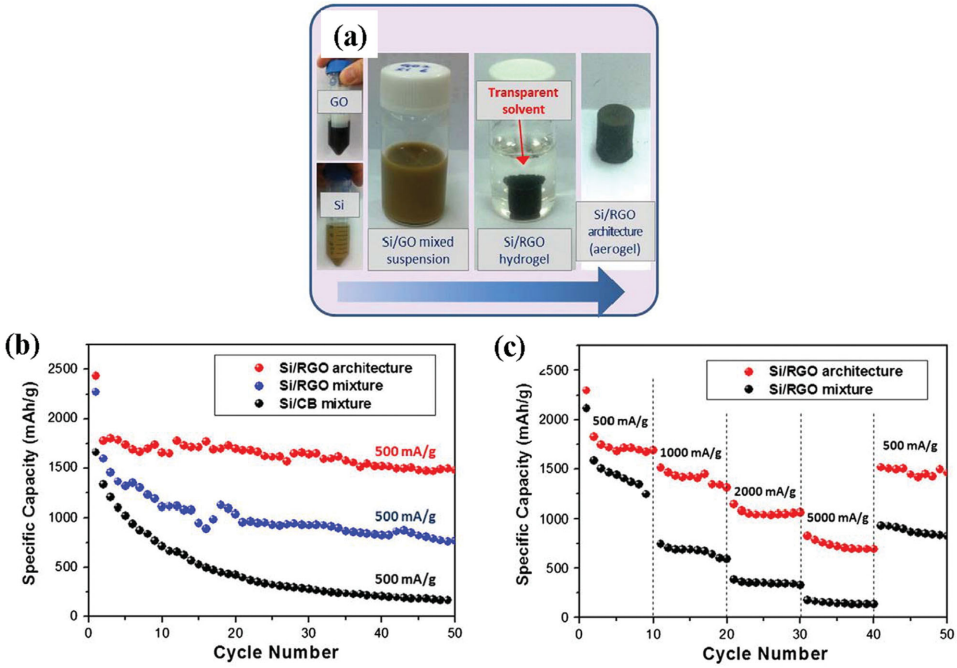

Figure 7. a) Preparation steps of Si/RGO architecture. b) Cyclability of the Si/carbon black (CB), Si/rGO mixture, and Si/rGO architecture electrodes at a current density of 500 mAg^{-1}. c) Rate capability of the Si/RGO mixture and Si/RGO architecture electrodes. Reproduced with permission.[110] Copyright 2013, Elsevier.

b) Introduction of metals: To overcome the inherent shortage of silicon as well as make up for its poor conductivity, metal nanoparticles were selectively incorporated into Si@graphene to produce binary metal/graphene composites. Si–Mn/rGO binary nanocomposites were yielded by mechanical complexation and subsequent thermal reduction of the mixtures of Si nanoparticles, MnO_2 nanorods, and rGO nanosheets. The resulting binary nanocomposite anodes displayed a specific capacity of 600 mAh g^{-1} after 50 cycles at a current density of 100 mA g^{-1}.[125] Ni-doped graphene-containing Si was produced by electrospinning, followed by thermal reduction. It possessed a specific capacity of 1045 mAh g^{-1} after 50 cycles at a current density of 100 mA g^{-1} and an enhanced rate capacity of 600 mAh g^{-1} at 1 A g^{-1} after 70 cycles.[126] A similar result was observed in gold-coated nanowire/graphene hybrid composite (Au–SiNWs/G) anode. It had a stable reversible capacity of approximately 1520 mAh g^{-1} at 200 mA g^{-1} after 20 cycles.[127]

Synthesized Si nanoparticles: a) Magnesiothermic reduction: The magnesiothermic reduction process is a common method for producing Si from silicon dioxide.[128] CAG/Si@SiOx composites produced via magnesiothemic reduction of mesoporous SiO_2, exhibiting a reversible capacity of 763 mAh g^{-1} at 100 mA g^{-1} after 50 cycles, were reported by Tao et al.[129] A comparable outcome was observed by Wong et al.[130] who developed a composite paper composed of graphene and rice husk-based Si NPs via magnesiothermic reduction process. It afforded a capacity of ≈650 mAh g^{-1} at 1 A g^{-1} after 30 cycles.

Higher capacity and better rate properties were achieved in other works focusing on higher dimensional materials. A 3D porous nano-architectured hybrid Si/graphene was synthesized through a magnesium reduction process by Xin et al.[131] The composite has a reversible capacity of ≈1000 mAh g^{-1} during charge rates ranging from 100 mA g^{-1} to 1 A g^{-1} after 30 cycles. More importantly, the material can be cycled at high Li^+ delivery rates such as 360 mAh g^{-1} at 5 A g^{-1} and 290 mAh g^{-1} at 10 A g^{-1} for more than 100 cycles.

In another study, Yi et al. synthesized micron-sized graphene/Si–C composites (G/Si–C) via high temperature hydrogen reduction of SiO.[132] The material possessed a capacity of 3.2 mAh cm^{-2} (≈1100 mAh g^{-1}) after 100 cycles with high Coulombic efficiency (average 99.51% from 2nd to 100th cycle). Notably, silicon nanoparticles produced by magnesiothermic reduction were encapsulated in graphene nanosheets via high-energy ball milling, followed by thermal treatment.[133]

b) Chemical Vapor Deposition (CVD) method: CVD is also used in the production of silicon/graphene composites. In 2010, Song et al.[134] reported that an array of sealed Si nanotubes was prepared by CVD of Si onto ZnO nanorods, followed by the selective removal of ZnO. It exhibited discharge capacities of 3360 and 2645 mAh g^{-1} at the rates of 0.05 and 0.2 C respectively, and high capacity retentions of about 81% after 50 cycles. Recently, a hybrid Si film/carbon nanofiber (CNF) synthesized via a two-step CVD method was employed as an anode for LIBs.[135] As reported by Ko et al.,[136] an amorphous silicon nanoparticle backbone graphene nanocomposite (a-SBG) produced from silane decomposition possessed a specific energy of 468 Wh kg^{-1} and 288 Wh kg^{-1} under a specific power of 7 kW kg^{-1} and 11 kW kg^{-1}, respectively. Notably, in situ growth of SiNPs@GNS–GrTr composites afforded an impressive capacity of 1528 mAh g^{-1} at 150 mA g^{-1}, cycle stability (88.6% after 50 cycles), and charge/discharge rate (412 mAh g^{-1} at 8 A g^{-1}).[137] In this work, silicon nanoparticles

were encapsulated in graphene nanosheets, which were then anchored on vertically aligned graphene trees. Very recently, Hassan[138] reported that carbon-coated Si nanowires on graphene (c-SiNW–G) produced via high temperature decomposition achieved a stable reversible capacity of 550 mAh g^{-1} after 100 cycles at 6.8 A g^{-1}. Additionally, recent study has demonstrated film deposition onto free-standing graphene foam via thermal decomposition of SiH_4.[139] Potential advantages of this technique include its inherent layer-by-layer setup, large surface coverage capability, controlled deposition of carbon coating by the injection of organic gas, and established industrial usage.

The representative studies on silicon/graphene composites are summarized in **Table 1**. Indeed, graphene–silicon composites are a promising and diverse group for high-capacity anode materials in LIBs owing to their low-cost, abundancy, and impressive lithium cyclability. However, some problems remain to be tackled. Of principle concern is the development of a low-cost, environmentally friendly synthesis technique for silicon and the related rational structure design. Addressing both of these points will help meet the supply demand for Si-graphene composite anode materials and lead to an improvement in conductivity and accommodation of volume expansion without unnecessary added production costs. So far, two different approaches to lithiation/delithiation have been investigated. Next, another approach is investigated whereby the method of releasing and absorbing lithium is different and dependent on the nature of the anode material. This approach is called intercalation and conversion.

2.3. Anodes Based on Intercalation and Conversion

Transition metal dichalcogenides of the form MX_2 (M = Mo, Ti, V, and W; X = S or Se) with a layered structure like graphite possess great potential for alternative anode materials. Generally speaking, MX_2 has strong covalent bonds within layers, and weak Van der Waals forces between layers, which provide ideal space for intercalation of Li ions. Molybdenum disulfide (molydisulphide, MoS_2) is classified as a representative metal dichalcogenide, where each Mo(IV) center occupies a trigonal prismatic coordination sphere that is bound to six sulfide ligands. Each sulfur center is pyramidal and connected to three molybdenum centers. The trigonal prisms are interconnected to form a layered structure, locating molybdenum atoms between layers of sulfur atoms. Their morphologies and properties are useful for energy storage applications such as electrodes for LIBs, supercapacitors,[140,141] and piezotronics.[143]

2.3.1. MoS_2–Graphene Hybrid

Li insertion and extraction into an idealized MoS_2/rGO[144] free-standing composite paper electrode can be summarized as follows (**Figure 8**):

$$\text{Intercalation}: MoS_2 + xLi^+ + xe^- \leftrightarrow Li_xMoS_2 \quad (4)$$

$$\text{Conversion}: Li_xMoS_2 + (4-x)Li^+ + (4-x)e^- \leftrightarrow Mo + 2Li_2S \quad (5)$$

Guo et al.[145] observed graphene-like MoS_2 flakes when using a thermal decomposition approach. Rana et al.[146] obtained flower-like MoS_2 particles anchored onto the surface of graphene films via CVD. The hybrid delivered a capacity of ≈580 mAh g^{-1} at 50 mA g^{-1}. Hou et al.[147] reported that layered-MoS_2 hybrids composed of N-doped graphene/porous G–C_3N_4 nanosheets, displayed a capacity of 800 mAh g^{-1} at 100 mA g^{-1} and a high cycling stability (maintaining 91% capacity after 100 cycles). Few-layer MoS_2/graphene (FL-MoS_2/GNS) composites produced via a hydrothermal method and a post-annealing process delivered a reversible capacity of around 1200 mAh g^{-1} with good cycle stability and enhanced rate capability.[148] Interestingly, a higher capacity has been recently achieved for MoS_2/GNS-15 nanocomposites via hydrolysis of $LiMoS_2$ by Liu et al.[149] The material had a reversible capacity of 1400 mAh g^{-1} in the initial cycle and retained 1351 mAh g^{-1} after 200 cycles at 100 mA g^{-1}. Moreover, the capacity reached 591 mAh g^{-1} even at 1 A g^{-1}. While molydisulphide is the leading example of layered materials for incorporation into graphene anodes, several others are also of great interest for similar applications.

2.3.2. WS_2, FeS_2, CuS, VS_4 and CoS/Graphene Hybrids

Other layered materials include WS_2, FeS_2, CuS. Interestingly, WS_2 possesses both Li and Na storage capability.[150,151] Shiva et al.[150] produced uniform graphene-like few-layer WS_2 supported on rGO which attained a specific capacity of 400–450 mAh g^{-1} at 100 mA g^{-1} at 50 cycles, and a steady capacity of 180–240 mAh g^{-1} at 4 A g^{-1}. In a recent interesting work, free-standing sandwich-type WS_2–NTs/GS hybrids were observed to maintain a capacity of 319 mA g^{-1} over 500 cycles at a current density of 1 A g^{-1}.[152]

A solvothermal method for making FeS_2/graphene composites recently attracted much interest. Qiu et al.[153] made FeS_2/N-doped graphene (FeS_2/N-G) composites which showed reversible discharge and charge capacities of 979 and 920 mAh g^{-1}, respectively (**Figure 9**). Cobalt sulfide/graphene composites were also investigated by Huang et al.[154] The uniform sphere-like cobalt sulfide particles (about 150 nm in diameter), consisting of CoS_2, CoS and Co_9S_8, were well dispersed on the surface and edge of graphene and offered a reversible capacity of 1018 mAh g^{-1} in the first cycle, which remained above 950 mAh g^{-1} after 50 cycles at 100 mA g^{-1}.

Li-cyclability of hexagonal CuS/graphene composites has been investigated by many groups.[155] Du et al.[156] reported a universal soft colloidal templating strategy for the synthesis of high-quality ultrathin metal sulphide nanocrystals, i.e., hexagonal CuS nanosheets, hexagonal ZnS nanowires, orthorhombic Bi_2S_3 nanowires and orthorhombic Sb_2S_3 nanowires. Among them, CuS nanosheet electrodes delivered capacities as high as 285 and 198 mAh g^{-1} at current densities of 2 and 3 A g^{-1}, respectively.

VS_4 and CoS adopt similar mechanisms when used as anode materials during cycling. Xu et al.[157] demonstrated that graphene-attached monoclinic VS_4 composite anode electrodes delivered a capacity of 630 and 314 mAh g^{-1} at 10 and 20 C. CoS/graphene composites have been synthesized by an ethylenediamine-mediated solvothermal method. The obtained

Table 1. Physical properties and electrochemical Li cycling data of elemental (Sn, Si, etc)

Morphology	Synthesis approach	Current rate [mA g^{-1}]	Reversible capacity [mAh g^{-1}]	Capacity retention after n cycles (cycling range)	Ref.
Sn NPs/graphene	hydrothermal and heat treatment	100	1839	45.7% (n = 100)	[100]
Porous Sn NPs @C/graphene	hydrothermal and heat treatment	100	693	87% (n = 50)	[99]
Sn–In/GNS	solvothermal/thermal treatment	100	865	83.9% (n = 50)	[102]
Sn NPs@G–PGNWs(porous graphene networks)	CVD	200	1245	87.5% (n = 100)	[103]
Sn NPs@G	microwave reduction/annealing	100	600	87% (n = 100)	[101]
Hollow Sn@C–graphene	hydrolysis followed by annealing	50	922.7	71.5% (n = 50)	[104]
Commercial silicon					
Si NPs/graphene	thermal reduction	100	2200 (n = 500)	<0.5% per cycle (n = 200) (1500 mAh g^{-1})	[116]
Si honeycomb graphene	"breath figure" method	50	1686	66% (n = 50)	[108]
Si NPs/rGO	dip-coating method	24000	724	87% (n = 200)	[114]
Si NPs/graphene	used as available	0.5 C	1258	86.5% (n = 50)	[113]
Si NPs/graphene	self-assembly	200	1100	73% (n = 100) (803 mAh g^{-1})	[107]
Si NPs/graphene	Microwave/heat treatment	500	1000	80% (n = 100)	[115]
Si NPs/N–graphene-like nanosheets	carbon-thermal method	200	1319	62% (n = 50)	[120]
Si NPs entrapped by rGO	self-assembly	500	1638	83.4% (discharge) (n = 50)	[110]
Si NPs/graphene	discharge-plasma-assisted milling	0.4 mA cm^{-2}	1474	58.8% (n = 200)	[119]
Si/graphite@graphene	spray-drying/heat treatment	100	803.3	62.2% (n = 50)	[121]
Si NPs/graphene sheets	freeze-drying/thermal reduction	100	1271	67% (n = 100)	[122]
Graphene wrapped Si	freeze-drying method	100	1248.8	78.8% (n = 100)	[123]
Grafted Si NPs/graphene	freeze-drying method	2000	1184	76% (n = 300)	[109]
Si from magnesiothermic reduction					
3D Si/graphene	sol–gel followed by reduction	5000	530	68% (n = 100)	[131]
Porous Si@SiO_x/graphene	chemical activation/reduction	100	831	91.8% (n = 50)	[129]
Si NPs/graphene	ball milling/thermal treatment	400	1314	31.2% (n = 50)	[133]
RH-Si NPs/graphene	precipitation/reduction	1000	1000	75% (n = 30)	[130]
Graphene/Si–C nanocomposite	vacuum filtration followed by reduction	400	1100	99% (n = 100)	[132]
Si from CVD and others					
Silicon film/ free-standing graphene foam	chemical vapor deposition	0.22 mA cm^{-2}	1.4 mAh cm^{-2}	57% at 0.45 mA cm^{-2} (n = 60)	[139]
Si nanowire–rGO	solvothermal followed by CVD	0.3 C	1812	80% (n = 100)	[142]
Silicon NPs/graphene	freeze-drying/thermal reduction	2800 (discharge)	≈1100	100% (n = 1000)	[136]
Si NWs–graphene	Ni-catalysis/thermal reduction	100	1416	65.7% (n = 30)	[138]
Sb NPs/graphene	solvothermal route	50	586	70% (n = 40)	[91]
Ni@graphene nanostructures	solvothermal/heat treatment	1000	490	490 mAh g^{-1} at 5 A g^{-1} (n = 1700)	[92]
Si–Mn/rGO	mechanical/thermal reduction	100	668	90% (n = 50)	[125]
Si–Ni–graphene	electrospinning/thermal treatment	1000	740	81% (n = 70)	[126]

CoS–graphene sheet-on-sheet composites with 26.2% graphene displayed reversible capacities of 898 mAh g^{-1} after 80 cycles at 0.1 C and 391 mAh g^{-1} after 200 cycles at 3 C.[158] Recently, cobalt sulfide nanoparticle–rGO composites showed a reversible capacity of 994 mAh g^{-1} after 150 cycles at 200 mA g^{-1}.[159] The advantage of such metal sulphides is that they are highly abundant and inexpensive.

Recently, layered sulfides with varied chemical compositions and unique crystal structure have attracted much attention due to their increasing applications in energy storage, especially for next-generation rechargeable battery technology.[160–162] Among them, graphene-containing MoS_2 has established itself as the most promising intercalation host candidate in LIBs owing to its unique graphene-like structure, high capacity and excellent rate properties.

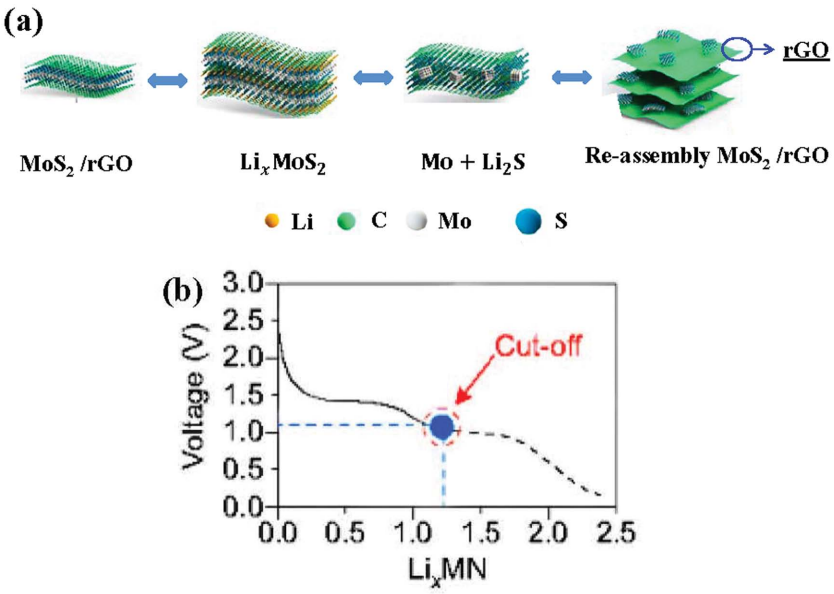

Figure 8. a) Schematic diagram of lithiation/ delithiation in MoS_2/rGO composite. b) charge–discharge curve of MX_2 electrode. Reproduced with permission.[140] Copyright 2013, Macmillan Publisher Lts.

2.4. Anodes Based on Conversion and Alloying: SnO_2, Metal Sulfides, Metal Nitrides and Germanium Compounds

In these anode materials, the oxides, nitrides, or sulfides are first reduced to the respective metals by lithium metal under electrochemical conditions, followed by lithium alloy (strictly, intermetallic compound) formation. In a typical example, SnO_2 experiences the following lithium cycling reactions:

$$\text{Conversion reaction}: SnO_2 + 4Li^+ + 4e^- \rightarrow Sn + 2Li_2O \quad (6)$$

$$\text{Alloying reaction}: Sn + 4.4Li^+ + 4.4e^- \leftrightarrow Li_{4.4}Sn \quad (7)$$

2.4.1. SnO_2

The mineral form of SnO_2 is called cassiterite, and adopts a rutile structure in which the tin atoms are coordinated by six oxygen atoms, and oxygen atoms are coordinated by three Tin atoms. SnO_2 is an extensively studied anode material possessing theoretical capacity of 782 mAh g^{-1}.[163] The incorporation of graphene may provide more opportunities for tin oxides in LIB applications. Several strategies have been developed to synthesize diverse SnO_2–graphene composites to meet various requirements in LIBs. The following sections will address some of the more promising strategies for producing tin oxide–graphene anode materials.

Reassembly or Self-Assembly: Assembly, such as layer-by-layer (LBL) assembly,[164] is a practical approach for SnO_2–graphene composites. Early studies on SnO_2–graphene composites were mainly concerned with lithium cycling under low current densities. In 2008, Paek et al.[165] attempted to reassemble graphene nanosheets (GNS) in the presence of rutile SnO_2 nanoparticles (≈5.4 ± 2.1 nm) and produced a delaminated nanoporous electrode material. The resulting SnO_2/GNS exhibited a reversible capacity of 810 mAh g^{-1}. Furthermore, it retained a capacity of 570 mAh g^{-1} at 50 mA g^{-1} after 30 cycles. This is in stark contrast to the specific capacity of the bare SnO_2 nanoparticle which quickly faded to 60 mAh g^{-1} only after 15 cycles. A comparable result was found in self-assembled free-standing 40 wt% graphene–SnO_2 electrodes.[166] In 2010, Wang et al.[166] developed a binary self-assembly approach to build SnO_2–graphene nanocomposites consisting of ordered alternating layers of nanocrystalline SnO_2 (≈3–5 nm) and graphene or graphene stacks. These devices delivered specific capacities of 760 mAh g^{-1} at 8 mA g^{-1}, 225 mAh g^{-1} at 80 mA g^{-1}, and 550 mAh g^{-1} at 20 mA g^{-1}, respectively. In another example, graphene-encapsulated SnO_2 hollow spheres[167] produced via a simple electrostatic self-assembly afforded a reversible capacity of 422 mAh g^{-1} after 100 cycles at 158 mA g^{-1} and a capacity of 237 mAh g^{-1} after 30 cycles at 1580 mA g^{-1}.

To date, high capacity and stable rate performance under large current densities have been realized for a 3D interconnected graphene framework based SnO_2 nanocomposite via self-assembly followed by a thermal treatment. Such devices have shown reversible capacities of 1244 mAh g^{-1} in 50 cycles at 100 mA g^{-1} and a rate capability of 754 mAh g^{-1} in 200 cycles at 1000 mA g^{-1}.[55] This transition from established low current density performance to similar high current density performance is an important step to increasing tin oxide–graphene anode material usage and application.

Wet Chemical Process: Wet chemical processes include redox reactions and co-precipitation. SnO_2–graphene composites based on a redox reaction approach are also of particular interest. Several examples of materials research in this large area are highlighted. The lithium cycling properties of 3D SnO_2–graphene nanocomposites produced by an in situ chemical reduction process[168] delivered a lithium storage capacity of 520 mAh g^{-1} at 55 mA g^{-1} after 100 cycles. Similarly, Wang et al.[169] adopted a redox reaction to produce SnO_2/graphene composites which delivered a charge capacity of 840 mAh g^{-1} after 30 cycles at 67 mA g^{-1}, and retained a charge capacity of about 590 and 270 mAh g^{-1} after 50 cycles at 400 and 1000 mA g^{-1}, respectively. Recently, Tripathi et al. reported Sn-doped SnO_2/graphene with a high capacity of 600 mAh g^{-1} at 700 mA g^{-1} after 35 cycles.[170] This material was produced by means of a DMF (dimethyl formamide)-assisted self-reduction method. Besides metal doping, metal ion doping has been demonstrated to produce high performance anodes.[171] Even phenomena which are often considered undesirable in wet synthesis have also proven useful in anode material synthesis.

Co-precipitation is the formation of one or more solid agglomerates, which pull another, typically soluble material, out of solution with them. Often, one of the precipitates is a contaminant. However, in anode research it can be used to great

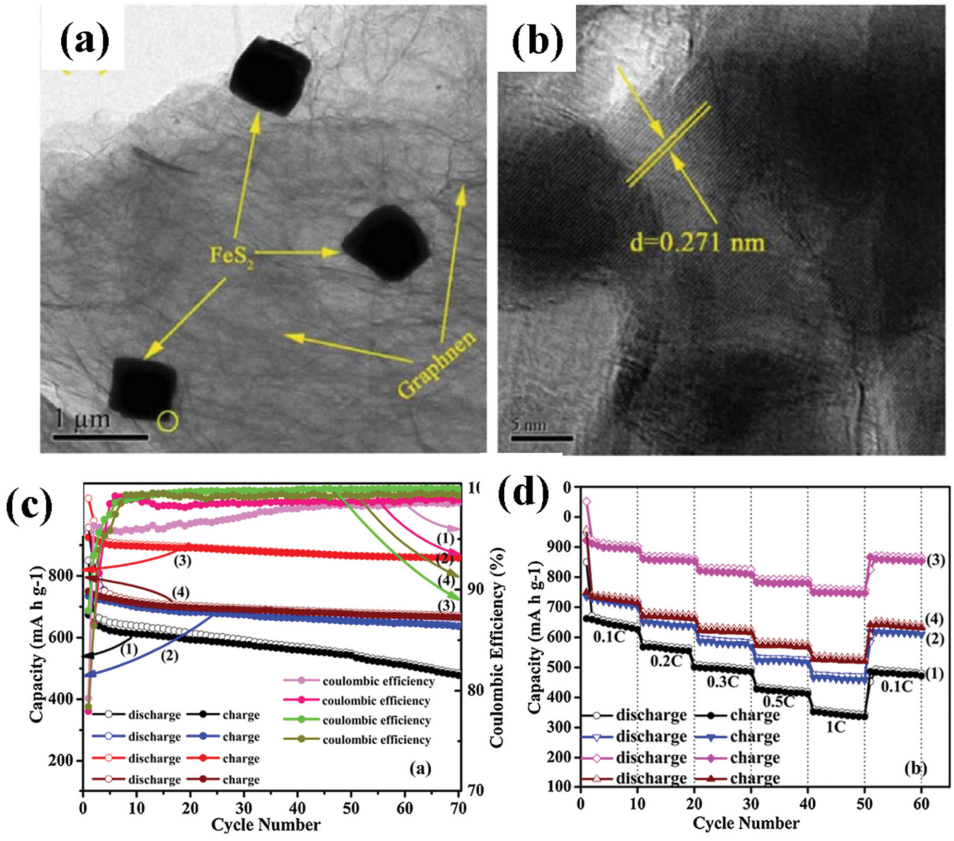

Figure 9. Microstructure of FeS_2/N-G (1:2) composite: a) TEM image. b) HRTEM image. c) Cycling performances and their columbic efficiencies of samples at a current density of 0.1 C: 1) FeS_2; 2) FeS_2/N–G (1:1); 3) FeS_2/N–G (1:2); 4) FeS_2/N–G (1:4). d) Rate capability of samples at different current densities: 1) FeS_2; 2) FeS_2/N–G (1:1); 3) FeS_2/N–G (1:2); (4) FeS_2/N–G (1:4). Reproduced with permission.[153] Copyright 2014, Elsevier.

benefit. The co-precipitation of SnO_2 on graphene followed by reduction is a feasible way to SnO_2/graphene composite anodes.[172,173] This rGO/SnO_2 composite offered a capacity of 2140 mAh g^{-1} and 1080 mAh g^{-1} for the first discharge and charge, respectively, at 50 mA g^{-1}, and good capacity retention with a capacity of 649 mAh g^{-1} after 30 cycles.[172] This synthesis approach is especially useful because it can be readily scaled up and requires minimal post processing.

Wet chemical reaction strategies provide a convenient, low-cost approach to produce various SnO_2 nanoparticle@graphene hybrid structures. The Li cycling property of composite produced via such routes commonly stabilizes around 500–700 mAh g^{-1}, and the rate capability of 423 mAh g^{-1} at 4 A g^{-1}[174] is impressive. More attention should be focused on the controllable synthesis of SnO_2, construction of 3D structures and the formation of flexible electrodes in the near future using these and many other wet chemical methods readily available to researchers and industry.

Hydrothermal or Solvothermal Methods: Hydrothermal methods are commonly used approaches to produce SnO_2-graphene composites.[175,176] Both processes are similar and are best described as crystallization processes conducted at high temperature and/or pressure. Variation of precursor solutions and other parameters including time, temperature, and ramp rate can be used to control the size and shape of resulting crystal materials. Earlier research in hydrothermally derived SnO_2-graphene composites consisting of 60 wt% SnO_2 nanocrystals have demonstrated a reversible specific capacity of 558 mAh g^{-1} after 50 cycles at C/5 (i.e., 264 mA g^{-1}). Subsequently, cycle performance of SnO_2-graphene nanocomposites under small current densities (50 mA g^{-1}) has been improved to 662 mAh g^{-1} after 150 cycles.[177] Again, pushing to higher current densities across many different LIB materials is a constant looming problem to be tackled.

More recently, hydrothermal graphene-containing SnO_2 materials have attained high marks, particularly for high and stable capacity performance. Hydrothermal binary SnO_2–Fe_2O_3/rGO samples showed a high reversible capacity of 976 mAh g^{-1} during the second cycle at 0.5 C (395 mA g^{-1}) and cycling stability of 958 mAh g^{-1} through the 100th cycle.[178] In a very different form, SnO_2/N-doped graphene aerogel (SnO_2–NGA) hybrids support lithium storage capacities of 1100 mAh g^{-1} under 0.2 A g^{-1} after 100 cycles.[179] Several other shape-varied materials including corn-like graphene/SnO_2/carbon nanofiber (GSCN) mixtures, and SnO_2/vertically aligned graphene nanosheets (VAGN) have also demonstrated high capacities at high current densities as high as 1813 mAh g^{-1} after over 1000 cycles under 2 A g^{-1}.[180]

Similarly, SnO_2 hollow spheres (HSs) enveloped by poly(3,4-ethylenedioxythiophene) or PEDOT, delivered a capacity of

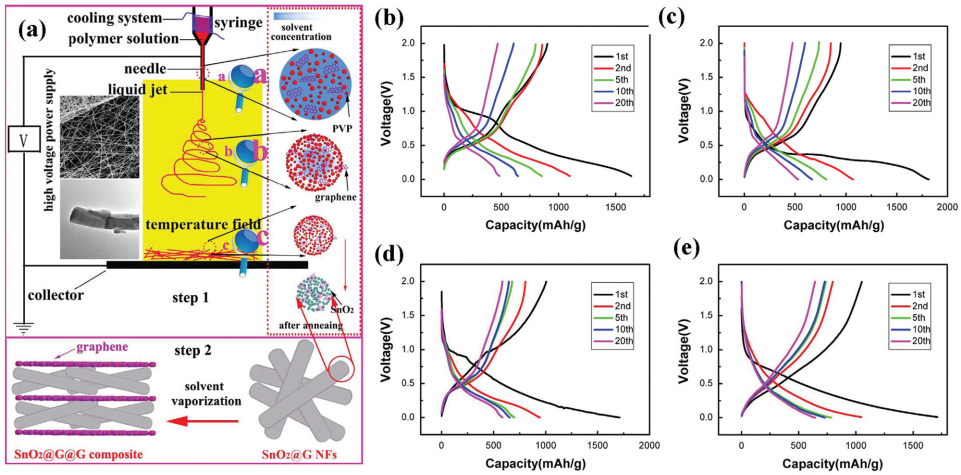

Figure 10. a) Schematic illustration of synthesis process of SnO_2@G nanofibers (NFs.) Charge and discharge curves of b) commercial SnO_2; c) pure SnO_2 NFs; d) SnO_2@G NFs; e) SnO_2@G@G composite obtained at the first, second, fifth, tenth, and twentieth cycles. Reproduced with permission.[185] Copyright 2014, Elsevier.

400 mAh g^{-1} after 30 cycles at 100 mA g^{-1}. More interestingly, a rate capability of 381 mAh g^{-1} at 2A g^{-1} was achieved.[181] In addition, nanosized SnO_2-graphene composites (with a discharge capacity of 504 mAh g^{-1} after 200 cycles) were produced by the microwave autoclave method, a variation on the traditional hydrothermal method.[182–184]

As discussed above, hydrothermal SnO_2-graphene composites afford various lithium cycling performance characteristics which are strongly dependent on the synthesis process and electrochemical cycle conditions. To date, lithium storage capacities of 1100 mAh g^{-1} at 0.2 A g^{-1}[179] and a rate capability of 381 mAh g^{-1} at 2 A g^{-1}[181] have been reliably attained by several hydrothermal/solvothermal-based synthesis techniques. Besides the main synthesis methods already outlined, several niche approaches have also been developed. The details of several such processes are presented in the next section.

Others: Several other routes have been utilized to synthesize SnO_2/graphene nanocomposites, such as electrospinning followed by calcination (**Figure 10**),[185] gas–liquid interfacial synthesis,[186,187] melting diffusion methods,[188] microwave-assisted non-aqueous sol–gel,[189] reactive e-beam evaporation of Sn granules,[190] and microwave-assisted reactions.[191] These techniques have been further applied to binary oxides, ternary oxide and complex wrapping morphologies such as graphene wrapped SnO/SnO_2 nanocrystals,[192] binary SnO_2–TiO_2/G ternary nanocomposites,[193] ZnO–SnO_2/graphene composites,[194] and SnO_2–CuO graphene nanocomposites.[195]

Many significant improvements in the cycling performance of SnO_2/rGO composite have been reported to date. Representative works summarizing key performance properties are listed in **Table 2**. Several overall observations can be gleaned from this table: 1) In general, the lithium cycling properties of SnO_2/graphene composites are fairly stable. 2) Several approaches have been employed to yield SnO_2/graphene composites with various structures and unique features. Among all synthesis methods, wet chemical assembly may likely gain even more attention due to the facile process and ease of control over the resulting composite morphologies as well as immediate application in emerging flexible electronics devices. Despite the abundance of structures and techniques developed, more systematic studies of individual parameters and performance characteristics are necessary to reveal the correlation between electrochemical performance and structure, such as finite size effects, coupling between SnO_2 and graphene, and interfacial effects on the surface of graphene. Peak performance reporting is indeed important and illustrative; however, structure–property relationships are even more insightful. Attention will now be directed to other metal oxides, nitrides and sulfides.

2.4.2. Layered Sulfides, Nitrides and Others

SnS_2 has a CdI_2-type of layered structure (a = 0.3648 nm, c = 0.5899 nm, space group P3m1) composed of a layer of tin atoms located between two layers of hexagonally close packed sulphur atoms. The large interlayer spacing of 0.5899 nm in this structure allows the insertion and extraction of guest species (such as Li or Na ions) and better accommodation for volume changes in the host during cycling.[162] SnS_2 experiences a similar Li cycling mechanism as SnO_2.

$$\text{Conversion reaction}: SnS_2 + 4Li^+ + 4e^- \rightarrow Sn + 2Li_2S \quad (8)$$

$$\text{Alloying reaction}: Sn + xLi^+ + xe^- \leftrightarrow Li_xSn (x \leq 4.4) \quad (9)$$

Various strategies have been developed to achieve layered metal dichalcogenides.[150,204,205] As reported by Qu. et al.,[162] hydrothermally synthesized SnS_2–rGO exhibited a discharge (sodiation) capacity of 839 mAh g^{-1} and a charge capacity of 630 mAh g^{-1} in the first cycle at 0.2 A g^{-1} between 0.01 and 2.5 V and discharge capacities of 628 mAh g^{-1} after 100 cycles. SnS_2–graphene nanocomposites with a reversible capacity of 766 mAh g^{-1} at 0.2 C rate and 570 mAh g^{-1} after 30 cycles were also reported.[206] The lithium cycling properties of SnS_2/graphene hybrid with a unique plate-on-sheet structure

Table 2. Physical properties and electrochemical Li cycling data of SnO_2

Morphology	Synthesis approach	Current rate [mA g^{-1}]	Reversible capacity [mAh g^{-1}]	Capacity retention after *n* cycles (cycling range)	Ref.
Graphene-encapsulated SnO_2 hollow spheres	electrostatic self-assembly	158	909	75% ($n = 30$)	[167]
				46.4% ($n = 100$)	
rGO/SnO_2	homogenous co-precipitation	50	1009	64.3% ($n = 30$)	[172]
SnO_2/graphene	solution-based process	100	690	63% ($n = 20$)	[196]
SnO_2 nanocrystals–porous activated graphene sheet	In situ synthesis	100	1017	60% ($n = 50$)	[197]
SnO_2@graphene@graphene	simple solution mixing	80	986.5	60% ($n = 120$)	[185]
SnO_2/rGO	vacuum filtration	200	700	100% ($n = 100$)	[198]
SnO_2@graphene	wet-mechano-chemical	100	773.6	80.1% ($n = 100$)	[199]
SnO_2–graphene	hydrothermal	0.5 C	786	71% ($n = 50$)	[200]
SnO_2 nanorods/graphene	hydrothermal	100	907	78% ($n = 50$)	[175]
SnO_2 nanocrystals/GS	hydrothermal	100	1024	82.4% (844 mAh g^{-1})	[201]
				($n = 50$)	
Carbon/SnO_2/graphene	hydrothermal/calcinations	200	785	58.6% ($n = 120$)	[202]
SnO_2–graphene	microwave autoclave method	100	590	100% ($n = 200$)	[182]
SnO_2/graphene	gas–liquid interfacial synthesis	100	936.4	123.5% ($n = 100$)	[186]
Porous SnO_2@C/graphene	gas–liquid interfacial synthesis and hydrothermal	100	1115	91% ($n = 100$)	[187]
Graphene–SnO_2	microwave-assisted method	500	890	100%, ($n = 80$)	[191
Sandwich-like graphene wrapped SnO_x@graphene	layer-by-layer self-assembly	200	904	58.6% ($n = 100$)	[192]
SnO_2–TiO_2/graphene	reflux method	100	1595.4	73.8% ($n = 100$)	[193]
ZnO–SnO_2/graphene	hydrothermal	1000	1209.4	66.2% ($n = 50$)	[194]
SnO_2–Fe_2O_3/rGO	wet-chemical method	395	976	98.2% ($n = 100$)	[178]
SnO_2/rGO	in situ chemical synthesis	50	1051	57.1% ($n = 20$)	[203]
Mono-disperse SnO_2 /rGO	wet chemical method	500	1057	98% ($n = 400$)	[174]

possessed a charge capacity of 704 mAh g^{-1} after 100 cycles at 1.6 mA cm^{-2} (around 0.6 C) and a charge capacity of 303 mA h g^{-1} at 25.6 mA cm^{-2} (around 10 C).

In_2S_3 adopts an analogous lithium cycle mechanism to that of SnS_2. Gu et al.[207] investigated hexagonal In_2S_3–graphene composites produced via hydrothermal synthesis. These composites possessed a reversible lithium-extraction capacity of 913 mAh g^{-1}, 782 mAh g^{-1}, and 690 mAh g^{-1} at 700 mA g^{-1}, 1400 mA g^{-1}, and 3500 mA g^{-1}, respectively. Interestingly, the lithium cyclability of ZnS–rGO composites made by spray pyrolysis has shown a discharge capacity of 437 mAh g^{-1} at 4 A g^{-1} after 700 cycles in a recent study.[208] More complex multi-metal indium sulfides such as tetragonal CuInZnS-decorated graphene (CIZS@graphene) delivered an initial discharge capacity of 1623 mAh g^{-1} at 100 mA g^{-1} and reversible capacity of 494 mAh g^{-1} at 2 A g^{-1} after 480 cycles.[209]

Sulphides have demonstrated huge potential as anode materials in LIBs due to their high capacity, low cost and abundance. Despite this, research into sulphide materials is fairly lacking compared to other materials including metal oxides and pure metal–graphene anode materials.

2.4.3. Layered Oxide (MWO_4)

The investigation of lithium cycling in layered oxides has also attracted considerable attention. In 2014, Wang et al.[210] fabricated 3D in situ self-assembled $FeWO_4$ graphene mesoporous composites through a hydrothermal route. Lithium cycling follows the conversion mechanism described below:

$$\text{Conversion reaction}: FeWO_4 + 8Li^+ + 8e^- \leftrightarrow W + Fe + 4Li_2O \quad (10)$$

The specific capacity of $ZnWO_4$/rGO hybrids via a hydrothermal treatment reached 477.3 mAh g^{-1} after 40 cycles at 100 mA g^{-1}.[211] The discharge capacity of lithium batteries produced 597 mAh g^{-1} at a current density of 100 mA g^{-1} after 100 cycles. SrWO4/graphene composites were synthesized via a sol–gel method by Zhang et al.[212] The first cycle of the reversible specific capacity of such a composite could reach to 575.9 mAh g^{-1} at 50 mA g^{-1}. It's clear that many other metals can be incorporated into these tungsten oxides.

Research seems to suggest that these layered oxides adopt only a conversion process rather than intercalation when

cycling lithium during charging/discharging. Thus, further investigation into the electrochemical mechanism of such materials needs to be implemented. However, due to the low theoretical capacity derived from such large formula weights, this area may not prove to be as promising when compared to materials considered so far. Besides metal–tungsten oxide–graphene anodes, other metals, metalloids, and metal oxides can be combined.

2.4.4. Germanium and Germanium Compounds

Early lithium cycling of GeO_2, $MGeO_3$ (M = Cu, Fe, and Co), and $CuO \cdot GeO_2$, composites in the voltage range 0–3.0 V were discussed by Kim et al.[213] During the first discharge the structure was destroyed, followed by the formation of Ge and M metal nanoparticles and the alloy $Li_{4.2}Ge$. Lv et al.[214] successfully synthesized an amorphous GeO_x/rGO ($1.01 < x < 1.07$) composite by a simple one-step reduction process. The composite had a high reversible capacity of 1600 mAh g^{-1} at 100 mA g^{-1} and rate capacity of 410 mAh g^{-1} at 20 A g^{-1}.

In our previous works, a facile one-step route to crystalline $CuGeO_3$ nanowire/graphene composites was developed.[215] Crystalline $CuGeO_3$ nanowires were tightly covered and anchored by graphene sheets, forming a layered structure. The $CuGeO_3$ containing 37 wt% graphene exhibited a superior lithium cycling performance with a reversible capacity of 1265 mAh g^{-1} in the first cycle, and 853 mAh g^{-1} after 50 cycles under a current density of 200 mA g^{-1} (**Figure 11**). Recent progress in $CuGeO_3$ has led to $Cu_3Ge/GeO_x/CuGeO_3$ nanowire electrodes[216] showing improved capacity retention of ≈645 mAh g^{-1} at 200 mA g^{-1} after 20 cycles.

In other works,[217] crystalline and amorphous regions were found to coexist in a single Zn_2GeO_4 nanorod. The partially crystalline ZGC (ZGC: Zn_2GeO_4/graphene composite) containing 10.2 wt% graphene possessed a high reversible capacity (1020 mAh g^{-1} in the first cycle), favorable cyclic performance (768 mAh g^{-1} after 50 cycles), and commendable rate capability (780 mAh g^{-1} at a current density of 0.8 A g^{-1}). The amorphous region in partially crystalline Zn_2GeO_4 nanorods and the elastic graphene sheets helped accommodate volume changes during the charge and discharge processes (**Figure 12**). Sandwiched Zn_2GeO_4–graphene oxide nanocomposites with a specific capacity of 1150 mAh g^{-1} at 200 mA g^{-1} after 100 discharge/charge cycles was also reported by Zou et al.[218] The unusual electrochemical performance may be ascribed to the synergetic chemical coupling effect between Zn_2GeO_4 and graphene oxide. Lithium cyclability of chestnut-like $Cd_2Ge_2O_6$/rGO nanocomposites synthesized via the hydrothermal method produced a capacity of 943 mAh g^{-1} for the first cycle and a capacity retention of 721 mAh g^{-1} even after 100 cycles.[219] Graphene nanosheets/$PbGeO_3$ composites synthesized via an in situ hydrothermal method delivered a discharge capacity of 607 mAh g^{-1} at 100 mA g^{-1} after 50 cycles.[220] Fe_2GeO_4 nanoparticles(NPs)/rGO hybrids afforded a high reversible capacity of 980 mAh g^{-1} at 0.4 A g^{-1} for 175 cycles.[221] However, the use of lead and cadmium in battery applications is less encouraged for safety reasons associated with heavy metal toxicity.

Additional investigations have centered on a freeze-drying method for making GeO_2–rGO with a high specific capacity (1200 mAh g^{-1} at 100 mA g^{-1}).[222] In general, germanium compounds, for example $CuGeO_3$, adopt a conversion and alloying process during lithium cycling as follows:

$$\text{Conversion reaction}: CuGeO_3 + 6Li^+ + 6e^- \rightarrow Cu + Ge + 3Li_2O \quad (11)$$

$$\text{Alloying reaction}: Ge + xLi^+ + xe^- \leftrightarrow Li_xGe \quad (12)$$

Germanium compounds possesses high conductivity,[223] stable cycling capacity in LIBs, and have attracted greater attention as a result.

2.4.5. Spinel

In 2014, inverse spinel Zn_2SnO_4 nanoflower/GNS 3D structures (with a reversible capacity of 850 mAh g^{-1} after 10 cycles at a current density of 300 mA g^{-1})[224] and hollow Zn_2SnO_4 boxes wrapped with flexible graphene (with 678.2 mAh g^{-1} after 45 cycles at 300 mA g^{-1})[225] aroused great interest due to their high conductivity and low cost. The overall electrochemical reaction mechanism can be described in the following equations:

$$\text{Conversion reaction}: Zn_2SnO_4 + 8Li^+ + 8e^- \rightarrow 2Zn + Sn + 4Li_2O \quad (13)$$

$$\text{Alloying reaction}: Zn + Sn + 5.4Li^+ + 5.4e^- \leftrightarrow Li_{4.4}Sn + ZnLi \quad (14)$$

As a normal spinel, $ZnMn_2O_4$ nanorods wrapped by rGO, delivering a reversible capacity of 707 mAh g^{-1} at 100 mA g^{-1} over 50 cycles and a rate capability of 440 mAh g^{-1} at 2 A g^{-1}, was recently reported by Zheng et al.[226] Another high reversible capacity of ≈650 mAh g^{-1} over 1500 cycles at 2A g^{-1} was recently gained for $ZnMn_2O_4$ graphene nanosheets whose cycle occurs by the following equations.[227]

$$ZnMn_2O_4 + 4Li^+ \rightarrow ZnO + 2MnO + 2Li_2O \quad (15)$$

$$ZnO + MnO + 5Li^+ + 5e^- \leftrightarrow ZnLi + 2Mn + 2Li_2O \quad (16)$$

2.5. Anodes Based on Conversion (Redox) Reaction

2.5.1. Spinel Structure

Mn_3O_4: Mn_3O_4 is found in nature as the mineral Hausmannite, and has a spinel structure, where the oxide ions are arranged in a cubic close-packed lattice and the Mn^{II} occupy tetrahedral sites and the Mn^{III} octahedral sites. The structure is distorted due to a Jahn-Teller effect. Mn_3O_4 experiences a conversion mechanism during lithium cycling as described below:

$$\text{Conversion reaction}: Mn_3O_4 + 8Li^+ + 8e^- \leftrightarrow 3Mn + 4Li_2O \quad (17)$$

Pasero et al.[228] reported pristine Mn_3O_4 showing a reversible and constant capacity of ≈250 mAh g^{-1} up to 10 cycles. In another work, cobalt-doped Mn_3O_4 surprisingly offered an

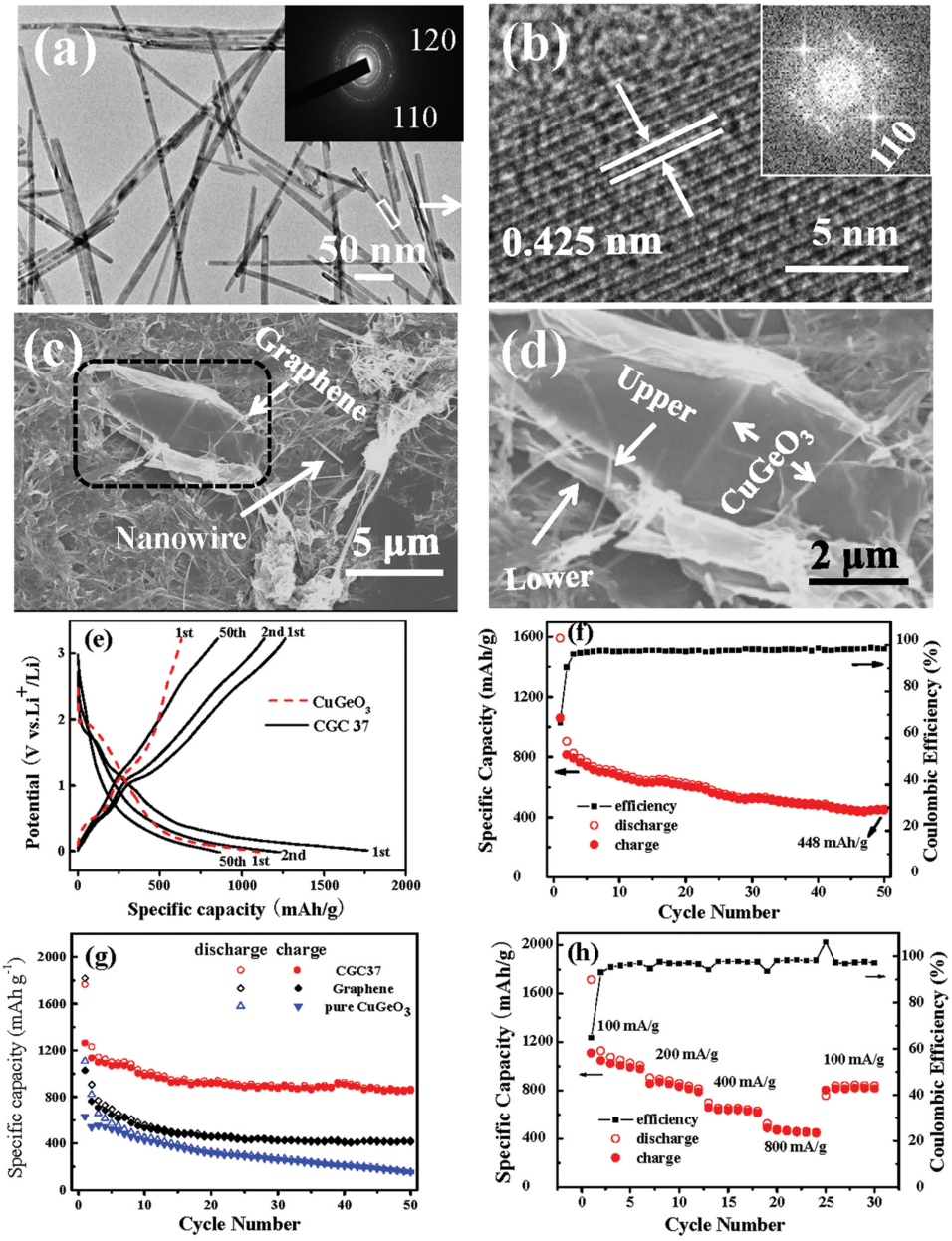

Figure 11. a) TEM image and b) HRTEM images of pure $CuGeO_3$ nanowires; the SAED pattern of (a) and the corresponding FFT pattern of (b) are shown as insets in (a) and (b), respectively. c) SEM image of CGC 37 (CGC: $CuGeO_3$/graphene composite) and d) the close-up of the black-box region in (c); the upper and lower layers of curved graphene sheet are labeled with "upper" and "lower" in (d). e) Galvanostatic charge/discharge profiles of CGC 37 at the first, second, and fiftieth cycles, and of pure crystalline $CuGeO_3$ nanowires at the first cycle under a current density of 200 mA g^{-1}. f) Cycling performances of pure crystalline $CuGeO_3$ nanowires, graphene and CGC 37 under current density of 200 mA $g^{-1}$for 50 cycles. g) Cycling performances of CGC 37 at a current density of 400 mAg^{-1} for 50 cycles. h) Rate performances of CGC 37 at different current densities. Reproduced with permission.[215] Copyright 2014, Royal Chemical Society.

enhanced constant capacity of ≈400 mAh g^{-1} in the voltage range 0.25–3.5 V at 0.2 C (1 Li per 5 h). However, such a low cycle performance is not satisfactory. As a consequence, carbon-coated Mn_3O_4,[229] Mn_3O_4/carbon nanotubes,[230] and Mn_3O_4 nanoparticle/graphene composites[231] have been prepared to potentially augment the electrochemical properties of Mn_3O_4.

Similar lithium cycling behavior of Mn_3O_4–graphene hybrids has been observed by several groups and found to be consistent. This suggests the hybrid materials possess reliable electrochemical properties which are not sensitive to processing considerations. However, the properties of neat or simple hybrids based on Mn_3O_4 are not sufficient. Several examples of spinel–graphene anode materials are subsequently addressed.

In 2010, Wang et al.[232] observed a stable capacity of ≈810 mAh g^{-1} (based on the composite) for the first five cycles at a current density of 40 mA g^{-1}. Good C-rate capability

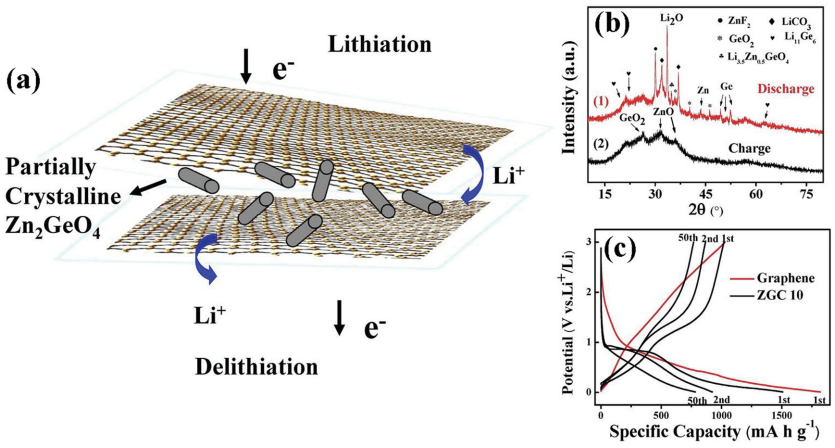

Figure 12. a) Scheme of lithiation/delithiation of composites. b) X-ray diffraction patterns of ZGC10 electrode after the 1st cycle of charge at 3 V and discharge at 0.01 V. c) Galvanostatic charge–discharge profiles of ZGC10 cycled at first, second, and fiftieth cycles at a current density of 200 mA g^{-1}. Reproduced with permission.[217] Copyright 2014, American Chemical Society.

and cycling stability was also observable, i.e., a capacity of ≈730 mAh g^{-1} at 400 mA g^{-1} after 40 cycles at various C-rates. Lavoie et al.[233] reported lithium cycling performances for Mn_3O_4/graphene composites with gravimetric capacities of ≈700 mAh g^{-1} and cycling stabilities of >100 cycles. More recently, Park et al.[234] presented a hydrothermal Mn_3O_4/N-doped graphene composite with a reversible capacity of 703 mAh g^{-1} at 200 mA g^{-1} after 40 cycles and rate capability of ≈400 mAh g^{-1} at 2.0 A g^{-1}.

Notably, free-standing N-doped graphene nanosheet/mesoporous Mn_3O_4 paper electrodes were synthesized via vacuum filtration, offering a high electrical conductivity (5.4 S cm^{-1}) and a reversible capacity of 740 mAh g^{-1} at 100 mA g^{-1}[235]

Co_3O_4: Co_3O_4 adopts the normal spinel structure, with Co^{2+} ions in tetrahedral interstices and Co^{3+} ions in the octahedral interstices of the cubic close-packed lattice of oxide anions. Co_3O_4 is also considered for anode materials in LIBs due to the satisfactory reversible capacity (about 710 ± 5 mAh g^{-1} at 600 mA g^{-1}). Typically this material is produced via molten salt synthesis[236] or electrospray pyrolysis.[237] Graphene/Co_3O_4 composites possess enhanced performance because of the combination of the advantages of Co_3O_4 nanoparticles and graphene.

Co-precipitation followed by calcination is a typical route to graphene/Co_3O_4 composites.[238,239] Under low current densities of 40–100 mA g^{-1}, the Co_3O_4/graphene composites produced via co-precipitation offer capacities as high as 935 mAh g^{-1} at 50 mA g^{-1} after 30 cycles,[238] 860 mAh g^{-1} at 40 mA g^{-1} after 120 cycles,[240] and 910 mAh g^{-1} over 100 cycles at 100 mA g^{-1} for Co_3O_4/NMEG hybrids (**Figure 13**).[241] However, the capacities reduce to 673 mAh g^{-1} over 100 cycles at 180 mA g^{-1}[242] and 400 mA h g^{-1} at 1000 mA g^{-1}.[240] The same goal of high capacity retention at high current density for large cycle numbers remains a challenge for this particular material class and synthesis technique.

Another potentially more effective approach is that of solvothermal reactions. This process has been recently utilized to synthesize mesoporous Co_3O_4@graphene nanostructures.[243,244] A Co_3O_4 (core) and graphene (shell) structure delivered a reversible capacity of 1076 mAh g^{-1} at 0.1 A g^{-1} and a reversible capacity over 600 mAh g^{-1} after 500 cycles at 1.0 A g^{-1} (**Figure 14**).[244] Hydrothermal methods are also a frequently utilized route to graphene-containing Co_3O_4,[245] such as Co_3O_4–GNs, offering a reversible capacity of 657 mAh g^{-1} after 100 cycles at 50 mA g^{-1}[246] and Co_3O_4 nanowire/graphene nanosheet possessing a reversible capacity of 906.6 mAh g^{-1} at 0.1 C rate and high cycle retention.[247]

Recently, mesoporous Co_3O_4 nanosheet–3D graphene hybrid materials, produced through a combination of CVD and hydrothermal method,[248] delivered a capacity of 630 mAh g^{-1} after 50 cycles at a rate of 0.2 C. In a more recent study,[249] Co_3O_4/ graphene aerogel, synthesized via a hydrothermal process followed by freeze-drying and a further heat treatment, offered a reversible capacity of 832 mAh g^{-1} after 200 cycles at 1000 mA g^{-1}. It is interesting to note that 3D materials seem to reach much higher performance measures when compared to their 2D counterparts.

Notably, various other promising chemical approaches including co-electrodeposition,[250] direct electrospray deposition,[251] thermal decomposition for mesoporous Co_3O_4 nanoparticles on graphene,[252] and microwave irradiation followed by heat treatment[253] have also been developed. As exhibited above, chemical reactions are crucial ways to produce Co_3O_4–graphene composites. In the following sections, physical routes to anode synthesis are addressed.

Sun et al.[254] reported a 3D hierarchical double porous Co_3O_4/graphene architecture via a so-called "dipping and drying" process for LIBs. Park et al.[255] demonstrated that the Co_3O_4 powders (<50 nm) mixed and wrapped by 10.5 μm^2 defect-free graphene has a capacity of 1050 $mAhg^{-1}$ at 500 mA g^{-1}, and a cycling stability of 900 mAh g^{-1} at 1 A g^{-1} after 200 cycles. Interestingly, Co_3O_4 quantum dot/graphene composites produced via a microwave irradiation method, showed a significantly enhanced cycling performance (1785 mAh g^{-1} at 0.1 C after 90 cycles).[256]

Quite intriguingly, vacuum filtration offers a facile strategy to flexible graphene-containing films. Take two recent examples: 1) 3D Co_3O_4/graphene composite films via replication and filtration processes were reported by Choi. et al.[257] The film possessed a rate capability of 71% retention at 1 A g^{-1} and a cycling performance with 90.6% retention during 50 cycles; and 2) free-standing and binder-free Co_3O_4/graphene films (cyclic stability of 1200 mAh g^{-1} at 200 mA g^{-1} after 100 cycles) were fabricated through a vacuum filtration and thermal treatment processes.[258] These processes are simple and easily scaled up making them attractive for industry. Vacuum filtration, in particular, naturally lends itself to the production of large-area films, which is a challenge for many other approaches.

Clearly, Co_3O_4/graphene composites possess a high reversible capacity up to 900–1000 mAh g^{-1} at 100 mA g^{-1} after

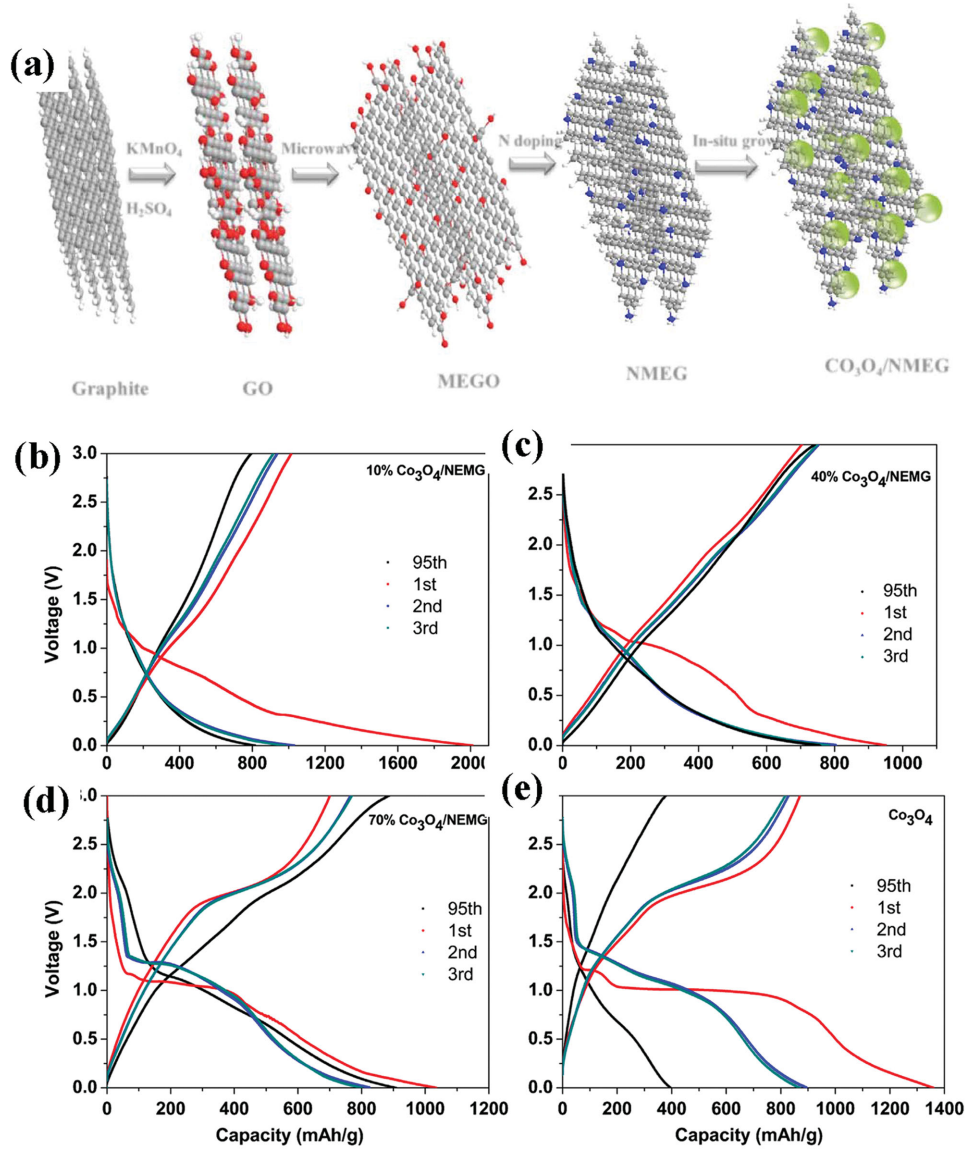

Figure 13. a) Schematic illustration of the preparation of Co_3O_4/NMEG composite. Typical charge–discharge curves of b–d) Co_3O_4/NMEG and e) Co_3O_4 cycled at the first, second, third, and 95th cycles between 0.01 V and 3.00 V. Reproduced with permission.[241] Copyright 2014, Elsevier.

30–120 cycles, and high rate performance (900 mAh g^{-1} at 1 A g^{-1} after 200 cycles).[254] The novel 3D structure design and flexible Co_3O_4/graphene electrode are a promising research area for future development at low cost.

Fe_3O_4: Fe_3O_4 occurs in nature as the mineral magnetite, and adopts an inverse spinel structure. It will be of great interest as an anode material in LIBs due to its high theoretical capacity value (928 mAh g^{-1}), low cost, and environmentally friendly nature. In 2006, Tarascon's group[259] found that nanostructured Fe_3O_4 rods and films grown on Cu substrates by electrodeposition possessed good lithium cyclability. As a typical carbon-based composite, Fe_3O_4/C core-shell nanorods produced by a hydrothermal method possessed an initial lithium storage capacity of 1120 mAh g^{-1} and a reversible capacity of 394 mAh g^{-1} after 100 cycles.[260]

- a) Hydrothermal process: In 2014, a hydrothermal approach for making Fe_3O_4/graphene nanocomposites drew much attention.[261] The rGO/66.7-wt% Fe_3O_4 composite afforded a stable capacity of 630 mAh g^{-1} at 100 mA g^{-1} for up to 200 cycles in the voltage range of 0.001–3.0 V.[262] Li et al.[263] showed that Fe_3O_4/GNSs nanocomposites, produced by hydrothermal treatment and calcination, exhibited a reversible capacity of 740 mAh g^{-1} after 100 cycles at 100 mA g^{-1}. In another study, Zhao et al.[264] reported that hydrothermally synthesized Fe_3O_4 nanoparticle/graphene oxide sheets delivered an improved discharge cycling performance of 1010 mAh g^{-1} over 50 cycles at 0.1 C. (**Figure 15**) In an analogous process, a solvothermal reaction was also discussed by Fu et al.[265] and Wang et al.,[266] and a reversible specific capacity of more than 963 mAh g^{-1}

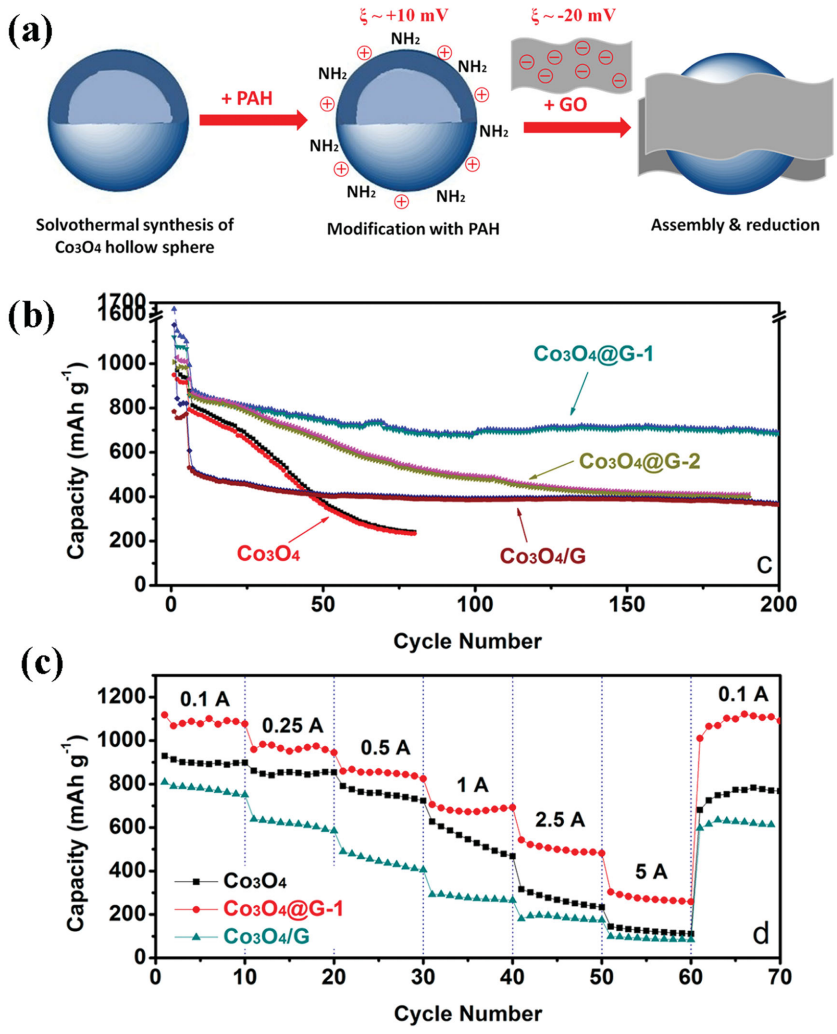

Figure 14. a) Scheme of the fabrication process of Co_3O_4@G core–shell composites. b) Comparison of the cycling performance of Co_3O_4, Co_3O_4@G-1, Co_3O_4@G-2 hybrid electrodes, and Co_3O_4/G mixture as the control sample at a current density of 1.0 A g^{-1}. c) Rate capability of the Co_3O_4, Co_3O_4@G-1, and Co_3O_4/G electrodes at various current densities between 0.1 and 5.0 A g^{-1}. Reproduced with permission.[244] Copyright 2014, American Chemical Society.

after 100 cycles at 100 mA g^{-1} was obtained in magnetite–graphene anode materials.[265]

- b) Self-assembly process: As noted above, self-assembly is a viable route to structured graphene-containing nanomaterials. This is no exception for Fe_3O_4 nanoparticles.[267] In 2011, Chen et al.[268] reported graphene-encapsulated ordered aggregates of Fe_3O_4 nanoparticles (30–50 nm) by a simple self-assembly process. The composite particles displayed a specific capacity of 832 mA h g^{-1} at 100 mA g^{-1} after 90 cycles. Subsequently, the rational design of graphene/Fe_3O_4 composites has led to stable reversible capacities of ≈1000–1200 mAh g^{-1} after ≈50–100 cycles at ≈100–200 mA g^{-1}. Highlights of this research are subsequently discussed. 3D architectures of N-doped graphene (N-G)/Fe_3O_4 (≈30–50 nm) composites were formed through the strong interaction between self-assembled N-G networks and Fe_3O_4 nanoparticles.[269] Lithium cyclability of this hybrid structure was 1037 mAh g^{-1} which then stabilized at 1014 mAh g^{-1} at 100 mA g^{-1} in the voltage range of 0.001–3 V vs. Li^+/Li for up to 50 cycles. The interconnected N-G sheets can effectively prevent the Fe_3O_4 nanoparticles from aggregating during cycling and further acted as a buffer matrix to accommodate the inherent volume change of Fe_3O_4. This helped maintain the structural integrity and electrochemical stabilization of the resulting composite electrodes. A self-assembled graphene-wrapped Fe_3O_4 hollow nanosphere material possessing cycling stability and a high discharge capacity of 1148 mAh g^{-1} through 50 cycles was developed by Jin et al.[270] Another self-assembled hierarchical Fe_3O_4 microsphere/graphene nanosheet composite, exhibiting a reversible capacity of 940.4 mAh g^{-1} at 500 mA g^{-1} after 70 cycles and a specific capacity of 745 mAh g^{-1} at 3 A g^{-1}, was recently reported by Wang et al.[266]
- c) Others: Various wet chemical processes have been used to produce Fe_3O_4-graphene composites. Deosarkar et al.[271] reported Fe_3O_4 nanoparticles (20 nm) loaded on graphene nanosheets by ultrasound assisted co-precipitation for use in anode materials in LIBs. Hydrolysis followed by heat treatment was also successfully applied for this material as well.[272,273] In 2010, Zhou et al.[272] reported that graphene nanosheet/Fe_3O_4 nanocubic (≈200 nm) composites demonstrated a capacity of 580 mAh g^{-1} at 700 mA g^{-1} after 100 cycles as cycled in 0.0–3.0 V. In particular, 3D flexible nanoarchitectures of a transition metal oxide (Fe_3O_4, Co_3O_4, NiO) loaded into nanoporous graphene papers through a general wet-immersion method were also observed by Huang et al.[274] The nanoporous Fe_3O_4-graphene composites could deliver a reversible specific capacity of 1428 mAh g^{-1} at 1 A g^{-1}.

To date, several other interesting novel routes are worth mentioning. These include a microwave assisted non-aqueous sol–gel approach by Yu et al.,[275] a stepwise hetero-coagulation method for graphene-encapsulated CMK-3-metal oxides (Fe_3O_4 and NiO)(CMK: carbon mesostructured by korea) by Tao et al.,[276] a microwave assisted combustion route to Fe_3O_4–rGO by Bhuvaneswari et al.,[277] solid-state reaction for FeO_x–graphene by Jiang et al.,[278] gas/liquid interface reaction for Fe_3O_4–22.7 wt% graphene nanocomposites (exhibiting a reversible capacity of 1048 mAh g^{-1} at the 90th cycle) by Lian et al.,[279] thermal decomposition followed by heat treatment to Fe_3O_4@GN-CE-20 (GN: graphene nanosheet; CE: CO_2-expanded ethanol) composite (displaying a reversible capacity of ≈800 mAh g^{-1} at 1 A g^{-1} after 100 cycles) by Zhuo,[280] and mesoporous Fe_3O_4 nanorods/rGO via low temperature plasma.[281] The understanding and degree of general applicability of these more recent techniques is still yet to be established. More work in these areas is necessary before any conclusions can be made.

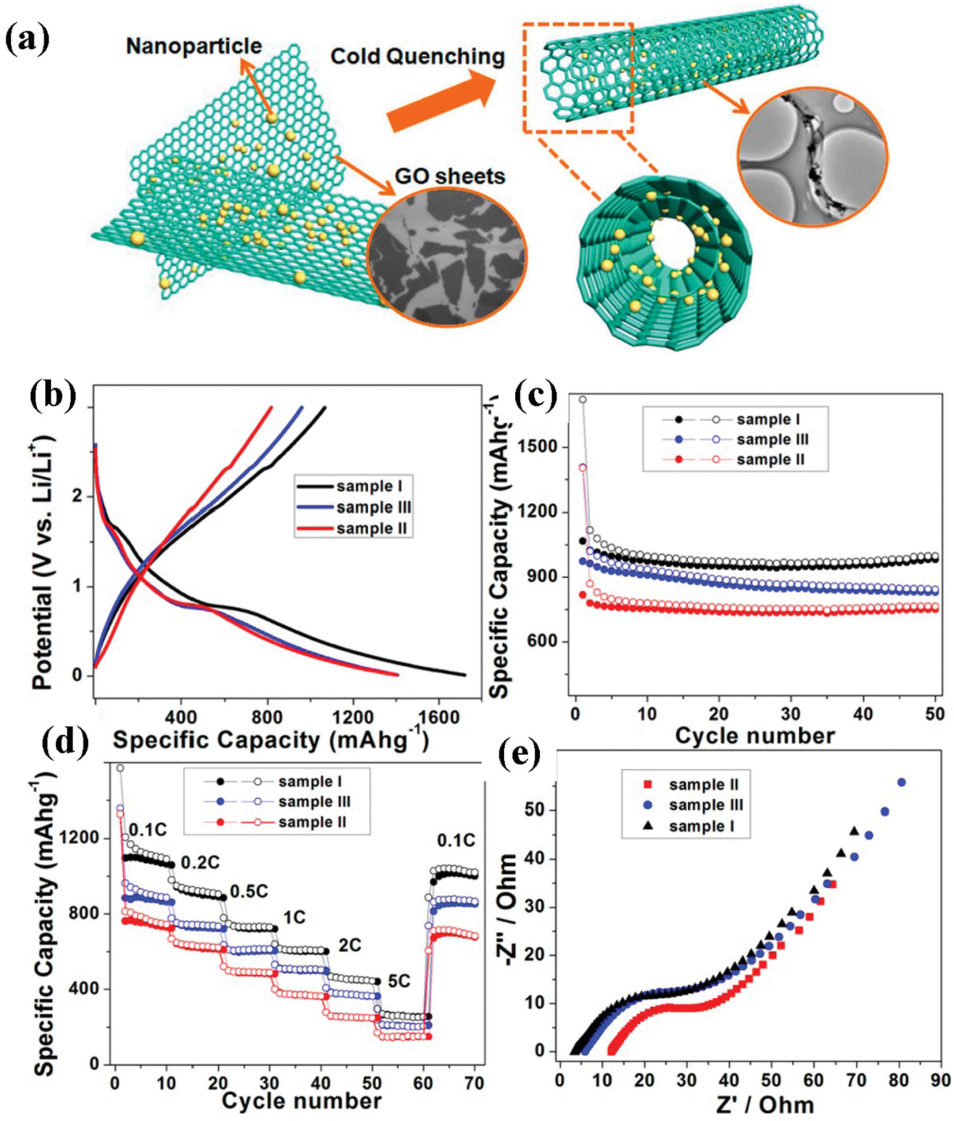

Figure 15. a) Schematic diagram of synthetic route to Fe_3O_4@GNSs composite. Electrochemical properties of sample I, sample II, and sample III; b) the first charge/discharge profiles. c) Cyclic stability test at 0.1 C. d) Rate capability from 0.1 to 5 C for 10 cycles. e) EIS (electrochemical impedance spectroscopy) presented as Nyquist plots. Reproduced with permission.[264] Copyright 2014, American Chemical Society.

Fe_3O_4/graphene nanocomposite possesses several advantages such as low-cost, abundant resources, facile synthesis routes, and high reversible capacity as anode materials in LIBs. The capacity and safety under extremely high rates need to be further verified to meet the requirements of practical battery applications in the future. It is also interesting to note the range of length scales of functional materials that can be used. Systems involving particles as small as several tens of nanometers up to planar structures of several microns have demonstrated good performance properties. Furthermore, hybrid systems involving mixed nano and micro scale elements have been presented. This underscores that nano isn't always better and that hierarchical systems of rational design can and do possess superior performance characteristics.

AB_2O_4 Spinels (A = Co, Ni, Mn, Sn; B = Fe, Co, Zn; A≠B):As a typical inverse spinel, the electrochemical reaction of $CoFe_2O_4$ during lithium cycling is described below:

$$CoFe_2O_4 + 8Li^+ + 8e^- \rightarrow Co + 2Fe + 4Li_2O \quad (18)$$

$$Co + 2Fe + 4Li_2O \leftrightarrow CoO + Fe_2O_3 + 8Li + 8e^- \quad (19)$$

Solvothermal processes are practical ways to produce $CoFe_2O_4$/rGO hybrids.[282,283] The porous $CoFe_2O_4$/rGO hybrids delivered an impressive reversible capacity of 1040 mAh g^{-1} at 91.4 mA g^{-1}.

In situ solvothermally sandwiched $CoFe_2O_4$/graphene sheet nanocomposites demonstrated a capacity of 1047 mAh g^{-1}

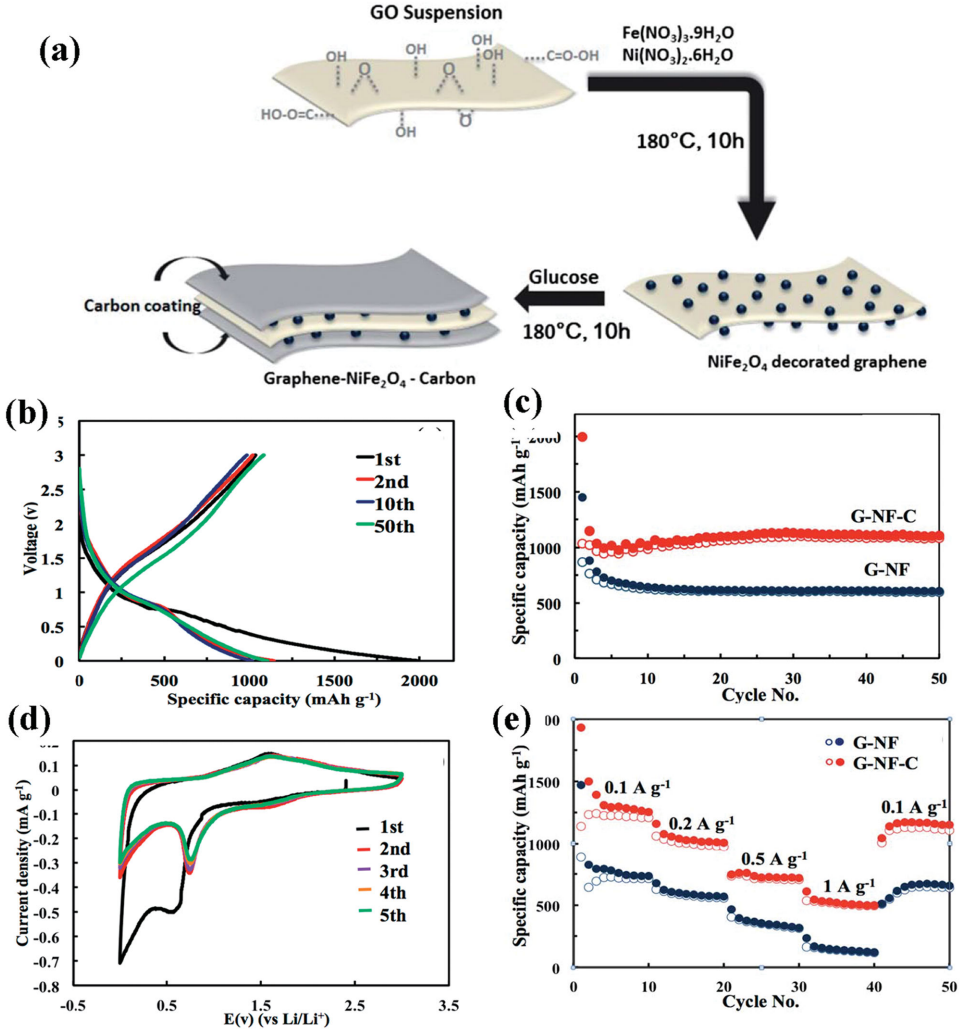

Figure 16. a) Schematic illustration of the synthesis procedure for graphene–$NiFe_2O_4$–carbon (G–NF–C) nanocomposites with a sandwich structure. b) Charge/discharge profiles of G–NF–C at 0.1 A g^{-1}. c) Cyclic performance of G–NF and G–NF–C electrodes at 0.1 A g^{-1}. d) Cyclic voltammetry curves of G–NF–C in the voltage window of 0.01–3.00 V and scanned at 0.001 mV s^{-1}. e) Rate performance of G–NF and G–NF–C electrodes at current densities in the range 0.1–1.0 A g^{-1}. Reproduced with permission.[286] Copyright 2014, Royal Chemical Society.

at 200 mA g^{-1} after 160 cycles. Even at 800 mA g^{-1}, a charge capacity of 565 mAh g^{-1} was measured after 300 cycles.[283] In a related study, Li et al.[284] reported $CoFe_2O_4$/GN nanocomposites self-assembled into a 3D network architecture which showed a high specific reversible capacity up to 651 mAh g^{-1} at 1 A g^{-1} for 50 cycles. Another promising result was observed in binder-free hierarchical $CoFe_2O_4$@graphene hybrid films,[285] measuring 866 mAh g^{-1} at 1 A g^{-1} after 125 cycles.

As in all previous examples, variety in anode materials comes not only from elemental composition but also morphology and spatial arrangement. Sandwich-structured inverse spinel $NiFe_2O_4$/graphene/carbon nanocomposites made by hydrothermal growth were explored by Heidari et al.[286] The composite presented a cycle stability of 1195 mAh g^{-1} after 200 cycles at 500 mA g^{-1} (**Figure 16**). In another work, polydopamine (PDA) functionalized graphene/$NiFe_2O_4$, produced through an in situ ultrasonic method, afforded a reversible capacity up to 947 mAh g^{-1} and improved rate capability.[287]

Inverse spinel $CuFe_2O_4$ has also attracted much attention for energy conversion, including Delafossite $CuFeO_2$ hexagonal platelet/graphene composites,[288] and $CuFe_2O_4$/graphene composites.[289,290] The latter delivered a capacity of 672 mAh g^{-1} after 200 cycles at 1 A g^{-1}.[289]

In a recent report by Chen et al.,[291] graphene-containing inverse $NiCo_2O_4$ nanosheet arrays possessed improved lithium storage properties (**Figure 17**) with reversible capacities up to 806 mAh g^{-1} after 85 cycles at various current densities.[292] In another interesting report, rGO/$NiCo_2O_4$ hierarchically porous films produced via citrate-assisted growth demonstrated reversible capacities of 954.3 mAh g^{-1} and 656.5 mAh g^{-1} over 50 cycles at 200 mA g^{-1} and 500 mA g^{-1}, respectively.[293] In addition, porous $CuCo_2O_4$ nanocubes wrapped by rGO sheets, offering a stable capacity of 570 mAh g^{-1} at 1 A g^{-1} after 350 cycles, were also produced.[294] These examples underscore the range of structures possible for only one inverse spinel material as well as the range of performance characteristics and

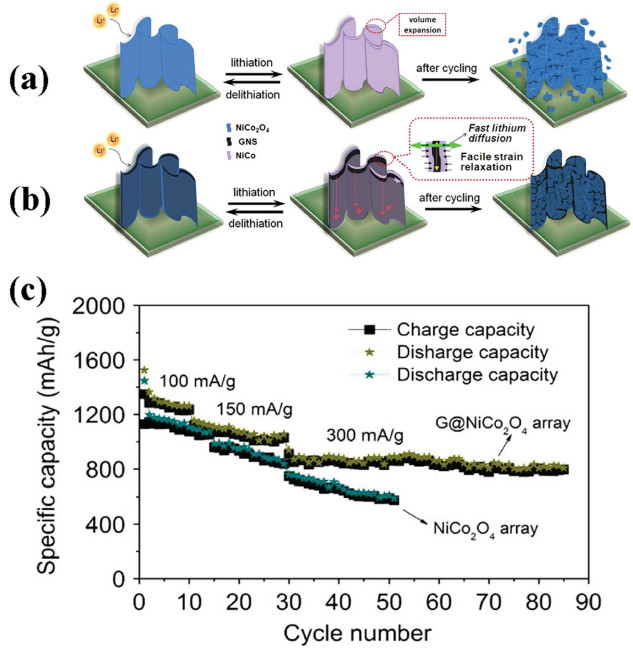

Figure 17. The deduction of electrochemical reaction of a) pure $NiCo_2O_4$ arrays and b) $NiCo_2O_4$/graphene arrays during Li-cycling. c) The cycling performance of $NiCo_2O_4$ and $NiCo_2O_4$/graphene nanosheet arrays at different current density. Reproduced with permission.[291] Copyright 2014, Elsevier.

processing options. In addition to normal and inverse spinel structures, there exist structures intermediate to these two extremes.

MFe_2O_4 (M = Mn, Mg) belongs to the partially inverse spinel structure.[295–297] In pure spinel structures, the divalent and trivalent cations are situated only in tetrahedral and octahedral sites respectively. The opposite is true for pure inverse spinel structures. Hence, a partially inverse spinel is essentially a mix of divalent and trivalent metal cations in both tetrahedral and octahedral sites. $MnFe_2O_4$–rGO nanocomposites were investigated,[297] producing a reversible capacity of 1017 mAh g^{-1} at 0.1 A g^{-1} after 90 cycles. Intriguingly, $MgFe_2O_4$/graphene nanocomposites produced by urea-assisted auto-combustion were also reported by Rai et al.[298] The results showed a reversible charge capacity of 764.4 mAh g^{-1} at 0.04 C over 60 cycles. The lithium cycling of $MgFe_2O_4$ during charging and discharging is proposed as below:[295]

$$MgFe_2O_4 + 6Li^+ + 6e^- \rightarrow MgO + 2Fe + 3Li_2O \quad (20)$$

$$Fe + Li_2O \leftrightarrow FeO + 2Li^+ + 2e^- \quad (21)$$

As noted above, AB_2O_4 spinel offers a similar lithium storage capability with the spinel M_3O_4 (M = Co, Fe, Mn) because they share the same lithium cyclability mechanism. However, the AB_2O_4 structure provides more pathways to change the elemental composition and crystal properties. This greater variability affords more options for application in LIBs.

Among the many spinels compositions, the ferro-based spinel/graphene group is a very promising candidate for anode materials in LIBs due to their low-cost, environmentally friendly nature, and high, stable reversible capacity. Furthermore, hydrothermal methods allow for the production of such nanomaterials on the large scale. These two points make large capacity graphene-containing spinel materials promising candidates for energy storage devices in both rigid and flexible forms. The advantage of inorganic crystalline structures is that there are an unlimited number of elemental combinations and the resulting crystal structures to be investigated for such devices. One of the most commonly encountered types is the aptly named "rock salt" group. Table salt is one such example of a metal chloride rock salt structure; however, many other combinations exist including metal-monoxide structures.

2.5.2. Rock Salt Structure (MO; M = Mn, Fe, Co, Ni, or Cu):

As monoxides, MO (M = Mn, Fe, Co, Ni, or Cu) adopt the rock salt structure, in which cations and anions are both octahedrally coordinated. In general, MO are often nonstoichiometric, and exhibit antiferromagnetic properties below the Néel temperature. Lithium cyclability of rock salts MO through the following conversion reaction was originally reported by Poizot et al.:[299]

$$MO + 2Li^+ + 2e^- \leftrightarrow M + Li_2O \quad (22)$$

Many studies have been devoted to material cataloguing for further insight into the generalizability of graphene-containing MO. Consequently they have become the focal point of research in recent years. Herein, several different representative metal oxides are described in detail.

CoO: CoO/rGO hydrides offer excellent lithium cyclability as reported by various groups. For example, the lithium cycling properties of CoO/rGO demonstrated a capacity of 732 mAh g^{-1} after 100 cycles at a 150 mA g^{-1} discharge current density.[242] A similar result was observed by Zhang et al.[300,301] with discharge capacities of 760 and 690 mAh g^{-1} after 252 and 352 cycles, respectively. In a related study, 1170 mAh g^{-1} at 150 mA g^{-1} and a 94% retention after 60 cycles was observed in hollow hierarchical CoO nanocube/rGO(COG) composites via a sacrificial-template method and subsequent thermal treatment.[302]

MnO: MnO possesses a theoretical capacity of 755 mAh g^{-1}. MnO/graphene nanosheet (MnO/GNS) hybrid materials have been synthesized by various approaches. The stable and reliable lithium cycling properties of MnO/GNS were also confirmed in several separate reports.[303,304] In early work, a reversible capacity of 635 mAh g^{-1} at 0.2 C in the voltage range between 0.01–3.5 V and a superior rate capability of 410 mAh g^{-1} at 5 C for MnO nanocrystal/GNS composites were explored by Hsieh et al.[303] The fact that early studies have already achieved such a high percentage of theoretical capacity is impressive.

Subsequently, performances approaching near-theoretical capacity (≈770–780 mAh g^{-1}) with good rate performance were achieved in MnO/GNS hybrids via various synthesis strategies. Several representative examples are discussed. N-doped MnO synthesized via a hydrothermal method delivered a reversible capacity of 772 mAh g^{-1} at 100 mA g^{-1} after 90 cycles, and a rate capability of 202 mAh g^{-1} at 5 A g^{-1}.[305] Lithium cycling

performance of a MnO nanoparticle/graphene composite synthesized via in situ carbo-thermal reduction exhibited a capacity of 460 mAh g^{-1} after 180 cycles at 1000 mA g^{-1}.[306] More recently, MnO/rGO was synthesized via spray pyrolysis and had discharge capacities of 1313 mAh g^{-1} after 130 cycles at 500 mA g^{-1}.[307]

NiO and NiS: Lithium cyclability of NiO via the conversion reaction was first realized by Poizot et al.,[299] who reported an initial reversible capacity of 600 mAh g^{-1} which slowly degraded to 200 mAh g^{-1} after 50 cycles. Much effort has been devoted to improving the capacity and reliability of NiO/Graphene nanosheets (GNS) as anode materials. As is the case for a lot of inorganic–graphene composites, several different simple and inexpensive preparation techniques exist.

Hydrothermal methods present a good strategy to NiO NS/graphene composites. The multilayer structure was formed through oxygen bridges originating from the pinning effect between hydroxyl/epoxy groups in graphene and the Ni atoms of NiO.[308] In earlier work, a low reversible capacity of 450 mAh g^{-1} at 300 mA g^{-1} after 100 cycles was reported for in situ formed NiO/grapheme synthesized via a solvo-hydrothermal approach.[309] Simultaneously, slightly higher capacities of 780 mAh g^{-1} at 0.1 C after 50 cycles[310] and 883 mAh g^{-1} at 50 mA g^{-1} after 50 cycles[308] were noted for NiO nanosheets/graphene via various synthesis strategies. More recently, these efforts have translated to higher reversible capacities of 1098 mAh g^{-1} at 100 mA g^{-1} after 50 cycles for a porous NiO nanosheets/graphene hierarchical structure[311] and a reversible capacity of 1031 mAh g^{-1} after 40 cycles at 0.1 C for hydrothermal NiO–graphene.[312]

Liquid phase deposition followed by annealing (i.e. spin coating and heating) has also been employed in NiO-graphene hybrid synthesis.[313–315] The rGO/NiO composites, produced by co-precipitation and annealing, delivered a discharge capacity of 1041 mAh g^{-1} after 50 cycles at 100 mA g^{-1}. More importantly, a good rate capacity of 727 mAh g^{-1} was available at 1600 mA g^{-1}.[315] However, lithium cycling performances reported by other groups have not been as promising. For example, a capacity of 646.1 mAh g^{-1} after 35 cycles at 100 mA g^{-1} for NiO-graphene hybrid,[313] and 700 mAh g^{-1} after 50 cycles at various current densities for NiO nanoplate–FGS nanocomposite by an in situ precipitation approach have been reported.[314] The possible reason for these observations is the different deposition agents and annealing processes.

Graphene-containing NiO nanomaterials with capacities of ≈1000 mAh g^{-1}, far more than the theoretical capacity of 717 mAh g^{-1}, have been reported by several groups. This first and foremost signifies that the mechanism of lithium storage is not yet fully understood for such materials. In particular, the concomitant effects, if any, of having the two materials together need to be better understood. Further insights into the mechanism are clearly required for this and many other types of materials. In addition to metal monoxides, metal monochalcogenides are of emerging interest. Quite intriguingly, NiS adopts the same mechanism as NiO for lithium cycling (Equation (23)). A sandwich-nanostructured NiS nanoflower/graphene afforded a reversible lithium-extraction capacity of 887 mAh g^{-1} after 60 cycles at 59 mA g^{-1}.[316] The cycling mechanism for metal monochalcogenides is provided below:

$$NiS + 2Li^+ + 2e^- \leftrightarrow Ni + Li_2S \quad (23)$$

CuO and ZnO: CuO and Cu_2O possess theoretical capacities of 674 mAh g^{-1} and 375 mAh g^{-1}, respectively. In an earlier study, reversible capacities of 743 mAh g^{-1} after 50 cycles at 50 mA g^{-1} were reported for hollow CuO nanoparticle/graphene (HNP/G) composites synthesized via the Kirkendall-effect approach.[317] One advantage of CuO-HNPs/G hybrids is a durable cycle life at high rates, with reported capacity retentions of 448 mAh g^{-1} after 300 cycles, as evaluated at 500 mA g^{-1}. Comparable performance characteristics have since been reported by other groups. For example, a low-temperature solution route was employed to produce shuttle, urchin-like, and fusiform CuO-GNS composites[318,319] A high capacity of 826 mAh g^{-1} was retained at 700 mA g^{-1}[319] and 532 mAh g^{-1} at 1400 mA g^{-1}[318] after 100 cycles for CuO–GNS. These reports underscore the morphology-dependency of performance and its equal importance to material composition in the overall properties of anode materials for batteries. In another instance, a hydrothermal method was similarly utilized to make high performance CuO/graphene nanocomposites.[320] After 50 cycles, the capacity of composites maintained at 692.5 mAh g^{-1} at 0.1 C rate (10 h per half cycle).

However, the presence of impurities, such as Cu_2O, may lead to a deterioration of lithium cycling performance,[321,322] with a lower discharge capacity of 423 mAh g^{-1} after 50 cycles at 67 mA g^{-1} for CuO/graphene composite,[321] and capacity 563 mAh g^{-1} after 100 cycles at 100 mA g^{-1} for CuO nanosheets/GNSs.[322] In addition to impurities, improper processing may also produce non-ideal results. For example, capacities of 600 mAh g^{-1} at 100 mA g^{-1} were reported for CuO nanoleaf/graphene sheets. As a representative example, a CuO–Cu_2O/graphene composite with the above two characteristics was synthesized by a microwave-assisted method. It possessed a reversible capacity of 487 mAh g^{-1} after 60 cycles at 200 mA g^{-1}.

Additional references, including but not limited to CuO/graphene composites with various morphologies produced via microwave-assisted method,[323] CVD[324] and electrophoresis deposition[325] have been reported. It is worth noting that a graphene/Si–CuO quantum dot layered structure produced via an electrophoresis deposition (EPD) technique, offering a specific capacity of 895 mAh g^{-1} at 1 C after 200 cycles, was recently reported by Rangasamy et al.[325] (**Figure 18**).

In addition, the lithium cyclability of the ZnO/graphene composites (with a stable capacity of 404 mAh g^{-1} after 100 cycles at 0.5 C) has been investigated.[326] Furthermore, complex graphene-encapsulated porous carbon–ZnO composites by Guo et al.[327] were recently reported.

Table 3 highlights the enhanced reversible capacity and excellent cyclability of MO/graphene when compared to bare MO. However, more attention should be directed to the controllable synthesis of rock salt MO (M = Mn, Fe, Co, Ni, or Cu) nanoparticles, particularly with uniform size and deliberate shape. In addition, many other d-block metals remain to be considered for such devices. Recent research on shape design and structuring of MO–graphene is certainly encouraging, but more work remains to be done in discovering different size effects and the ideal (if any) effective coupling between MO and graphene in such devices.

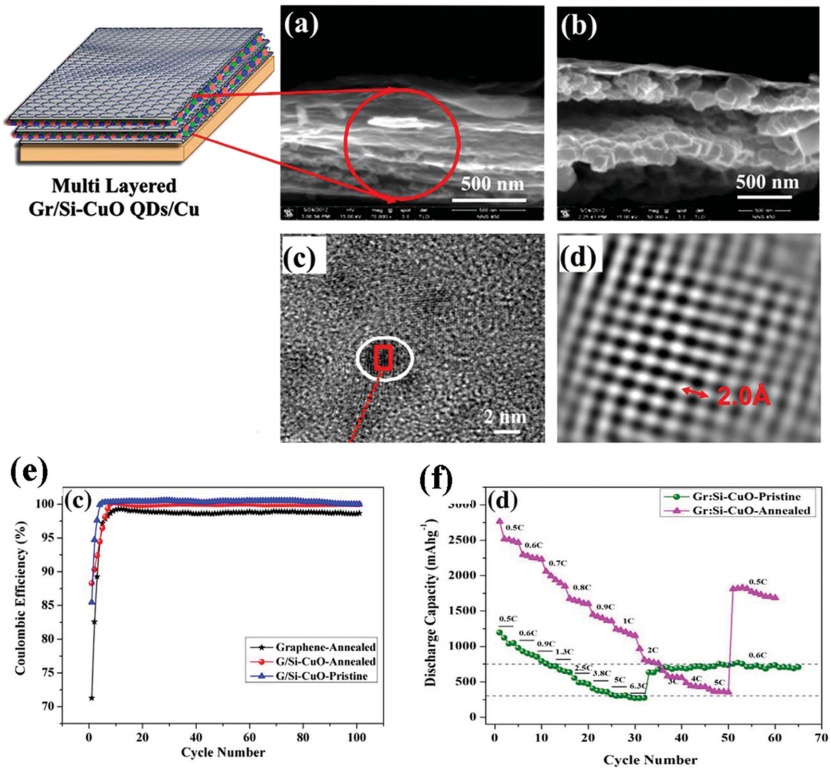

Figure 18. a) FESEM cross section image of Gr/Si–CuO QD (quantum dot) showing multi layered structure of Si–CuO QD embedded into the graphene layer (inset: Scheme of Gr/Si–CuO multi-layered structure). b) Cross section view of high magnified Gr/Si–CuO QD, which shows Si–CuO QD layer wrapped with graphene layer. c) HRTEM image showing the nano-crystalline QD. d) Filtered inverse FFT image obtained from white circle in (c). e) Coulombic efficiency as a function of cycle number for Gr/Si–CuO samples. f) C rate capability of as-prepared and annealed Gr/Si–CuO QD. Reproduced with permission.[325] Copyright 2014, Elsevier.

2.5.3. Corundum Structure (M_2O_3, M = Fe, Cr)

Known as hematite, the α-Fe_2O_3 possesses a hexagonal corundum structure. Owing to its high theoretical capacity (1005 mAh g^{-1}) and low cost, lithium cycling of Fe_2O_3 has been the focus of several studies.[330]

As has been the case for several other anode material synthesis techniques, the hydrothermal method is a simple route to Fe_2O_3-graphene nanocomposites.[331–335] To date, reversible capacities for hydrothermal Fe_2O_3/graphene hybrids of 1000 ± 50 mAh g^{-1} after 90–450 cycles at ≈100–200 mA g^{-1} have been reported. Zhao et al.[333] investigated nanorod-like Fe_2O_3/graphene nanocomposites, which presented a large reversible capacity of 1063.2 mAh g^{-1} at a charge/discharge rate of 0.1 C. High capacity retention Fe_2O_3-graphene nanocomposites synthesized via a hydrothermal method maintained a capacity of 1049 mAh g^{-1} after cycling at 200 mA g^{-1} for 450 cycles. The trend observed for previous research is to take simple doping approaches and expand them to include more complex doping, co-doping and morphologically complex material structures.[334] Recently, Wu et al.[335] investigated Fe@Fe_2O_3 core–shell nanoparticles anchored on graphene. This material possessed a reversible charge capacity of 959.3 mAh g^{-1} up to 90 cycles at 100 mA g^{-1}. In contrast, the lithium storage capacities of hydrothermal materials of the same kind were reported as 570 mAh g^{-1} after 20 cycles.[331] and 582 mAh g^{-1} after 100 cycles at 1000 mA g^{-1}.[332]

Recently, the electrochemical performance of Fe_2O_3–graphene synthesized via a wet chemical process was also investigated. As reported by Zhu et al,[336] a reversible specific capacity of 883 mAh g^{-1} after 100 cycles at 1 A g^{-1} was observed in 10% Fe_2O_3–nanomesh graphene (NMG) composites by an adsorption precipitation process (**Figure 19**). Fe_2O_3/graphene nanocomposites, obtained via precipitation followed by thermal decomposition method, delivered a delithiation capacity of ≈900 mAh g^{-1} at 100 mA g^{-1} for up to 50 cycles, and a rate capability of 500 mAh g^{-1} at 5 A g^{-1}.[337] Flexible Fe_2O_3@SnO_2/graphene films were synthesized via vacuum filtration followed by thermal reduction. This material exhibited an excellent cycling performance of 1015 mAh g^{-1} at 100 mA g^{-1} even after 200 cycles.[338] Such material properties are very encouraging from an easily processable and low-cost material.

Lithium cyclability of nonstoichiometric hollow and yolk–shell iron oxide (FeO_x), sandwiched between few-layer graphene (FLG) sheets via chemical precipitation followed by heat treatment, was also explored. Rather low reversible specific capacities of ≈335 mAh g^{-1} after 120 cycles at 1 A g^{-1} in the voltage range of 0.1–3.0 V were reported. This is included to underscore that morphologically complex materials are not necessarily better performing. Many factors, not all of which are well understood or even known, contribute to the ultimate performance and consistency of performance of such devices.

CVD was likewise employed to produce Fe_2O_3@graphene.[339] It was reported that conductive-additive-free Fe_2O_3@C@graphene showed a reversible specific capacity of 864 mAh g^{-1} after 100 cycles at 100 mA g^{-1}. In other literature,[340] a specific capacity of ≈1118 mAh g^{-1} at a discharge current density of ≈0.17 C with 88% retention after 100 cycles was reported for a heterogeneous Fe_2O_3/Fe_3C–graphene via CVD (**Figure 20**). Other investigations into the lithium cyclability of Fe_2O_3/graphene composites were also tackled by Zhang et al.,[341] Chen et al.,[342] and Tian et al.[343]

In one interesting study, Lin et al.[344] reported a composite material made of graphene nanoribbons and iron oxide nanoparticles, in which graphene was synthesized via the treatment of MWCNTs with a K/Na alloy, followed by heat treatment. This material exhibited a discharge capacity of 910 mAh g^{-1} at 100 mA g^{-1} after 134 cycles. The electrochemical performance of half cells has been fully discussed above, the performance of the full battery, comprising Fe_2O_3@ graphene anode and $LiFePO_4$ cathode, has also received attention,[345] suggesting the potential for practical application in LIBs.

In addition, a hydrothermal method followed subsequently by a thermal treatment has been used to produce

Table 3. Physical properties and electrochemical Li cycling data of MO (M = Co, Mn, Ni, Cu, or Zn)

Morphology	Synthesis approach	Current rate [mA g^{-1}]	Reversible capacity [mAh g^{-1}]	Capacity retention after n cycles (cycling range)	Ref.
Micro-sized CoO	commercial available	0.2 C	640	100% (n = 100)	[299]
CoO/rGO	hydrothermal/thermal pyrolysis	150 (0.2 C)	890	74.5% (n = 100)	[242]
CoO–graphene–carbon	electrospinning/thermal treatment	100	1030	73.8% (n = 252) at 0.5 A g^{-1}	[301]
MnO nanocrystals/GNS	chemical-wet impregnation/thermal reduction	0.2 C	635	≈410 mAh g^{-1} at 5C	[303]
MnO/graphene	in situ reduction method	50	747	94.5% (n = 100)	[304]
MnO/GNS	hydrothermal method/annealing	100	670	782 mAh g^{-1} (n = 60)	[306]
NiO Ns/graphene	hydrothermal/heat treatment	50	1000	≈90% (n = 50)	[308]
NiO Ns/graphene	hydrothermal	100	982	112% (n = 50)	[311]
NiO nanowalls/GNs	hydrothermal	0.1 C	844.9	92.9% (n = 50)	[310]
NiO–graphene	hydrothermal	0.1 C	1056	97.6% (n = 40)	[312]
graphene/NiO	hydrothermal/heat treatment	300	≈580	77% (n = 100)	[309]
NiO–graphene hybrid	liquid phase deposition	100	748	86.3% (n = 35)	[313]
NiO nanoplate–FGS	hydrothermal	100	750	93.3% (n = 50)	[314]
Ni/NiO–graphene	spray pyrolysis	1500	845	100% (n = 300)	[328]
CuO/graphene	chemical reduction	67	583.5	75.5% (n = 50)	[321]
Shuttle- and urchin-like CuO/GNS	low-temperature solution	70	771	107% (n = 100)	[319]
fusiform CuO/GNS	low-temperature solution	1400	925	57.5% (n = 100)	[318]
CuO nanoleaves/GNs	microwave-assisted method	100	1419	42.3% (n = 50)	[323]
CuO nanorods/graphene	hydrothermal method	0.1 C	605.6	114% (n = 50)	[320]
CuO NPs/graphene	Kirkendall-effect	50	640	116% (n = 50)	[317]
Gr/Si–CuO QD	electrophoresis deposition	1 C	1552	71% at 1C (n = 100)	[325]
CuO–Cu_2O/graphene	microwave-assisted process/annealing	200	705	69% (n = 60)	[329]
ZnO NPs/graphene	solution-based method	0.5 C	700	57.7% (n = 100)	[326]
Graphene–carbon–ZnO	hydrothermal	0.1 C	≈750	86.6% (n = 100)	[327]

graphene-containing Cr_2O_3 hybrids as anode materials for LIBs.[346,347] Such materials are of interest due to their extremely high thermal stability and chemical resistance. In a recent example, graphene–Cr_2O_3 nanosheets offered a reversible capacity of 850 mAh g^{-1} at a current density of 200 mA g^{-1} after 50 cycles. However, more work on these chromium materials is required.

Clearly, hybrid graphene/M_2O_3 nanomaterials, primarily based on Fe_2O_3, have produced various composites with unique structures and compositions. The stable lithium storage performance of graphene/Fe_2O_3 has been verified to around 1000 mAh g^{-1} at ≈100 mA g^{-1} for various specimens reported by several groups. Representative data on high performance Fe_2O_3/graphene composites are summarized in **Table 4**.

2.5.4. Molybdenum Compounds and Others

Molybdenum dioxide (MoO_2) adopts a distorted rutile structure with a low electronic resistivity because of its electronic band structure. Early studies[348,349] demonstrated that MoO_2 nanoparticle/graphene hybrids possess lithium cyclability in the voltage range 0.01–3.0 V, with a reversible storage capacity of 765.3 mAh g^{-1} after 40 cycles at 60 mA g^{-1},[348] and a reversible capacity of 986.9 mAh g^{-1} at 200 mA g^{-1} after 150 cycles.[349] As important as peak performance characteristics are, they are only as good as their ability to be reproduced and verified. Hence, when several groups work on the same material and achieve similar results, it is indicative of a strong potential research area as is already known for molybdenum-based dichalcogenides.

MoO_3, rather than MoO_2, occurs as the rare mineral molybdite, and has also received much attention recently. Anhydrous MoO_3 is composed of layers of distorted MoO_6 octahedra in an orthorhombic crystal. In 2014, Choi et al.[350] produced a graphene–MoO_3 composite by spray pyrolysis, leading to initial discharge capacities of 1490 mAh g^{-1} at a current density of 2 A g^{-1}. Moreover, the reversible discharge capacity decreased slightly from 1228 mAh g^{-1} to 845 mAh g^{-1} as the current density increased from 0.5 A g^{-1} to 3 A g^{-1}.

Similar lithium storage properties were confirmed by other researchers as well. Liu et al.[351] reported that alpha-MoO_3/graphene composite (MoO_3/G) prepared via hydrothermal synthesis revealed an initial charge capacity of 977.7 mAh g^{-1} at a current density of 50 mA g^{-1}, and the electrode still retained a capacity of 869.2 mAh g^{-1} after eighty cycles. The

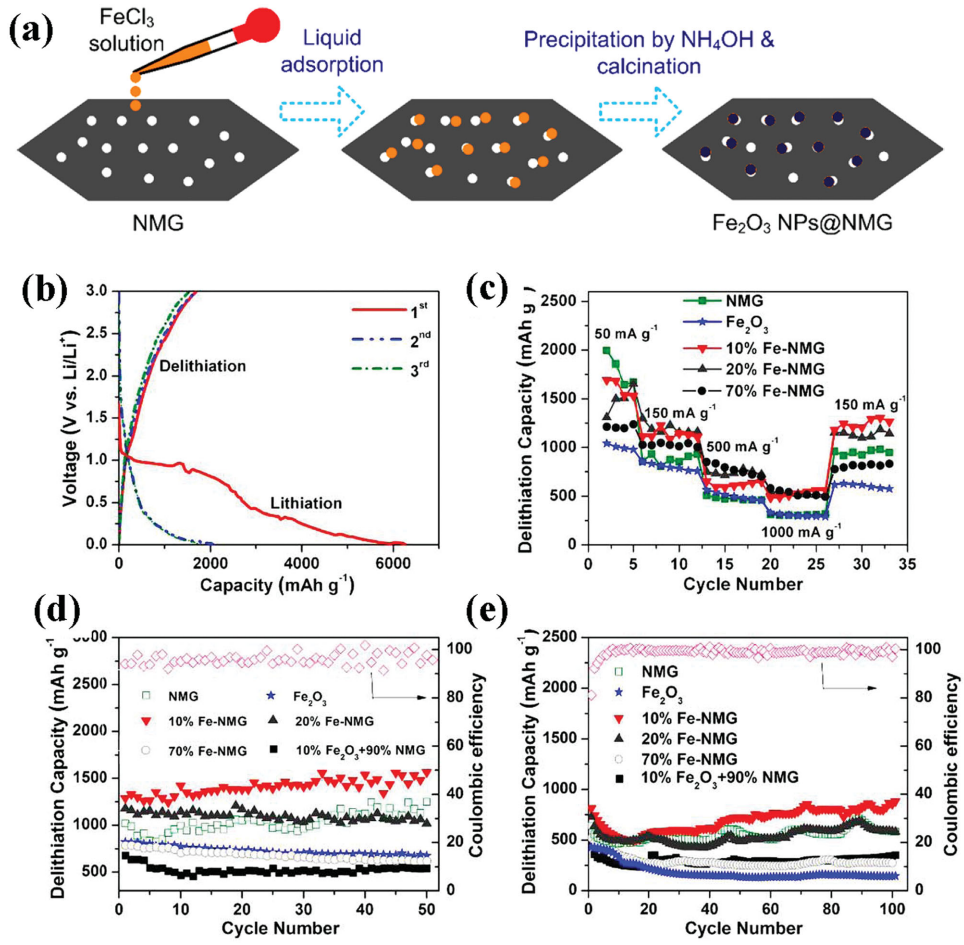

Figure 19. a) Schematic illustration of the synthesis of Fe_2O_3–NMG composites. b) Lithium insertion and extraction curves of the 10%Fe–NMG composite cycled between 3 and 0.01 V (vs. Li+/Li) at the current density of 50 mA g^{-1}. c) Rate capability and d,e) cycling stability at current densities of 150 mA g^{-1} and 1000 mA g^{-1} for as-prepared materials. The pink circles in (c) and (d) represent the Coulombic efficiency of the 10% Fe–NMG during the cycling process. Reproduced with permission.[336] Copyright 2014, American Chemical Society.

graphene-encapsulated MoO_3 nanoribbons synthesized via a self-assembly process[352] showed a specific capacity of 754 mAh g^{-1} after 200 cycles at 1000 mA g^{-1}. In addition, $Mn_2Mo_3O_8$–graphene delivered a reversible capacity of 494 mAh g^{-1} at a current density of 200 mA g^{-1} after 20 cycles.[353] Mixed-metal oxides offer a new area of unexplored materials, but with added complexity in processing and mechanistic understanding.

2.6. Anodes Based on Both Alloying–Dealloying and the Conversion Reaction

Fewer material systems follow the alloying–conversion reaction mechanism, which is essentially a hybrid of two separate mechanisms of lithium cycling. One such example is normal spinel $ZnFe_2O_4$/graphene ($ZnFe_2O_4$/G) hybrids. In one study, this material was synthesized by an in situ solvothermal process[354] and retained a charge capacity of 600 and 398 mAh g^{-1} at 200 and 400 mA g^{-1} after 90 cycles, respectively. As an obvious contrast, the charge capacity of bare $ZnFe_2O_4$ dropped rapidly from 510 mAh g^{-1} to 72 mAh g^{-1} after 50 cycles at 50 mA g^{-1}. $ZnFe_2O_4$ nanocrystals/graphene hybrids synthesized by in situ hydrothermal route were also recently noted by Xie et al.[355]

An inverse spinel Co_2SnO_4 hollow cube/graphene composite, delivering a capacity over 1000 mAh g^{-1} at 100 mA g^{-1}, was synthesized by a pyrolysis-induced transformation.[356] The reaction mechanism was expressed as follows:

$$Co_2SnO_4 + 8Li^+ + 8e^- \rightarrow 2Co + 4Li_2O + Sn \quad (24)$$

$$Sn + 4.4Li^+ \leftrightarrow Li_{4.4}Sn \quad (25)$$

$$Sn + 2Li_2O \leftrightarrow SnO_2 + 4Li \quad (26)$$

$$Co + Li_2O \leftrightarrow CoO + 2Li \quad (27)$$

The conversion-like component of the reaction is seen in Equation (24) and the alloying-like component is evident in Equation (25). Of particular note is amorphous $CoSnO_3$.[357] This material can be synthesized via a simple hydrothermal

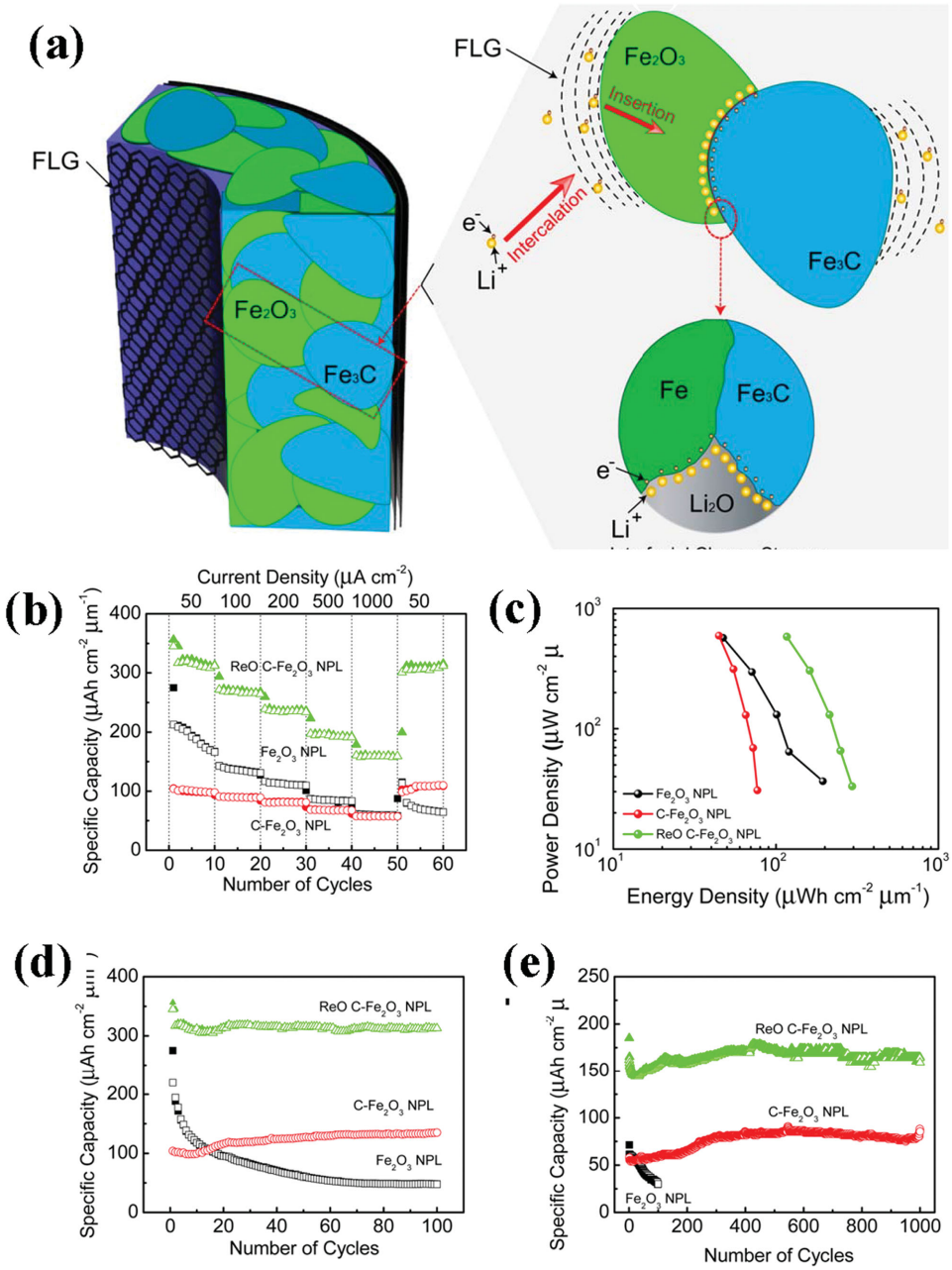

Figure 20. a) Proposed lithium storage by intercalation into the graphene interlayer and insertion into the lattice of active material, followed by additional charge separation at two-phase boundaries to form space charge layers. Electrochemical performance of the nanoporous thin film for LIBs. b) Capacity obtained at different current densities from 50 μA cm^{-2} to 1000 μA cm^{-2}. c) Ragone plot. d,e) Cycling tests measured at 50 μA cm^{-2} for 100 cycles and 1000 μA cm^{-2} for 1000 cycles, respectively. The solid and hollow symbols in (b). Panels (d) and (e) denote discharge and charge, respectively. Reproduced with permission.[340] Copyright 2014, American Chemical Society.

method, followed by annealing. It delivered a charge capacity of 724 mAh g^{-1} after 50 cycles at 200 mA g^{-1} by following the previously described lithium cycling mechanism.

2.7. Summary of Graphene-Containing Anode Materials

The range of inorganic materials suitable for graphene-containing hybrid anodes in LIBs is extensive; covering most of the base-metal oxides and part of the light main-group elements. Graphene can effectively accommodate the inherent volume expansion of inorganic materials, and thus provide an immense opportunity for inorganic compounds to achieve improved lithium storage performance through a combination of structure design, synthesis procedure and performance optimization. Of further importance, graphene-containing hybrids make flexible electrodes possible for emerging applications in pliable and wearable electronic devices. The future of next generation

Table 4. Physical properties and electrochemical Li cycling data of M_2O_3 (M = Fe or Cr)

Morphology	Synthesis approach	Current rate [mA g^{-1}]	Reversible capacity [mAh g^{-1}]	Capacity retention after *n* cycles (cycling range)	Ref.
α-Fe_2O_3/graphene–carbon	hydrothermal method	C/10	727	78.4% ($n = 20$)	[331]
Fe_2O_3NPs/GNS	microwave-induced hydrolysis	100 (0.1 C)	1120	27.8% ($n = 40$)	[332]
Fe_2O_3rice/GNS		100 (0.1 C)	1184	62% ($n = 40$)	
Nanorod-like Fe_2O_3/graphene	hydrothermal followed by calcination	100 (0.1 C)	1042	57.8% ($n = 30$)	[333]
Fe_2O_3 nanocrystals/GNS	hydrothermal method	200	946	110% ($n = 450$)	[334]
Fe@ Fe_2O_3NPs/graphene	hydrothermal and thermal reduction	100	1110	86.4% ($n = 90$)	[335]
γ-Fe_2O_3 NPs/graphene	thermal decomposition method	100	900	100% ($n = 50$)	[337]
3 nm Fe_2O_3 NPs/NMG	adsorption–precipitation process	50	1692	100% ($n = 50$)	[336]
Fe_2O_3@SnO_2 GNs films	vacuum filtration/thermal reduction	100	1255	80.8% ($n = 200$)	[338]
Fe_2O_3NPs @C@G	CVD	100	891	97% ($n = 100$)	[339]
Fe_2O_3/Fe_3C–graphene	CVD	0.17 C	1118	88% ($n = 100$)	[340]
Fe_2O_3 NPs/graphene	Hydrolysis	0.2 C	850	94% ($n = 100$)	[341]
α- Fe_2O_3 NPs/graphene	In situ wet chemistry approach	100	827	90% ($n = 50$)	[342]
GNR/Fe_2O_3–P	MWCNT'S split/heat treatment	200	1190	76.5% ($n = 134$)	[344]
GNR/Fe_2O_3_250		200	1003	74.3% ($n = 128$)	
GNR/ Fe_2O_3 -300		200	1291	31% (n = 50)	
C–graphene/$Cr_2O_3NP_s$	hydrothermal followed by thermal treatment	0.1 C	763.9	58.9% ($n = 100$)	[346]

battery research will not hinge on one particular material, as a variety of promising candidates are emerging. Issues concerning the repeatability, stability and scale-up considerations of devices are the next hurdle in development beyond benchtop curiosity. In the following sections, a similar review of graphene-based cathode materials and preparation techniques is described.

3. Cathode Materials

As is well known, the biggest obstacle for the development of high-power and long-lasting LIBs is the limited capacity ascribed to current commercial cathode materials. Much effort has been devoted to improving the energy density of commercial ternary cathode materials to satisfy the high power demand.[358] It is highly likely that graphene can positively impact the development and improvement of cathode materials due to several key properties, including improved electrical conductivity, augmented kinetics of electrons and lithium ion transportation,[359] and reduced particle agglomeration during cycling, as demonstrated in anode materials. The key material groups for cathodes will be reviewed in the subsequent sections.

3.1. Phosphate Materials

3.1.1. Li(Fe,Mn)PO_4

$LiFePO_4$ is a 3.5 V cathode and adopts an orthorhombic olivine-type structure, and is generally considered as a strong cathode material owing to its low cost and good lithium-cyclability. The reversible lithium storage capacity of $LiFePO_4$/graphene composites is stable between 150 to 170 mAh g^{-1}. In fact, $LiFePO_4$ has already been successfully implemented in numerous commercial batteries for the automotive market.

Yang et al.[360] have demonstrated a straightforward, template-free sol–gel route to synthesize a novel porous 3D hierarchical $LiFePO_4$/graphene (LFP/G) composite. When used as a cathode for LIBs, the as-prepared composites possessed good electrochemical properties, i.e., reversible capacity of 146 mAh g^{-1} at 17 mA g^{-1} after 100 cycles. This is higher than reports for pristine LFP (104 mAh g^{-1}). Related formulations were also investigated, including $LiFePO_4$/5%-GS composites (delivering a capacity of 155.4 mA h g^{-1} at 0.2 C),[361] graphene–$LiFePO_4$ composites via a hydrothermal method (specific discharge capacity of 149 mAh g^{-1} at 0.17 C),[359] graphene nanoribbon-wrapped $LiFePO_4$ via electrostatic interaction[362] (delivering a specific discharge capacity of 152 mAh g^{-1} at 0.1 C) and $LiFePO_4$@GNS nanoparticles via solid state reaction (discharge and charge capacities of 145 mAh g^{-1} and 150 mAh g^{-1}, respectively).[363] As was encountered for anode development, a wealth of material combinations, morphologies and preparation techniques are available and the challenge is narrowing down the list to the best among many.

It is worth noting that a specific capacity higher than 158 mAh g^{-1} has been achieved for $LiFePO_4$ composites by several groups in 2014. Reversible lithium storage capacities of 158 mAh g^{-1},[364] 170 mAh g^{-1},[365] 160 mAh g^{-1},[366] 164 mAh g^{-1},[367] and 190 Wh kg^{-1} energy density for over 80 charge–discharge cycles (**Figure 21**)[368] were consistently reported.

The rate performance of $LiFePO_4$/graphene composites is also promising. Wu et al.[369] reported amorphous carbon and graphene co-modified $LiFePO_4$ nanocomposites via a facile polyol process, followed by thermal treatment. The composites deliv-

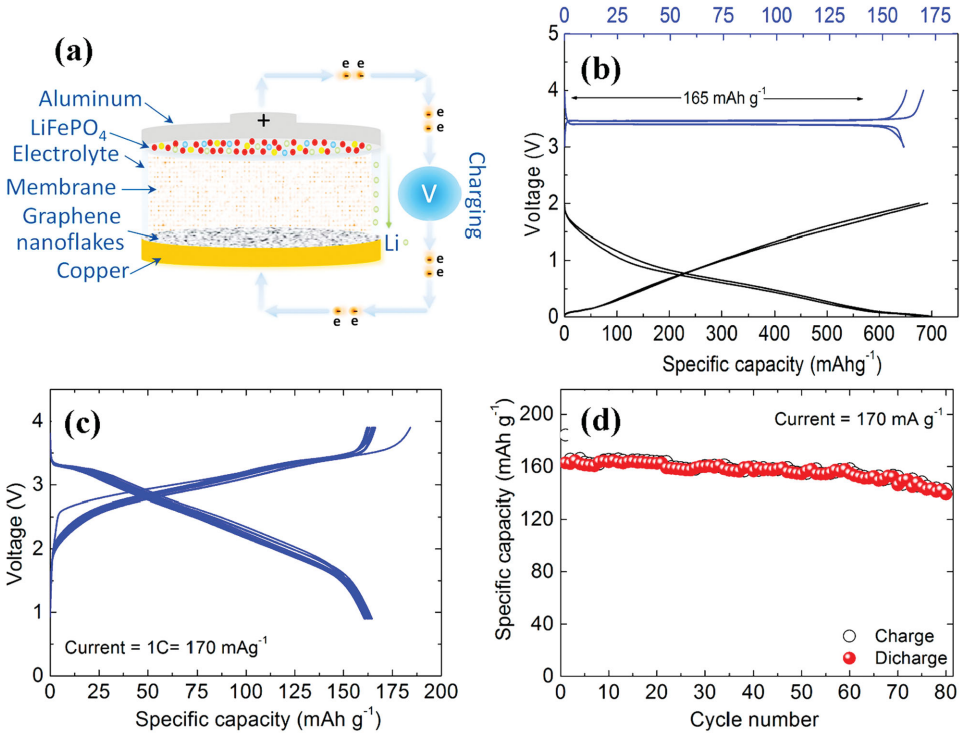

Figure 21. Electrochemical test of a graphene nanoflakes /lithium iron phosphate lithium ion battery. a) Schematic of graphene/Lithium iron phosphate battery. b) Charge-discharge voltage profiles of the single electrodes, that is, the graphene nanoflakes anodes (black curve) and the $LiFePO_4$ cathode (blue curve) as reported versus lithium. Current rate of 170 ($LiFePO_4$) and 700 mA g^{-1} (graphene nanoflakes). c) Voltage profile of the graphene / $LiFePO_4$ full battery. d) Specific capacity versus cycles number of the battery. Electrolyte: LP 30. Cycling rate: 1C (170 mA g^{-1} vs $LiFePO_4$). Voltage limits: 0.9–3.9 V. Temperature 25 °C. Reproduced with permission.[368] Copyright 2014, American Chemical Society.

ered a reversible specific capacity of 97 mAh g^{-1} at 10 C after 200 cycles. Liu et al.[370] reported that $LiFePO_4$ nanograin/graphene composites maintained an operating flat voltage at more than 3.0 V with a discharge capacity up to 107.8 mAh g^{-1}. Additional works on graphene encapsulated $LiFePO_4$ composites (capacity of 96 mAh g^{-1} after 950 cycles at 10 C),[371] graphene encapsulated $LiFePO_4$ composite via hydrothermal followed by annealing (with ≈88 mAh g^{-1} at 10 C after 40 cycles),[372] graphene nanoribbon-wrapped $LiFePO_4$ by electrostatic absorbing,[373] and carbon-coated $LiFePO_4$ via electrochemical exfoliation (specific capacity of 208 mAh g^{-1})[374] were also recently published. While such studies are promising, the variability in performance characteristics is large and the underlying mechanisms are not well understood. For each morphology, the effect on the underlying mechanism and kinetics must be considered.

Recently, $LiMnPO_4$–C/GNPs composites have attracted much attention. Zong et al.[375] reported a $LiMnPO_4$–C/GNPs composite that displayed reversible capacities of 139 mAh g^{-1} at 0.05 C and 119 mAh g^{-1} at 1 C. A carbon-coated $LiMnPO_4$ nanoplate/graphene material displayed a specific capacity of 159 mAh g^{-1} at C/20 and a retention of 72.3% of its initial capacity after 100 cycles.[376] In another work, a $LiMnPO_4$–C/GNPs composite cathode material delivered a capacity of 105.1 mAh g^{-1} at 0.05 C over a voltage range of 2.5–4.4 V.[377] Graphene oxide-assisted facile hydrothermal synthesis of $LiMn_{0.6}Fe_{0.4}PO_4$ nanoparticles[378] and rGO/carbon double-coated $LiMn_{0.9}Mg_{0.1}PO_4$ nanoplates[379] are also discussed as cathode material for LIBs.

3.1.2. $Li_3(V, Ti)_2(PO_4)_3$

$Li_3V_2(PO_4)_3$ is another phosphate material with a monoclinic structure that has been researched for use in cathodes in LIBs due to its high operating voltage and high rate capabilities. In 2014, Cheng et al.[380] suggested that nano-$Li_3V_2(PO_4)_3$-wrapped rGO sheets delivered a capacity of 105.7 mAh g^{-1} at 20 C for 3.0–4.3 V, and a discharge capacity of 123.2 mAh g^{-1} after 100 cycles at 0.1 C. Another recent work provided a similar result with a capacity of 141.6 mAh g^{-1} at 0.075 C, and a rate capacity of 119.0 mAh g^{-1} at 15 C for a $Li_3V_2(PO_4)_3$/rGO composite.[381] In Choi's study[382], $Li_3V_2(PO4)_3$/Ag–graphene (LVP/Ag–G) hybrids were synthesized as cathode materials with a simple sol–gel route. The LVP/Ag–G electrode afforded a discharge capacity of 118 and 133 mAh g^{-1} at 10 C in the potential range 3.0–4.3 V and 3.0–4.8 V, respectively.

Recently, two other important phosphate materials, $LiVPO_4F$ and $LiTi_2(PO_4)_3$, have also attracted much attention. $LiVPO_4F$ has been widely investigated as a potential cathode material for LIBs operating at 4.2 V vs. Li/Li^+.[61,383] Cyclability of a nano-sized $LiVPO_4F$/graphene composite (LVPF/G) synthesized via a facile mechano-chemical approach exhibited an initial charge capacity of 287 mAh g^{-1} at rate of 0.1 C (1 C = 310 mA g^{-1}) with no capacity fading after 100 cycles and a good rate capability of 168 mAh g^{-1} at 10 C under 0.01–3 V vs. Li/Li^+.[384]

Roh et al.[385] developed a $LiTi_2(PO_4)_3$/rGO nanocomposite with a NASICON-type structure that delivered a reversible

capacity of 138 mAh g^{-1} at a 0.1 C rate. Trasmission electron microscopy (TEM) imaging revealed that almost all of the $LiTi_2(PO_4)_3$ nanoparticles remained unchanged after 200 cycles. The $LiTi_2(PO_4)_3$ possessed an average voltage at which Li insertion–extraction occurred from 2.4 V to 2.6 V. This voltage, unfortunately, is too high for use as an anode and too low for use as a cathode in LIBs.

3.2. Spinel

$LiMn_2O_4$ adopts a spinel structure, in which manganese is located in the octahedral sites and lithium occupies the tetrahedral sites. $LiMn_2O_4$ is a 4.0 V cathode.[386] Lithium cycling performance of ZnO-ALD-modified $LiMn_2O_4$/graphene possessing a capacity of 122 mAh g^{-1} after 100 electrochemical cycles was reported by Aziz et al.[387] A $LiMn_2O_4$–graphene composite produced by electrophoretic co-deposition delivered an improved average energy density of 59.6 Wh kg^{-1} along with a power density of 697 W kg^{-1}.[388]

Other transition metals (such as nickel, cobalt and iron) were also incorporated into $LiMn_2O_4$ to improve its properties.[389] Binary spinel structures, such as sandwiched $LiNi_{0.5}Mn_{1.5}O_4$ synthesized via sol–gel as a 5 V cathode, were recently discussed.[390] Moreover, ternary systems have also been investigated.

One such example is graphene-modified $LiCo_{1/3}Ni_{1/3}Mn_{1/3}O_2$,[391] which possessed a discharge capacity of 198.5 mAh g^{-1} after 50 cycles at 0.2 C. Consequently, much interest has been invested in such materials. The graphene-coated $Li(Li_{0.2}Mn_{0.54}Ni_{0.13}Co_{0.13})O_2$ synthesized via a spray drying method exhibited a capacity of 153 mAh g^{-1} at 250 mA g^{-1} after 50 cycles. This is higher than values reported for the graphene-free cathode materials.[392] Another group[393] also investigated a Li-rich cathode material $Li(Li_{0.2}Mn_{0.54}Ni_{0.13}Co_{0.13})O_2$/GO synthesized by a sol–gel method. It possessed a very high discharge capacity of 313 mAh g^{-1} at 12.5 mA g^{-1}, and 201 mAh g^{-1} charge capacity at 2.5 A g^{-1}.

Among all considered materials, binary spinel structures achieve a balance between cost and performance. Consequently, they are one of the primary candidates for cathode materials in batteries.

3.3. Vanadium Compounds

V_2O_5 is one of the most investigated layered metal oxides for its lithium cyclability via the intercalation–deintercalation reaction:[394]

$$V_2O_5 + xLi^+ + xe^- \leftrightarrow Li_xV_2O_5 \quad (28)$$

As reported by Yang et al.,[395] nanocrystalline V_2O_5 particles were successfully entrapped by graphene nanoribbons (GNRs). The composite delivered an impressive capacity of 217 mAh g^{-1} at 0.1 C after 100 cycles (**Figure 22**). A similar lithium storage performance, i.e. discharge capacities of 214 mAh g^{-1} at 1 A g^{-1} after 100 cycles for rGB–V_2O_5 composite, was reported by Choi et al.[396] As a comparison, pure V_2O_5 only delivers a capacity of 152 mAh g^{-1}.

Additional work has further investigated more complex cathode architectures involving vanadium oxide and graphene. Some representative reports include single-crystalline V_2O_5 nanowire/graphene possessing a high reversible capacity of 357 mAh g^{-1},[397] V_2O_5/graphene synthesized by a facile solvothermal approach,[398] rGO/V_2O_5 with a discharge capacity of 140 mAh g^{-1} at 150 mA g^{-1} for 100 cycles,[399] V_2O_5 thin film/graphene sheet composites offering a specific capacity of 122 mAh g^{-1} after 300 cycles at 500 mA g^{-1},[400] and rGO/V_2O_5 NWs[401] with discharge capacities of 138 mAh g^{-1} after 30 cycles. Other vanadium compounds including VO_2/rGO composites,[402] and V_3O_7/GO[403] were recently reported as well.

Similar to $LiTi_2(PO_4)_3$, the voltage range (2.2–2.6 V) of V_2O_5 makes its assignment as either a cathode or anode ambiguous. In general, it can be defined as a cathode material when graphite is used as a counter electrode material. Furthermore,

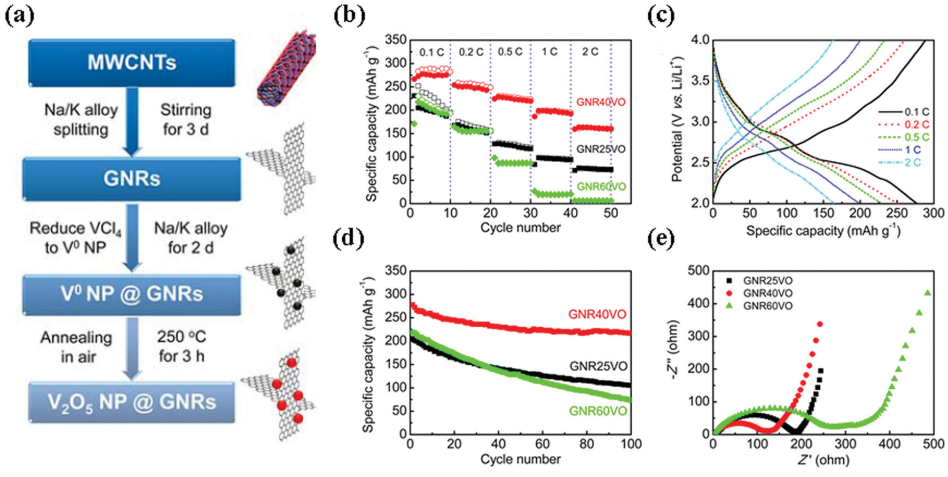

Figure 22. a) Synthesis scheme and schematic diagrams of the fabricated GNR–V_2O_5 NP composites. b–e) Rate performance and cyclability of composites. b) Variation in the capacity of composites with different applied current densities from 0.1 C to 2 C. c) Discharge/charge profiles of GNR40VO at different current densities from 0.1 C to 2 C. d) 100 discharge/charge cycle testing of composites at 0.1 C. e) EIS of composites. Reproduced with permission.[395] Copyright 2014, American Chemical Society.

V_2O_5 is highly toxic and expensive, limiting its extensive application in LIB research.[404]

3.4. $Li_2(Fe, Mn)SiO_4$

3D macroporous graphene-containing Li_2FeSiO_4 composites (3D-G/Li_2FeSiO_4/C) were synthesized by Zhu et al.[405] and tested as a cathode material for LIBs. 3D-G/Li_2FeSiO_4/C demonstrated improved performance characteristics with a discharge capacity of 108 mAh g^{-1} at a rate of 20 C (1 C = 166 rnA g^{-1}) after 1000 cycles. Recently, Gong et al.[406] reported that lithium cyclability of nanospherical Li_2MnSiO_4/C/graphene composites produced an initial discharge capacity of 215.3 mAh g^{-1} under 0.05 C together with a stable discharge capacity of 175 mAh g^{-1} after 40 cycles.

3.5. Summary of Graphene-Containing Cathode Materials

As listed in **Table 5**, graphene in cathode materials is not as essential a contribution when compared to anode materials. This is due largely to the limited contribution of its electrochemical properties. Owing to the inherent nature of the active materials in cathodes, the addition of graphene may only produce incrementally higher reversible capacity and cycling stability than those of the corresponding pristine active materials. Furthermore, graphene may even result in decreased performance and higher cost. The synthesis of well-dispersed active material/graphene cathode composites is also rather complex because of the generally incompatible fabrication processes between the inorganic active materials and graphene. Therefore, more attention should to be devoted to the investigation of graphene incorporation in cathode materials to solve such issues.

4. Conclusions and Outlook

Lithium-ion batteries are widely used in consumer electronics, electrical vehicles and other new energy sectors. It is important to note that electric vehicles in developed countries, such as the United States, have been commercialized in recent years. By 2013, the total global unit sales for electric vehicles had reached 500,000 units for three years and the United States occupied the dominant position of about 200,000 units. As a crucial component of electrical vehicles, battery pack development and performance is directly tethered to the cost and key technology concerns such as lifetime and safety of electric vehicles. Therefore, battery development is an essential piece in the industrial chain. The large number and variety of research efforts being undertaken are certainly encouraging and will hopefully yield positive results and help to drive the progress of LIB technology.

In this review, a brief commentary on the current state-of-the-art and challenges of inorganic/graphene anode and cathode materials synthesis and performance has been presented. From the viewpoint of technology, both anode and cathode materials derived from graphene-containing nanomaterials all possess several interesting properties motivating the use of graphene. First, nanoparticles (nanorods and nanowires) likely prevent graphene from detaching during cycling. Second, graphene prevents the aggregation of nanoparticles (nanorods and nanowires) during lithium cycling. Third, graphene sheets impart an increased specific surface area and an improved conductivity.

Lastly, the use of graphene has allowed accommodation for volume changes during cycling, thus reducing electrode destruction and improving cycle number and performance. Consequently, nanomaterial/graphene composites-based electrode materials have achieved great success for use in both the anode and cathode of lithium-ion batteries.

With specific attention to anodes, a number of reports have provided a framework of graphene-containing material categories. These range from transition metal oxides, main group oxides, and elementals with doping, co-doping and other morphological variations within each. However, several challenges remain and need to be tackled in the future: a) Composites with different structure and morphology offer opportunities to understand the influence of material nature on lithium storage performance. Clearly, more novel architectures need to be rationally designed and created to enrich the family of anode/graphene composites, and thus further improve the performance of the resulting LIBs. b) Despite graphene-containing composites exhibiting many unique synergistic attributes, a deep understanding of the coupling between graphene and nanomaterials can provide critical insight into the properties and performance relationship in graphene-containing composites and impart the optimization of their architecture. c) The

Table 5. Physical properties and electrochemical Li cycling data of typical cathode materials

Morphology	Synthesis approach	Current rate [mA g^{-1}]	Reversible capacity [mAh g^{-1}]	Capacity retention after *n* cycles (cycling range)	Ref.
$LiFePO_4$/5%GS	solution phase	5 C	124.3	100% ($n = 100$)	[361]
Graphene nanoribbons/$LiFePO_4$	electrostatic interaction	10 C	103	100% ($n = 200$)	[362]
$LiFePO_4$@GNS	solid state reaction	1 C (170 mA g^{-1})	128	95.3% ($n = 1000$)	[363]
$LiFePO_4$/rGO	co-precipitation/heat treatment	0.06 C	172	97.5% ($n = 50$)	[365]
Graphene/$LiMnPO_4$	sol–gel method	0.05 C	134	90% ($n = 40$)	[375]
V_2O_5–SnO_2/nanocapsules	solvothermal/heat treatment	250	947	71% ($n = 50$)	[394]
V_2O_5/graphene nanoribbons	chemical reduction/annealing	0.1 C	278	78% ($n = 100$)	[395]
3D-G/Li_2FeSiO_4	sol–gel	1 C	255	90% ($n = 100$)	[405]

finite size effects of nanomaterials needs to be scrutinized to clarify the correlation between the particle dimension and lithium storage properties, which in turn will provide guidance on composite synthesis and practical applications. d) For viable industrial applications, easily controlled, cost-effective preparative approaches need to be developed. e) Large scale and environmentally friendly production of graphene at low cost is also crucial in the application of graphene-containing composite. CVD is a common method used to grow large-area, single, or multilayer graphene sheets on metal substrates. Solution-based intercalation, chemical functionalization, and/or sonication of bulk graphite are proven to be advantageous due to their high yield and easy implementation. However, cost-effective approaches that yield large-scale high-quality graphene still need to be developed along these lines.[57]

With regard to cathode materials, synthesis of well-dispersed cathode material/graphene composites is rather complex because of the incompatible fabrication processes between the inorganic active materials and graphene. Obviously, much effort needs to be concentrated on the use of graphene in cathode materials. Graphene has emerged as one of the best electron conducting additives due to its flexibility, high electronic conductivity and large surface area. With progress being made in low-cost, large scale production of graphene, it will certainly find widespread applications among industrialized cathode materials and thus open up possibilities for future advances in LIBs.

There is much current interest in lithium-sulphur and lithium-air batteries due to their high energy density. The incorporation of graphene in lithium-sulphur and lithium-air batteries has been shown to be effective and promising. For lithium-sulphur batteries, a graphene matrix is advantageous in addressing issues such as the poor electronic conductivity of sulphur, large volume expansion and dissolution of polysulfides in electrolyte, thereby greatly enhancing the rate and cycle stabilities of Li-sulphur battery. For lithium-air batteries, graphene has promising applications as a catalyst on its own or as a catalyst substrate. The large surface area of graphene enables a high discharge capacity. The catalytic activity of graphene or graphene-supported catalysts reduces the large overpotential and thus enhances the cycle stability and round-trip efficiency of lithium-air batteries.Nonetheless, graphene-containing nanomaterials will remain as an active field of exploration for next-generation energy storage devices.

Acknowledgements

This work is supported by The South China University of Technology (S.W.) and National Science Foundation (ECCS-1305087) (Z.L.).

Received: February 25, 2015
Revised: April 14, 2015
Published online: July 14, 2015

[1] Q. Wang, Z. H. Wen, J. H. Li, *Adv. Funct. Mater.* **2006**, *16*, 2141.
[2] LiFeng Cui, Yuan Yang, C. Hsu, Y. Cui, *Nano Lett.* **2009**, *9*, 3370.
[3] R. V. Noorden, *Nature* **2014**, *498*, 416.
[4] P. G. Bruce, S. A. Freunberger, L. J. Hardwick, J. M. Tarascon, *Nat. Mater.* **2012**, *11*, 19.
[5] X. L. Ji, K. T. Lee, L. F. Nazar, *Nat. Mater.* **2009**, *8*, 500.
[6] D. Larcher, J. M. Tarascon, *Nat. Chem.* **2015**, *7*, 19.
[7] C. K. Chan, X. F. Zhang, Y. Cui, *Nano Lett.* **2008**, *8*, 307.
[8] G. Jo, I. Choi, H. Ahn, M. J. Park, *Chem. Commun.* **2012**, *48*, 3987.
[9] X. W. Lou, Y. Wang, C. Yuan, J. Y. Lee, L. A. Archer, *Adv. Mater.* **2006**, *18*, 2325.
[10] G. Zhou, D. Wang, F. Li, L. Zhang, N. Li, Z. Wu, L. Wen, G. Q. Lu, H. Cheng, *Chem. Mater.* **2010**, *22*, 5306.
[11] M. D. Stoller, S. Park, Y. Zhu, J. An, R. S. Ruoff, *Nano Lett.* **2008**, *8*, 3498.
[12] K. S. Novoselov, A. K. Geim, S. V. Morozov, D. Jiang, Y. Zhang, S. V. Dubonos, I. V. Grigorieva, A. A. Firsov, *Science* **2004**, *306*, 666.
[13] A. A. Balandin, *Nat. Mater.* **2011**, *10*, 569.
[14] P. Lian, X. Zhu, S. Liang, Z. Li, W. Yang, H. Wang, *Electrochim. Acta* **2010**, *55*, 3909.
[15] S. Q. Chen, P. Chen, Y. Wang, *Nanoscale* **2011**, *3*, 4323.
[16] C. D. Wang, Y. S. Chui, Y. Li, X. F. Chen, W. J. Zhang, *Appl. Phys. Lett.* **2013**, *103*, 253903.
[17] Y. L. Zou, X. Y. Zhou, J. Yang, *RSC Adv.* **2014**, *4*, 25552.
[18] O. Vargas, A. Caballero, J. Morales, E. Rodriguez-Castellon, *ACS Appl. Mater. Interfaces* **2014**, *6*, 3290.
[19] H. J. Peng, J. Q. Huang, M. Q. Zhao, Q. Zhang, X. B. Cheng, X. Y. Liu, W. Z. Qian, F. Wei, *Adv. Funct. Mater.* **2014**, *24*, 2772.
[20] R. Raccichini, A. Varzi, S. Passerini, B. Scrosati, *Nat. Mater.* **2015**, *14*, 271.
[21] Q. Li, N. Mahmood, J. Zhu, Y. Hou, S. Sun, *Nano Today* **2014**, *9*, 668.
[22] a) D. D. Cai, S. Q. Wang, L. X. Ding, P. C. Lian, S. Q. Zhang, F. Peng, H. H. Wang, *J. Power Sources* **2014**, *254*, 198; b) W. Ai, Z. Z. Du, Z. X. Fan, J. Jiang, Y. L. Wang, H. Zhang, L. H. Xie, W. Huang, T. Yu, *Carbon* **2014**, *76*, 148.
[23] D. Wei, M. R. Astley, N. Harris, R. White, T. Ryhanen, J. Kivioja, *Nanoscale* **2014**, *6*, 9536.
[24] a) S. Han, D. Wu, S. Li, F. Zhang, X. Feng, *Small* **2013**, *9*, 1173; b) E. J. Yoo, J. Kim, E. Hosono, H. S. Zhou, T. Kudo, I. Honma, *Nano Lett.* **2008**, *8*, 2277.
[25] X. F. Zhou, Z. P. Liu, *IOP 3rd Int. Congress on Ceramics (ICC): Nano-Crystals and Advanced Powder Technology IOP, Bristol*, 2011 IOP Conf.Ser. : Mater. Sci. Eng. **2011**, *18*, 001001.
[26] D. Yoon, K. Y. Chung, W. Chang, S. M. Kim, M. J. Lee, Z. Lee, J. Kim, *Chem. Mater.* **2015**, *27*, 266.
[27] S. Petnikota, N. K. Rotte, V. Srikanth, B. S. R. Kota, M. V. Reddy, K. P. Loh, B. V. R. Chowdari, *J. Solid State Electrochem.* **2014**, *18*, 941.
[28] J. H. Li, L. F. Li, B. W. Zhang, M. Yu, H. J. Ma, J. Y. Zhang, C. Zhang, J. Y. Li, *Ind. Eng. Chem. Res.* **2014**, *53*, 13348.
[29] W. Ahn, H. S. Song, S. H. Park, K. B. Kim, K. H. Shin, S. N. Lim, S. H. Yeon, *Electrochim. Acta* **2014**, *132*, 172.
[30] D. D. Cai, L. X. Ding, S. Q. Wang, Z. Li, M. Zhu, H. H. Wang, *Electrochim. Acta* **2014**, *139*, 96.
[31] Y. S. Yun, V. D. Le, H. Kim, S. J. Chang, S. J. Baek, S. Park, B. H. Kim, Y. H. Kim, K. Kang, H. J. Jin, *J. Power Sources* **2014**, *262*, 79.
[32] R. P. Hardikar, D. Das, S. S. Han, K. R. Lee, A. K. Singh, *Phys. Chem. Chem. Phys.* **2014**, *16*, 16502.
[33] a) T. Hu, X. Sun, H. T. Sun, G. Q. Xin, D. L. Shao, C. S. Liu, J. Lian, *Phys. Chem. Chem. Phys.* **2014**, *16*, 1060; b) M. I. Bodnarchuk, K. V. Kravchyk, F. Krumeich, S. T. Wang, M. V. Kovalenko, *ACS Nano* **2014**, *8*, 2360.
[34] a) X. L. Ma, G. Q. Ning, C. L. Qi, C. G. Xu, J. S. Gao, *ACS Appl. Mater. Interfaces* **2014**, *6*, 14415; b) J. P. Jegal, K. C. Kim, M. S. Kim, K. B. Kim, *J.Mater. Chem. A* **2014**, *2*, 9594.

[35] W. Ai, Z. M. Luo, J. Jiang, J. H. Zhu, Z. Z. Du, Z. X. Fan, L. H. Xie, H. Zhang, W. Huang, T. Yu, *Adv. Mater.* **2014**, *26*, 6186.
[36] C. Tang, Q. Zhang, M. Q. Zhao, J. Q. Huang, X. B. Cheng, G. L. Tian, H. J. Peng, F. Wei, *Adv. Mater.* **2014**, *26*, 6100.
[37] H. Chakraborti, S. K. Pal, *Chem. Phys. Lett.* **2014**, *600*, 118.
[38] Y. Yang, K. C. He, P. Yan, D. Wang, X. Y. Wu, X. Zhao, Z. L. Huang, C. M. Zhang, D. N. He, *Electrochim. Acta* **2014**, *138*, 481.
[39] F. Ouhib, A. Aqil, J. M. Thomassin, C. Malherbe, B. Gilbert, T. Svaldo-Lanero, A. S. Duwez, F. Deschamps, N. Job, A. Vlad, S. Melinte, C. Jerome, C. Detrembleur, *J.Mater. Chem. A* **2014**, *2*, 15298.
[40] J. Shim, D. G. Kim, H. J. Kim, J. H. Lee, J. H. Baik, J. C. Lee, *J.Mater. Chem. A* **2014**, *2*, 13873.
[41] Y. X. Yu, *J.Mater. Chem. A* **2014**, *2*, 8910.
[42] Z. Z. Du, W. Ai, L. H. Xie, W. Huang, *J. Mater. Chem. A* **2014**, *2*, 9164.
[43] Y. Z. Su, Y. X. Liu, P. Liu, D. Q. Wu, X. D. Zhuang, F. Zhang, X. L. Feng, *Angew. Chem., Int. Ed.* **2015**, *54*, 1812.
[44] B. Luo, L. Zhi, *Energy Environ. Sci.* **2015**, *8*, 456.
[45] Y. L. Zou, X. Y. Zhou, J. Yang, *Phys. Chem. Chem. Phys.* **2014**, *16*, 10429.
[46] J. X. Zhang, Z. W. Xie, W. Li, S. Q. Dong, M. Z. Qu, *Carbon* **2014**, *74*, 153.
[47] J. X. Qiu, C. Lai, S. Li, S. Q. Zhang, *RSC Adv.* **2014**, *4*, 18899.
[48] J. J. Tang, G. H. Chen, J. Yang, X. Y. Zhou, L. N. Zhou, B. Huang, *Nano Energy* **2014**, *8*, 62.
[49] C. Kang, R. Baskaran, J. Hwang, B. C. Ku, W. Choi, *Carbon* **2014**, *68*, 493.
[50] Y. L. Zhao, J. G. Feng, X. Liu, F. C. Wang, L. F. Wang, C. W. Shi, L. Huang, X. Feng, X. Y. Chen, L. Xu, M. Y. Yan, Q. J. Zhang, X. D. Bai, H. A. Wu, L. Q. Mai, *Nat. Commun.* **2014**, *5*, 4565.
[51] P. Goli, S. Legedza, A. Dhar, R. Salgado, J. Renteria, A. A. Balandin, *J. Power Sources* **2014**, *248*, 37.
[52] T. D. Dao, J. E. Hong, K. S. Ryu, H. M. Jeong, *Chem. Eng. J.* **2014**, *250*, 257.
[53] K. M. Oh, S. W. Cho, G. O. Kim, K. S. Ryu, H. M. Jeong, *Electrochim. Acta* **2014**, *135*, 478.
[54] a) X. W. Liu, H. Zhao, X. M. Huang, Y. H. Hu, H. Q. Gao, X. X. Liu, L. Y. Shen, *Eur. Phys. J.: Appl. Phys.* **2014**, *66*, 30301; b) K. W. Shu, C. Y. Wang, M. Wang, C. Zhao, G. G. Wallace, *J.Mater. Chem. A* **2014**, *2*, 1325.
[55] X. Liu, J. Cheng, W. Li, X. Zhong, Z. Yang, L. Gu, Y. Yu, *Nanoscale* **2014**, *6*, 7817.
[56] J. Zang, S. Ryu, N. Pugno, Q. Wang, Q. Tu, M. J. Buehler, X. Zhao, *Nat. Mater.* **2013**, *12*, 321.
[57] K. R. Paton, E. Varrla, C. Backes, R. J. Smith, U. Khan, A. O'Neill, C. Boland, M. Lotya, O. M. Istrate, P. King, T. Higgins, S. Barwich, P. May, P. Puczkarski, I. Ahmed, M. Moebius, H. Pettersson, E. Long, J. Coelho, S. E. O'Brien, E. K. McGuire, B. M. Sanchez, G. S. Duesberg, N. McEvoy, T. J. Pennycook, C. Downing, A. Crossley, V. Nicolosi, J. N. Coleman, *Nat. Mater.* **2014**, *13*, 624.
[58] J. M. Tour, *Nat. Mater.* **2014**, *13*, 545.
[59] J. A. Torres, R. B. Kaner, *Nat. Mater.* **2014**, *13*, 328.
[60] N. Mahmood, C. Z. Zhang, H. Yin, Y. L. Hou, *J. Mater. Chem. A* **2014**, *2*, 15.
[61] M. V. Reddy, G. V. S. Rao, B. V. R. Chowdari, *Chem. Rev.* **2013**, *113*, 5364.
[62] a) J. X. Zhu, D. Yang, Z. Y. Yin, Q. Y. Yan, H. Zhang, *Small* **2014**, *10*, 3480; b) D. Chen, W. Chen, L. Ma, G. Ji, K. Chang, J. Y. Lee, *Mater. Today* **2014**, *17*, 184; c) Mahmood, C. Zhang, H. Yin, Y. Hou, *J.Mater. Chem. A* **2014**, *2*, 15; d) W. W. Sun, Y. Wang, *Nanoscale* **2014**, *6*, 11528.
[63] R. Yi, J. Feng, D. Lv, M. L. Gordin, S. Chen, D. Choi, D. Wang, *Nano Energy* **2013**, *2*, 498.
[64] H. Xiong, M. D. Slater, M. Balasubramanian, C. S. Johnson, T. Rajh, *J. Phys. Chem. Lett.* **2011**, *2*, 2560.
[65] Y. Xu, E. Memarzadeh Lotfabad, H. Wang, B. Farbod, Z. Xu, A. Kohandehghan, D. Mitlin, *Chem. Commun.* **2013**, *49*, 8973.
[66] D. H. Wang, D. W. Choi, J. Li, Z. G. Yang, Z. M. Nie, R. Kou, D. H. Hu, C. M. Wang, L. V. Saraf, J. G. Zhang, I. A. Aksay, J. Liu, *ACS Nano* **2009**, *3*, 907.
[67] D. W. Choi, D. H. Wang, V. V. Viswanathan, I. T. Bae, W. Wang, Z. M. Nie, J. G. Zhang, G. L. Graff, J. Liu, Z. G. Yang, T. Duong, *Electrochem. Commun.* **2010**, *12*, 378.
[68] S. Yang, X. Feng, K. Müllen, *Adv. Mater.* **2011**, *23*, 3575.
[69] J. Qiu, P. Zhang, M. Ling, S. Li, P. Liu, H. Zhao, S. Zhang, *ACS Appl. Mater. Interfaces* **2012**, *4*, 3636.
[70] M. M. Zhen, X. J. Guo, G. D. Gao, Z. Zhou, L. Liu, *Chem. Commun.* **2014**, *50*, 11915.
[71] C. M. Ban, M. Xie, X. Sun, J. J. Travis, G. K. Wang, H. T. Sun, A. C. Dillon, J. Lian, S. M. George, *Nanotechnology* **2013**, *24*, 424002.
[72] X. Jiang, X. L. Yang, Y. H. Zhu, H. L. Jiang, Y. F. Yao, P. Zhao, C. Z. Li, *J.Mater. Chem. A* **2014**, *2*, 11124.
[73] J. Wang, L. F. Shen, H. S. Li, X. Y. Wang, P. Nie, B. Ding, G. Y. Xu, H. Dou, X. G. Zhang, *Electrochim. Acta* **2014**, *133*, 209.
[74] J. Wang, L. F. Shen, P. Nie, G. Y. Xu, B. Ding, S. Fang, H. Dou, X. G. Zhang, *J.Mater. Chem. A* **2014**, *2*, 9150.
[75] J. X. Qiu, C. Lai, Y. Z. Wang, S. Li, S. Q. Zhang, *Chem. Eng. J.* **2014**, *256*, 247.
[76] Y. M. Li, Z. G. Wang, X. J. Lv, *J.Mater. Chem. A* **2014**, *2*, 15473.
[77] Y. F. Tang, Z. Q. Liu, X. J. Lu, B. F. Wang, F. Q. Huang, *RSC Adv.* **2014**, *4*, 36372.
[78] B. C. Qiu, M. Y. Xing, J. L. Zhang, *J. Am. Chem. Soc.* **2014**, *136*, 5852.
[79] X. L. Li, Y. L. Zhang, T. T. Li, Q. N. Zhong, H. Y. Li, J. M. Huang, *J. Power Sources* **2014**, *268*, 372.
[80] Y. Luo, J. Luo, W. Zhou, X. Qi, H. Zhang, D. Y. W. Yu, C. M. Li, H. J. Fan, T. Yu, *J.Mater. Chem. A* **2013**, *1*, 273.
[81] N. Zhu, W. Liu, M. Xue, Z. Xie, D. Zhao, M. Zhang, J. Chen, T. Cao, *Electrochim. Acta* **2010**, *55*, 5813.
[82] Y. Shi, L. Wen, F. Li, H.-M. Cheng, *J. Power Sources* **2011**, *196*, 8610.
[83] Y. Oh, S. Nam, S. Wi, J. Kang, T. Hwang, S. Lee, H. H. Park, J. Cabana, C. Kim, B. Park, *J.Mater. Chem. A* **2014**, *2*, 2023.
[84] H. F. Ni, W. L. Song, L. Z. Fan, *Electrochem. Commun.* **2014**, *40*, 1.
[85] X. Li, P. X. Huang, Y. Zhou, H. Peng, W. Li, M. Z. Qu, Z. L. Yu, *Mater. Lett.* **2014**, *133*, 289.
[86] Y. C. Yang, B. H. Qiao, X. M. Yang, L. B. Fang, C. C. Pan, W. X. Song, H. S. Hou, X. B. Ji, *Adv. Funct. Mater.* **2014**, *24*, 4349.
[87] B. Zhang, Y. Yu, Y. S. Liu, Z. D. Huang, Y. B. He, J. K. Kim, *Nanoscale* **2013**, *5*, 2100.
[88] Y. Tang, L. Yang, Z. Qiu, J. Huang, *J. Mater. Chem.* **2009**, *19*, 5980.
[89] C. K. Chan, H. Peng, G. Liu, K. McIlwrath, X. F. Zhang, R. A. Huggins, Y. Cui, *Nat. Nanotechnol.* **2008**, *3*, 31.
[90] Y. Oumellal, A. Rougier, G. A. Nazri, J. M. Tarascon, L. Aymard, *Nat. Mater.* **2008**, *7*, 916.
[91] Y. D. Zhang, J. Xie, T. J. Zhu, G. S. Cao, X. B. Zhao, S. C. Zhang, *J. Power Sources* **2014**, *247*, 204.
[92] H. W. Song, H. Cui, C. X. Wang, *ACS Appl. Mater. Interfaces* **2014**, *6*, 13765.
[93] F. W. Yuan, H. Y. Tuan, *Chem. Mater.* **2014**, *26*, 2172.
[94] J. W. Qin, X. Wang, M. H. Cao, C. W. Hu, *Chem. – Eur. J.* **2014**, *20*, 9675.
[95] X. Li, M. Gu, S. Hu, R. Kennard, P. Yan, X. Chen, C. Wang, M. J. Sailor, J.-G. Zhang, J. Liu, *Nat. Commun.* **2014**, *5*, 4105.
[96] K. Ogata, E. Salager, C. J. Kerr, A. E. Fraser, C. Ducati, A. J. Morris, S. Hofmann, C. P. Grey, *Nat. Commun.* **2014**, *5*, 3127.

[97] L. L. Luo, J. S. Wu, J. Y. Luo, J. X. Huang, V. P. Dravid, *Sci. Rep.* **2014**, *4*, 3863.
[98] a) H. S. Im, Y. J. Cho, Y. R. Lim, C. S. Jung, D. M. Jang, J. Park, F. Shojaei, H. S. Kang, *ACS Nano* **2013**, *7*, 11103; b) Y. Zhao, X. F. Li, B. Yan, D. J. Li, S. Lawes, X. L. Sun, *J. Power Sources* **2015**, *274*, 869.
[99] P. C. Lian, J. Y. Wang, D. D. Cai, G. X. Liu, Y. Y. Wang, H. H. Wang, *J. Alloys Compd.* **2014**, *604*, 188.
[100] X. Y. Zhou, Y. L. Zou, J. Yang, *J. Power Sources* **2014**, *253*, 287.
[101] F. R. Beck, R. Epur, D. H. Hong, A. Manivannan, P. N. Kumta, *Electrochim. Acta* **2014**, *127*, 299.
[102] H. X. Yang, L. Li, *J. Alloys Compd.* **2014**, *584*, 76.
[103] J. Qin, C. N. He, N. Q. Zhao, Z. Y. Wang, C. S. Shi, E. Z. Liu, J. J. Li, *ACS Nano* **2014**, *8*, 1728.
[104] X. Y. Zheng, W. Lv, Y. B. He, C. Zhang, W. Wei, Y. Tao, B. H. Li, Q. H. Yang, *J. Nanomater.* **2014**, *2014*, 974285.
[105] N. Li, H. W. Song, H. Cui, C. X. Wang, *Nano Energy* **2014**, *3*, 102.
[106] a) C. K. Chan, H. Peng, G. Liu, K. McIlwrath, X. F. Zhang, R. A. Huggins, Y. Cui, *Nat. Nanotechnol.* **2008**, *3*, 31; b) N. Liu, Z. Lu, J. Zhao, M. T. McDowell, H.-W. Lee, W. Zhao, Y. Cui, *Nat. Nanotechnol.* **2014**, *9*, 187; c) A. Magasinski, P. Dixon, B. Hertzberg, A. Kvit, J. Ayala, G. Yushin, *Nat. Mater.* **2010**, *9*, 353.
[107] Y. S. Ye, X. L. Xie, J. Rick, F. C. Chang, B. J. Hwang, *J. Power Sources* **2014**, *247*, 991.
[108] H. Tang, J. P. Tu, X. Y. Liu, Y. J. Zhang, S. Huang, W. Z. Li, X. L. Wang, C. D. Gu, *J. Mater. Chem. A* **2014**, *2*, 5834.
[109] Z. F. Li, H. Y. Zhang, Q. Liu, Y. D. Liu, L. Stanciu, J. Xie, *ACS Appl. Mater. Interfaces* **2014**, *6*, 5996.
[110] S. H. Park, H. K. Kim, D. J. Ahn, S. I. Lee, K. C. Roh, K. B. Kim, *Electrochem. Commun.* **2013**, *34*, 117.
[111] a) R. C. de Guzman, J. H. Yang, M. M. C. Cheng, S. O. Salley, K. Y. S. Ng, *J. Power Sources* **2014**, *246*, 335; b) H. Li, C. X. Lu, *New Carbon Mater.* **2014**, *29*, 295.
[112] H. Li, C.-x. Lu, *Carbon* **2015**, *81*, 851.
[113] K. Eom, T. Joshi, A. Bordes, I. Do, T. F. Fuller, *J. Power Sources* **2014**, *249*, 118.
[114] J. B. Chang, X. K. Huang, G. H. Zhou, S. M. Cui, P. B. Hallac, J. W. Jiang, P. T. Hurley, J. H. Chen, *Adv. Mater.* **2014**, *26*, 758.
[115] F. Maroni, R. Raccichini, A. Birrozzi, G. Carbonari, R. Tossici, F. Croce, R. Marassi, F. Nobili, *J. Power Sources* **2014**, *269*, 873.
[116] J. K. Lee, K. B. Smith, C. M. Hayner, H. H. Kung, *Chem. Commun.* **2010**, *46*, 2025.
[117] V. C. Tung, M. J. Allen, Y. Yang, R. B. Kaner, *Nat. Nanotechnol.* **2009**, *4*, 25.
[118] H. Li, C. X. Lu, C. L. Ma, B. P. Zhang, *Funct. Mater. Lett.* **2014**, *7*, 1350067.
[119] R. Z. Hu, W. Sun, Y. L. Chen, M. Q. Zeng, M. Zhu, *J.Mater. Chem. A* **2014**, *2*, 9118.
[120] H. W. Mi, Y. L. Li, P. Y. Zhu, X. Y. Chai, L. N. Sun, H. T. Zhuo, Q. L. Zhang, C. X. He, J. H. Liu, *J. Mater. Chem. A* **2014**, *2*, 11254.
[121] M. R. Su, Z. X. Wang, H. J. Guo, X. H. Li, S. L. Huang, W. Xiao, L. Gan, *Electrochim. Acta* **2014**, *116*, 230.
[122] Y. Chen, X. J. Zhang, Y. H. Tian, X. Zhao, *J. Nanomater.* **2014**,*2014*, 734751.
[123] V. Chabot, K. Feng, H. W. Park, F. M. Hassan, A. R. Elsayed, A. P. Yu, X. C. Xiao, Z. W. Chen, *Electrochim. Acta* **2014**, *130*, 127.
[124] J. Shin, K. Park, W. H. Ryu, J. W. Jung, I. D. Kim, *Nanoscale* **2014**, *6*, 12718.
[125] A. R. Park, J. S. Kim, K. S. Kim, K. Zhang, J. Park, J. H. Park, J. K. Lee, P. J. Yoo, *ACS Appl. Mater. Interfaces* **2014**, *6*, 1702.
[126] Z. L. Xu, B. Zhang, Z. Q. Zhou, S. Abouali, M. A. Garakani, J. Q. Huang, J. K. Kim, *RSC Adv.* **2014**, *4*, 22359.
[127] H. J. Kim, S. E. Lee, J. Lee, J. Y. Jung, E. S. Lee, J. H. Choi, J. H. Jung, M. Oh, S. Hyun, D. G. Choi, *Phys. E* **2014**, *61*, 204.
[128] P. Wu, H. Wang, Y. W. Tang, Y. M. Zhou, T. H. Lu, *ACS Appl. Mater. Interfaces* **2014**, *6*, 3546.
[129] H. C. Tao, X. L. Yang, L. L. Zhang, S. B. Ni, *Mater. Chem. Phys* **2014**, *147*, 528.
[130] D. P. Wong, R. Suriyaprabha, R. Yuvakumar, V. Rajendran, Y. T. Chen, B. J. Hwang, L. C. Chen, K. H. Chen, *J. Mater. Chem. A* **2014**, *2*, 13437.
[131] X. Xin, X. F. Zhou, F. Wang, X. Y. Yao, X. X. Xu, Y. M. Zhu, Z. P. Liu, *J. Mater. Chem.* **2012**, *22*, 7724.
[132] R. Yi, J. T. Zai, F. Dai, M. L. Gordin, D. H. Wang, *Nano Energy* **2014**, *6*, 211.
[133] D. Chen, R. Yi, S. R. Chen, T. Xu, M. L. Gordin, D. H. Wang, *Solid State Ionics* **2014**, *254*, 65.
[134] T. Song, J. Xia, J.-H. Lee, D. H. Lee, M.-S. Kwon, J.-M. Choi, J. Wu, S. K. Doo, H. Chang, W. I. Park, D. S. Zang, H. Kim, Y. Huang, K.-C. Hwang, J. A. Rogers, U. Paik, *Nano Lett.* **2010**, *10*, 1710.
[135] H. Kim, X. Huang, Z. Wen, S. Cui, X. Guo, J. Chen, *J.Mater. Chem. A* **2015**, *3*, 1947.
[136] M. Ko, S. Chae, S. Jeong, P. Oh, J. Cho, *ACS Nano* **2014**, *8*, 8591.
[137] N. Li, S. X. Jin, Q. Y. Liao, H. Cu, C. X. Wang, *Nano Energy* **2014**, *5*, 105.
[138] F. M. Hassan, A. R. Elsayed, V. Chabot, R. Batmaz, X. C. Xiao, Z. W. Chen, *ACS Appl. Mater. Interfaces* **2014**, *6*, 13757.
[139] F. Li, H. W. Yue, Z. B. Yang, X. W. Li, Y. L. Qin, D. Y. He, *Mater. Lett.* **2014**, *128*, 132.
[140] M. Chhowalla, H. S. Shin, G. Eda, L.-J. Li, K. P. Loh, H. Zhang, *Nat. Chem.* **2013**, *5*, 263.
[141] J. Kibsgaard, Z. Chen, B. N. Reinecke, T. F. Jaramillo, *Nat. Mater.* **2012**, *11*, 963.
[142] J. G. Ren, C. D. Wang, Q. H. Wu, X. Liu, Y. Yang, L. F. He, W. J. Zhang, *Nanoscale* **2014**, *6*, 3353.
[143] W. Wu, L. Wang, Y. Li, F. Zhang, L. Lin, S. Niu, D. Chenet, X. Zhang, Y. Hao, T. F. Heinz, J. Hone, Z. L. Wang, *Nature* **2014**, *514*, 470.
[144] R. Wang, C. Xu, J. Sun, Y. Liu, L. Gao, H. Yao, C. Lin, *Nano Energy* **2014**, *8*, 183.
[145] J. Guo, X. Chen, Y. J. Yi, W. Z. Li, C. H. Liang, *RSC Adv.* **2014**, *4*, 16716.
[146] K. Rana, J. Singh, J. T. Lee, J. H. Park, J. H. Ahn, *ACS Appl. Mater. Interfaces* **2014**, *6*, 11158.
[147] Y. Hou, J. Y. Li, Z. H. Wen, S. M. Cui, C. Yuan, J. H. Chen, *Nano Energy* **2014**, *8*, 157.
[148] L. Ma, G. Huang, W. Chen, Z. Wang, J. Ye, H. Li, D. Chen, J. Y. Lee, *J. Power Sources* **2014**, *264*, 262.
[149] Y. C. Liu, Y. P. Zhao, L. F. Jiao, J. Chen, *J.Mater. Chem. A* **2014**, *2*, 13109.
[150] K. Shiva, H. Matte, H. B. Rajendra, A. J. Bhattacharyya, C. N. R. Rao, *Nano Energy* **2013**, *2*, 787.
[151] D. W. Su, S. X. Dou, G. X. Wang, *Chem. Commun.* **2014**, *50*, 4192.
[152] R. J. Chen, T. Zhao, W. P. Wu, F. Wu, L. Li, J. Qian, R. Xu, H. M. Wu, H. M. Albishri, A. S. Al-Bogami, D. Abd El-Hady, J. Lu, K. Amine, *Nano Lett.* **2014**, *14*, 5899.
[153] W. D. Qiu, J. Xia, H. M. Zhong, S. X. He, S. H. Lai, L. P. Chen, *Electrochim. Acta* **2014**, *137*, 197.
[154] G. C. Huang, T. Chen, Z. Wang, K. Chang, W. X. Chen, *J. Power Sources* **2013**, *235*, 122.
[155] C. Feng, L. Zhang, Z. Wang, X. Song, K. Sun, F. Wu, G. Liu, *J. Power Sources* **2014**, *269*, 550.
[156] Y. Du, Z. Yin, J. Zhu, X. Huang, X.-J. Wu, Z. Zeng, Q. Yan, H. Zhang, *Nat. Commun.* **2012**, *3*, 1177.
[157] X. Xu, S. Jeong, C. S. Rout, P. Oh, M. Ko, H. Kim, M. G. Kim, R. Cao, H. S. Shin, J. Cho, *J. Mater. Chem. A* **2014**, *2*, 10847.
[158] S. F. Kong, Z. T. Jin, H. Liu, Y. Wang, *J. Phys. Chem. C* **2014**, *118*, 25355.

[159] Z. P. Li, W. Y. Li, H. T. Xue, W. P. Kang, X. Yang, M. L. Sun, Y. B. Tang, C. S. Lee, *RSC Adv.* **2014**, *4*, 37180.
[160] C. B. Zhu, X. K. Mu, P. A. van Aken, Y. Yu, J. Maier, *Angew. Chem., Int. Ed.* **2014**, *53*, 2152.
[161] L. David, R. Bhandavat, G. Singh, *ACS Nano* **2014**, *8*, 1759.
[162] B. H. Qu, C. Z. Ma, G. Ji, C. H. Xu, J. Xu, Y. S. Meng, T. H. Wang, J. Y. Lee, *Adv. Mater.* **2014**, *26*, 3854.
[163] a) D. Aurbach, A. Nimberger, B. Markovsky, E. Levi, E. Sominski, A. Gedanken, *Chem. Mater.* **2002**, *14*, 4155; b) G. F. Ortiz, I. Hanzu, P. Lavela, P. Knauth, J. L. Tirado, T. Djenizian, *Chem. Mater.* **2010**, *22*, 1926; c) J. Y. Huang, L. Zhong, C. M. Wang, J. P. Sullivan, W. Xu, L. Q. Zhang, S. X. Mao, N. S. Hudak, X. H. Liu, A. Subramanian, H. Fan, L. Qi, A. Kushima, J. Li, *Science* **2010**, *330*, 1515.
[164] M. Shahid, N. Yesibolati, M. C. Reuter, F. M. Ross, H. N. Alshareef, *J. Power Sources* **2014**, *263*, 239.
[165] S.-M. Paek, E. Yoo, I. Honma, *Nano Lett.* **2008**, *9*, 72.
[166] D. Wang, R. Kou, D. Choi, Z. Yang, Z. Nie, J. Li, L. V. Saraf, D. Hu, J. Zhang, G. L. Graff, J. Liu, M. A. Pope, I. A. Aksay, *ACS Nano* **2010**, *4*, 1587.
[167] H. Yang, Z. H. Hou, N. B. Zhou, B. H. He, J. G. Cao, Y. F. Kuang, *Ceram. Int.* **2014**, *40*, 13903.
[168] J. Yao, X. Shen, B. Wang, H. Liu, G. Wang, *Electrochem. Commun.* **2009**, *11*, 1849.
[169] X. Wang, X. Zhou, K. Yao, J. Zhang, Z. Liu, *Carbon* **2011**, *49*, 133.
[170] A. M. Tripathi, S. Mitra, *ChemElectroChem* **2014**, *1*, 1327.
[171] Y. Li, X. Lv, J. Lu, J. Li, *The J. Phys. Chem. C* **2010**, *114*, 21770.
[172] X. Zhu, Y. Zhu, S. Murali, M. D. Stoller, R. S. Ruoff, *J. Power Sources* **2011**, *196*, 6473.
[173] G. L. Wu, M. B. Wu, D. Wang, L. H. Yin, J. S. Ye, S. Z. Deng, Z. Y. Zhu, W. J. Ye, Z. T. Li, *Appl. Surf. Sci.* **2014**, *315*, 400.
[174] J. X. Guo, B. Jiang, X. Zhang, H. T. Liu, *J. Power Sources* **2014**, *262*, 15.
[175] C. Xu, J. Sun, L. Gao, *J. Mater. Chem.* **2012**, *22*, 975.
[176] Q. Guo, S. S. Chen, X. Qin, *Mater. Lett.* **2014**, *119*, 4.
[177] M. Ara, K. Wadumesthrige, T. J. Meng, S. O. Salley, K. Y. S. Ng, *RSC Adv.* **2014**, *4*, 20540.
[178] J. Zhu, Z. Lu, M. O. Oo, H. H. Hng, J. Ma, H. Zhang, Q. Yan, *J. Mater. Chem.* **2011**, *21*, 12770.
[179] C. Tan, J. Cao, A. M. Khattak, F. Cai, B. Jiang, G. Yang, S. Hu, *J. Power Sources* **2014**, *270*, 28.
[180] a) Y. Chen, B. H. Song, R. M. Chen, L. Lu, J. M. Xue, *J. Mater. Chem. A* **2014**, *2*, 5688; b) N. Li, H. Sonsg, H. Cui, C. Wang, *Electrochim. Acta* **2014**, *130*, 670; c) Y. Chen, B. Song, R. M. Chen, L. Lu, J. Xue, *J. Mater. Chem. A* **2014**, *2*, 5688.
[181] A. Bhaskar, M. Deepa, M. Ramakrishna, T. N. Rao, *J. Phys. Chem. C* **2014**, *118*, 7296.
[182] C. Zhong, J. Wang, Z. Chen, H. Liu, *J. Phys. Chem. C* **2011**, *115*, 25115.
[183] X. Huang, X. Zhou, L. Zhou, K. Qian, Y. Wang, Z. Liu, C. Yu, *ChemPhysChem* **2011**, *12*, 278.
[184] S.-Y. L. Jian Xie, Xue-Fei Chen, Yun-Xiao Zheng, Wen-Tao Song, Gao-Shao Cao, Tie-Jun Zhu, Xin-Bing Zhao, *Int. J. Electrochem. Sci.* **2011**, *6*, 5539.
[185] J. Zhu, G. H. Zhang, X. Z. Yu, Q. H. Li, B. A. Lu, Z. Xu, *Nano Energy* **2014**, *3*, 80.
[186] P. Lian, X. Zhu, S. Liang, Z. Li, W. Yang, H. Wang, *Electrochim. Acta* **2011**, *56*, 4532.
[187] P. C. Lian, J. Y. Wang, D. D. Cai, L. X. Ding, Q. M. Jia, H. H. Wang, *Electrochim. Acta* **2014**, *116*, 103.
[188] F. H. Du, Y. S. Liu, J. Long, Q. C. Zhu, K. X. Wang, X. Wei, J. S. Chen, *Chem. Commun.* **2014**, *50*, 9961.
[189] S. Baek, S. H. Yu, S. K. Park, A. Pucci, C. Marichy, D. C. Lee, Y. E. Sung, Y. Z. Piao, N. Pinna, *RSC Adv.* **2012**, *2*, 13038.
[190] R. Thomas, G. M. Rao, *Electrochim. Acta* **2014**, *125*, 380.
[191] H. L. Lu, N. W. Li, M. B. Zheng, L. Qiu, S. T. Zhang, J. F. Zheng, G. B. Ji, J. M. Cao, *Mater. Lett.* **2014**, *115*, 125.
[192] J. J. Tang, J. Yang, L. M. Zhou, J. Xie, G. H. Chen, X. Y. Zhou, *J. Mater. Chem. A* **2014**, *2*, 6292.
[193] S. S. Chen, X. Qin, *J. Solid State Electrochem.* **2014**, *18*, 2893.
[194] Q. Guo, S. S. Chen, X. Qin, *Mater. Lett.* **2014**, *128*, 50.
[195] J. Zhao, W. F. Shan, X. B. Xia, Q. Wang, L. L. Xing, *Sci. China: Technol. Sci.* **2014**, *57*, 1081.
[196] J. F. Liang, W. Wei, D. Zhong, Q. L. Yang, L. D. Li, L. Guo, *ACS Appl. Mater. Interfaces* **2012**, *4*, 454.
[197] Y. C. Yang, X. B. Ji, F. Lu, Q. Y. Chen, C. E. Banks, *Phys. Chem. Chem. Phys.* **2013**, *15*, 15098.
[198] T. Gao, K. Huang, X. Qi, H. X. Li, L. W. Yang, J. X. Zhong, *Ceram. Int.* **2014**, *40*, 6891.
[199] S. Li, Y. Z. Wang, C. Lai, J. X. Qiu, M. Ling, W. Martens, H. J. Zhao, S. Q. Zhang, *J. Mater. Chem. A* **2014**, *2*, 10211.
[200] A. Bhaskar, M. Deepa, M. Ramakrishna, T. N. Rao, *The J. Phys. Chem. C* **2014**, *118*, 7296.
[201] D. P. Cai, T. Yang, B. Liu, D. D. Wang, Y. Liu, L. L. Wang, Q. H. Li, T. H. Wang, *J. Mater. Chem. A* **2014**, *2*, 13990.
[202] G. L. Wu, Z. T. Li, W. T. Wu, M. B. Wu, *J. Alloys Compd.* **2014**, *615*, 582.
[203] H. J. Zhang, P. P. Xu, Y. Ni, H. Y. Geng, G. H. Zheng, B. Dong, Z. Jiao, *J. Mater. Res.* **2014**, *29*, 617.
[204] X. Huang, B. Sun, K. Li, S. Chen, G. Wang, *J. Mater. Chem. A* **2013**, *1*, 13484.
[205] H. C. Tao, X. L. Yang, L. L. Zhang, S. B. Ni, *J. Electroanal. Chem.* **2014**, *728*, 134.
[206] Q. Wang, Y. X. Nie, B. He, L. L. Xing, X. Y. Xue, *Solid State Sci.* **2014**, *31*, 81.
[207] Y. Gu, Y. Wang, *RSC Adv.* **2014**, *4*, 8582.
[208] G. D. Park, S. H. Choi, J. K. Lee, Y. C. Kang, *Chem. – Eur. J.* **2014**, *20*, 12183.
[209] X. S. Tang, X. Y. Yao, Y. Chen, B. H. Song, D. Zhou, J. H. Kong, C. Y. Zhao, X. H. Lu, *J. Power Sources* **2014**, *257*, 90.
[210] W. Wang, L. W. Hu, J. B. Ge, Z. Q. Hu, H. B. Sun, H. Sun, H. Q. Zhang, H. M. Zhu, S. Q. Jiao, *Chem. Mater.* **2014**, *26*, 3721.
[211] X. Wang, B. L. Li, D. P. Liu, H. M. Xiong, *Sci. China: Chem.* **2014**, *57*, 122.
[212] L. S. Zhang, Q. L. Bai, L. Z. Wang, A. Q. Zhang, Y. Zhang, Y. Xing, *Funct. Mater. Lett.* **2014**, *7*, 1450010.
[213] C. H. Kim, Y. S. Jung, K. T. Lee, J. H. Ku, S. M. Oh, *Electrochim. Acta* **2009**, *54*, 4371.
[214] D. P. Lv, M. L. Gordin, R. Yi, T. Xu, J. X. Song, Y. B. Jiang, D. Choi, D. H. Wang, *Adv. Funct. Mater.* **2014**, *24*, 1059.
[215] S. Wu, R. Wang, Z. Wang, Z. Lin, *Nanoscale* **2014**, *6*, 8350.
[216] G. H. Lee, J. C. Kim, D. H. Lee, S. D. Seo, H. W. Shim, D. W. Kim, *ChemElectroChem* **2014**, *1*, 673.
[217] R. Wang, S. Wu, Y. Lv, Z. Lin, *Langmuir* **2014**, *30*, 8215.
[218] F. Zou, X. L. Hu, L. Qie, Y. Jiang, X. Q. Xiong, Y. Qiao, Y. H. Huang, *Nanoscale* **2014**, *6*, 924.
[219] J. K. Feng, C. S. Wang, Y. T. Qian, *Mater. Lett.* **2014**, *122*, 327.
[220] J. Wang, C. Q. Feng, Z. Q. Sun, S. L. Chou, H. K. Liu, J. Z. Wang, *Sci. Rep.* **2014**, *4*, 7030.
[221] S. Jin, C. Wang, *Nano Energy* **2014**, *7*, 63.
[222] D. L. Ma, S. Yuan, X. L. Huang, Z. Y. Cao, *Energy Technol.* **2014**, *2*, 342.
[223] S. Wu, Q. Ma, F. He, *J. Am. Ceram. Soc.* **2013**, *96*, 2046.
[224] K. Wang, Y. Huang, Y. Y. Shen, L. L. Xue, H. J. Huang, H. W. Wu, Y. L. Wang, *Ceram. Int.* **2014**, *40*, 15183.
[225] Y. Zhao, Y. Huang, X. Sun, H. J. Huang, K. Wang, M. Zong, Q. F. Wang, *Electrochim. Acta* **2014**, *120*, 128.

[226] Z. M. Zheng, Y. L. Cheng, X. B. Yan, R. T. Wang, P. Zhang, *J. Mater. Chem. A* **2014**, *2*, 149.
[227] P. Xiong, B. R. Liu, V. Teran, Y. Zhao, L. L. Peng, X. Wang, G. H. Yu, *ACS Nano* **2014**, *8*, 8610.
[228] D. Pasero, N. Reeves, A. R. West, *J. Power Sources* **2005**, *141*, 156.
[229] C. Wang, L. Yin, D. Xiang, Y. Qi, *ACS Appl. Mater. Interfaces* **2012**, *4*, 1636.
[230] Z.-H. Wang, L.-X. Yuan, Q.-G. Shao, F. Huang, Y.-H. Huang, *Mater. Lett.* **2012**, *80*, 110.
[231] a) I. Nam, N. D. Kim, G. P. Kim, J. Park, J. Yi, *J. Power Sources* **2013**, *244*, 56; b) H. Huang, L. Y. Zhang, Y. Xia, Y. P. Gan, X. Y. Tao, C. Liang, W. K. Zhang, *New J. Chem.* **2014**, *38*, 4743.
[232] H. Wang, L.-F. Cui, Y. Yang, H. Sanchez Casalongue, J. T. Robinson, Y. Liang, Y. Cui, H. Dai, *J. Am. Chem. Soc.* **2010**, *132*, 13978.
[233] N. Lavoie, P. R. L. Malenfant, F. M. Courtel, Y. Abu-Lebdeh, I. J. Davidson, *J. Power Sources* **2012**, *213*, 249.
[234] S. K. Park, A. Jin, S. H. Yu, J. Ha, B. Jang, S. Bong, S. Woo, Y. E. Sung, Y. Piao, *Electrochim. Acta* **2014**, *120*, 452.
[235] Y. S. Yun, H. J. Jin, *RSC Adv.* **2014**, *4*, 38310.
[236] M. V. Reddy, Z. Beichen, L. J. e. Nicholette, Z. Kaimeng, B. V. R. Chowdari, *Electrochem. Solid-State Lett.* **2011**, *14*, A79.
[237] M. Valvo, E. García-Tamayo, U. Lafont, E. M. Kelder, *J. Power Sources* **2011**, *196*, 10191.
[238] Z.-S. Wu, W. Ren, L. Wen, L. Gao, J. Zhao, Z. Chen, G. Zhou, F. Li, H.-M. Cheng, *ACS Nano* **2010**, *4*, 3187.
[239] B. Li, H. Cao, J. Shao, G. Li, M. Qu, G. Yin, *Inorg. Chem.* **2011**, *50*, 1628.
[240] L. Y. Pan, H. B. Zhao, W. C. Shen, X. W. Dong, J. Q. Xu, *J. Mater. Chem. A* **2013**, *1*, 7159.
[241] L. F. Lai, J. X. Zhu, Z. G. Li, D. Y. W. Yu, S. R. Jiang, X. Y. Cai, Q. Y. Yan, Y. M. Lam, Z. X. Shen, J. Y. Lin, *Nano Energy* **2014**, *3*, 134.
[242] J. X. Zhu, Y. K. Sharma, Z. Y. Zeng, X. J. Zhang, M. Srinivasan, S. Mhaisalkar, H. Zhang, H. H. Hng, Q. Y. Yan, *J. Phys. Chem. C* **2011**, *115*, 8400.
[243] K. H.Kim, D. W.Tung, V. H. Phm, J. S. Chung, B. S.Kong, J. K.Lee, K. Kim, E. S. Oh, *Electrochim. Acta* **2012**, *69*, 358.
[244] H. T. Sun, X. Sun, T. Hu, M. P. Yu, F. Y. Lu, J. Lian, *J. Phys. Chem. C* **2014**, *118*, 2263.
[245] L. Li, G. M. Zhou, X. Y. Shan, S. F. Pei, F. Li, H. M. Cheng, *J. Power Sources* **2014**, *255*, 52.
[246] L. N. Wang, H. Wang, J. C. Wang, J. B. Bai, *Synth. React. Inorg., Met.-Org., Nano-Met. Chem.* **2015**, *45*, 614.
[247] Q. Wang, C.-Y. Zhang, X.-B. Xia, L.-L. Xing, X.-Y. Xue, *Mater. Lett.* **2013**, *112*, 162.
[248] H. Y. Sun, Y. G. Liu, Y. L. Yu, M. Ahmad, D. Nan, J. Zhu, *Electrochim. Acta* **2014**, *118*, 1.
[249] M. A. Garakani, S. Abouali, B. Zhang, C. A. Takagi, Z. L. Xu, J. Q. Huang, J. K. Kim, *ACS Appl. Mater. Interfaces* **2014**, *6*, 18971.
[250] G.-P. Kim, I. Nam, N. D. Kim, J. Park, S. Park, J. Yi, *Electrochem. Commun.* **2012**, *22*, 93.
[251] T. Hu, G. Q. Xin, H. T. Sun, X. Sun, M. P. Yu, C. S. Liu, J. Lian, *RSC Adv.* **2014**, *4*, 1521.
[252] D. F. Qiu, G. Bu, B. Zhao, Z. X. Lin, L. Pu, L. J. Pan, Y. Shi, *Mater. Lett.* **2014**, *119*, 12.
[253] S. Q. Chen, Y. Wang, *J. Mater. Chem.* **2010**, *20*, 9735.
[254] F. Sun, K. Huang, X. Qi, T. Gao, Y. P. Liu, X. H. Zou, J. X. Zhong, *Ceram. Int.* **2014**, *40*, 2523.
[255] K. H. Park, D. Lee, J. Kim, J. Song, Y. M. Lee, H. T. Kim, J. K. Park, *Nano Lett.* **2014**, *14*, 4306.
[256] X. Zhou, J. Shi, Y. Liu, Q. Su, J. Zhang, G. Du, *Electrochim. Acta* **2014**, *143*, 175.
[257] B. G. Choi, S.-J. Chang, Y. B. Lee, J. S. Bae, H. J. Kim, Y. S. Huh, *Nanoscale* **2012**, *4*, 5924.
[258] R. Wang, C. Xu, J. Sun, Y. Liu, L. Gao, C. Lin, *Nanoscale* **2013**, *5*, 6960.
[259] P. L. Taberna, S. Mitra, P. Poizot, P. Simon, J. M. Tarascon, *Nat. Mater.* **2006**, *5*, 567.
[260] H. Liu, G. Wang, J. Wang, D. Wexler, *Electrochem. Commun.* **2008**, *10*, 1879.
[261] A. P. Hu, X. H. Chen, Q. L. Tang, B. Zeng, *Ceram. Int.* **2014**, *40*, 14713.
[262] Y. H. Chang, J. Li, B. Wang, H. Luo, L. J. Zhi, *J. Mater. Sci. Technol.* **2014**, *30*, 759.
[263] Y. Li, S. M. Zhu, Z. Y. Yu, Q. Meng, T. Zhang, Q. L. Liu, J. J. Gu, W. Zhang, T. Lu, C. L. Zhu, Z. P. Guo, J. Ma, D. Zhang, *Sci. Adv. Mater.* **2014**, *6*, 283.
[264] J. P. Zhao, B. J. Yang, Z. M. Zheng, J. Yang, Z. Yang, P. Zhang, W. C. Ren, X. B. Yan, *ACS Appl. Mater. Interfaces* **2014**, *6*, 9890.
[265] C. J. Fu, G. G. Zhao, H. J. Zhang, S. Li, *Int. J. Electrochem. Sci.* **2014**, *9*, 46.
[266] T. Q. Wang, X. L. Wang, Y. Lu, Q. Q. Xiong, X. Y. Zhao, J. B. Cai, S. Huang, C. D. Gu, J. P. Tu, *RSC Adv.* **2014**, *4*, 322.
[267] J. W. Yin, H. M. Shi, P. Wu, Q. Y. Zhu, H. Wang, Y. W. Tang, Y. M. Zhou, T. H. Lu, *New J. Chem.* **2014**, *38*, 4036.
[268] D. Chen, G. Ji, Y. Ma, J. Y. Lee, J. Lu, *ACS Appl. Mater. Interfaces* **2011**, *3*, 3078.
[269] Y. H. Chang, J. Li, B. Wang, H. Luo, H. Y. He, Q. Song, L. J. Zhi, *J. Mater. Chem. A* **2013**, *1*, 14658.
[270] B. Jin, G. Y. Chen, X. B. Zhong, Y. Liu, K. Y. Zhou, P. Sun, P. Lu, W. X. Zhang, J. C. Liang, *Ceram. Int.* **2014**, *40*, 10359.
[271] M. P. Deosarkar, S. M. Pawar, B. A. Bhanvase, *Chem. Eng. Process.* **2014**, *83*, 49.
[272] G. Zhou, D.-W. Wang, F. Li, L. Zhang, N. Li, Z.-S. Wu, L. Wen, G. Q. Lu, H.-M. Cheng, *Chem. Mater.* **2010**, *22*, 5306.
[273] D. L. Ma, S. Yuan, Z. Y. Cao, *Chin. Sci. Bull.* **2014**, *59*, 2017.
[274] X. D. Huang, B. Sun, S. Q. Chen, G. X. Wang, *Chem. – Asian J.* **2014**, *9*, 206.
[275] S. H. Yu, D. E. Conte, S. Baek, D. C. Lee, S. K. Park, K. J. Lee, Y. Piao, Y. E. Sung, N. Pinna, *Adv. Funct. Mater.* **2013**, *23*, 4293.
[276] S. S. Tao, W. B. Yue, M. Y. Zhong, Z. J. Chen, Y. Ren, *ACS Appl. Mater. Interfaces* **2014**, *6*, 6332.
[277] S. Bhuvaneswari, P. M. Pratheeksha, S. Anandan, D. Rangappa, R. Gopalan, T. N. Rao, *Phys. Chem. Chem. Phys.* **2014**, *16*, 5284.
[278] W. Jiang, F. Liang, J. W. Wang, L. Su, Y. M. Wu, L. M. Wang, *RSC Adv.* **2014**, *4*, 15394.
[279] P. Lian, X. Zhu, H. Xiang, Z. Li, W. Yang, H. Wang, *Electrochim. Acta* **2010**, *56*, 834.
[280] L. H. Zhuo, Y. Q. Wu, L. Y. Wang, J. Ming, Y. C. Yu, X. B. Zhang, F. Y. Zhao, *J. Mater. Chem. A* **2013**, *1*, 3954.
[281] Q. Zhou, Z. B. Zhao, Z. Y. Wang, Y. F. Dong, X. Z. Wang, Y. Gogotsi, J. S. Qiu, *Nanoscale* **2014**, *6*, 2286.
[282] P. R. Kumar, P. Kollu, C. Santhosh, K. E. V. Rao, D. K. Kim, A. N. Grace, *New J. Chem.* **2014**, *38*, 3654.
[283] S. Y. Liu, J. Xie, C. C. Fang, G. S. Cao, T. J. Zhu, X. B. Zhao, *J. Mater. Chem.* **2012**, *22*, 19738.
[284] S. M. Li, B. Wang, J. H. Liu, M. Yu, *Electrochim. Acta* **2014**, *129*, 33.
[285] B. Wang, S. M. Li, J. H. Liu, M. Yu, B. Li, X. Y. Wu, *Electrochim. Acta* **2014**, *146*, 679.
[286] E. K. Heidari, B. A. Zhang, M. H. Sohi, A. Ataie, J. K. Kim, *J. Mater. Chem. A* **2014**, *2*, 8314.
[287] Y. L. Xiao, J. T. Zai, X. M. Li, Y. Gong, B. Li, Q. Y. Han, X. F. Qian, *Nano Energy* **2014**, *6*, 51.
[288] Y. S. Fu, Q. Chen, M. Y. He, Y. H. Wan, X. Q. Sun, H. Xia, X. Wang, *Ind. Eng. Chem. Res.* **2012**, *51*, 11700.
[289] Y. C. Dong, Y. S. Chui, R. G. Ma, C. W. Cao, H. Cheng, Y. Y. Li, J. A. Zapien, *J. Mater. Chem. A* **2014**, *2*, 13892.

[290] Y. C. Dong, C. W. Cao, Y. S. Chui, J. A. Zapien, *Chem. Commun.* **2014**, *50*, 10151.
[291] Y. J. Chen, J. Zhu, B. H. Qu, B. A. Lu, Z. Xu, *Nano Energy* **2014**, *3*, 88.
[292] Y. J. Chen, M. Zhuo, J. W. Deng, Z. Xu, Q. H. Li, T. H. Wang, *J. Mater. Chem. A* **2014**, *2*, 4449.
[293] G. Gao, H. B. Wu, X. W. Lou, *Adv. Energy Mater.* **2014**, *4*, 1400422.
[294] W. P. Kang, Y. B. Tang, W. Y. Li, Z. P. Li, X. Yang, J. Xu, C. S. Lee, *Nanoscale* **2014**, *6*, 6551.
[295] N. Sivakumar, S. R. P. Gnanakan, K. Karthikeyan, S. Amaresh, W. S. Yoon, G. J. Park, Y. S. Lee, *J. Alloys Compd.* **2011**, *509*, 7038.
[296] H. Tang, P. B. Gao, A. Xing, S. Tian, Z. H. Bao, *RSC Adv.* **2014**, *4*, 28421.
[297] Y. L. Xiao, J. T. Zai, L. Q. Tao, B. Li, Q. Y. Han, C. Yu, X. F. Qian, *Phys. Chem. Chem. Phys.* **2013**, *15*, 3939.
[298] A. K. Rai, T. V. Thi, J. Gim, J. Kim, *Mater. Charact.* **2014**, *95*, 259.
[299] P. Poizot, S. Laruelle, S. Grugeon, L. Dupont, J. M. Tarascon, *Nature* **2007**, *407*, 496.
[300] M. Zhang, Y. Wang, M. Q. Jia, *Electrochim. Acta* **2014**, *129*, 425.
[301] M. Zhang, F. L. Yan, X. Tang, Q. H. Li, T. H. Wang, G. Z. Cao, *J. Mater. Chem. A* **2014**, *2*, 5890.
[302] X. Guan, J. Nai, Y. Zhang, P. Wang, J. Yang, L. Zheng, J. Zhang, L. Guo, *Chem. Mater.* **2014**, *26*, 5958.
[303] C.-T. Hsieh, C.-Y. Lin, J.-Y. Lin, *Electrochim. Acta* **2011**, *56*, 8861.
[304] T. H. Wu, F. Y. Tu, S. Q. Liu, S. X. Zhuang, G. H. Jin, C. Y. Pan, *J. Mater. Sci.* **2014**, *49*, 1861.
[305] K. Zhang, P. Han, L. Gu, L. Zhang, Z. Liu, Q. Kong, C. Zhang, S. Dong, Z. Zhang, J. Yao, H. Xu, G. Cui, L. Chen, *ACS Appl. Mater. Interfaces* **2012**, *4*, 658.
[306] D. Qiu, L. Ma, M. Zheng, Z. Lin, B. Zhao, Z. Wen, Z. Hu, L. Pu, Y. Shi, *Mater. Lett.* **2012**, *84*, 9.
[307] S. M. Lee, S. H. Choi, J. K. Lee, Y. C. Kang, *Electrochim. Acta* **2014**, *132*, 441.
[308] G. Zhou, D.-W. Wang, L.-C. Yin, N. Li, F. Li, H.-M. Cheng, *ACS Nano* **2012**, *6*, 3214.
[309] I. R. M. Kottegoda, N. H. Idris, L. Lu, J.-Z. Wang, H.-K. Liu, *Electrochim. Acta* **2011**, *56*, 5815.
[310] Q. Wang, C. Y. Zhang, W. F. Shan, L. L. Xing, X. Y. Xue, *Mater. Lett.* **2014**, *118*, 66.
[311] Y. Huang, X.-l. Huang, J.-s. Lian, D. Xu, L.-m. Wang, X.-b. Zhang, *J. Mater. Chem.* **2012**, *22*, 2844.
[312] Y. Zou, Y. Wang, *Nanoscale* **2011**, *3*, 2615.
[313] Y. J. Mai, S. J. Shi, D. Zhang, Y. Lu, C. D. Gu, J. P. Tu, *J. Power Sources* **2012**, *204*, 155.
[314] D. Qiu, Z. Xu, M. Zheng, B. Zhao, L. Pan, L. Pu, Y. Shi, *J. Solid State Electrochem.* **2012**, *16*, 1889.
[315] X.-J. Zhu, J. Hu, H.-L. Dai, L. Ding, L. Jiang, *Electrochim. Acta* **2012**, *64*, 23.
[316] H. Geng, S. F. Kong, Y. Wang, *J.Mater. Chem. A* **2014**, *2*, 15152.
[317] J. Zhou, L. Ma, H. Song, B. Wu, X. Chen, *Electrochem. Commun.* **2011**, *13*, 1357.
[318] L. Q. Lu, Y. Wang, *J. Mater. Chem.* **2011**, *21*, 17916.
[319] L. Q. Lu, Y. Wang, *Electrochem. Commun.* **2012**, *14*, 82.
[320] Q. Wang, J. Zhao, W. F. Shan, X. B. Xia, L. L. Xing, X. Y. Xue, *J. Alloys Compd.* **2014**, *590*, 424.
[321] Y. J. Mai, X. L. Wang, J. Y. Xiang, Y. Q. Qiao, D. Zhang, C. D. Gu, J. P. Tu, *Electrochim. Acta* **2011**, *56*, 2306.
[322] X. Zhang, J. Zhou, H. Song, X. Chen, Y. V. Fedoseeva, A. V. Okotrub, L. G. Bulusheva, *ACS Appl. Mater. Interfaces* **2014**, *6*, 17236.
[323] X. Y. Zhou, J. Zhang, Q. M. Su, J. J. Shi, Y. Liu, G. H. Du, *Electrochim. Acta* **2014**, *125*, 615.
[324] Y. Qi, J. R. Eskelsen, U. Mazur, K. W. Hipps, *Langmuir* **2012**, *28*, 3489.
[325] B. Rangasamy, J. Y. Hwang, W. Choi, *Carbon* **2014**, *77*, 1065.
[326] L. L. Xu, S. W. Bian, K. L. Song, *J. Mater. Sci.* **2014**, *49*, 6217.
[327] R. Guo, W. B. Yue, Y. M. An, Y. Ren, X. Yan, *Electrochim. Acta* **2014**, *135*, 161.
[328] S. H. Choi, Y. N. Ko, J.-K. Lee, Y. C. Kang, *Sci. Rep.* **2014**, *4*,5786.
[329] X. Y. Zhou, J. J. Shi, Y. Liu, Q. M. Su, J. Zhang, G. H. Du, *J. Alloys Compd.* **2014**, *615*, 390.
[330] D. Larcher, C. Masquelier, D. Bonnin, Y. Chabre, V. Masson, J.-B. Leriche, J.-M. Tarascon, *J. Electrochem. Soc.* **2003**, *150*, A133.
[331] X.-Y. Xue, C.-H. Ma, C.-X. Cui, L.-L. Xing, *Solid State Sci.* **2011**, *13*, 1526.
[332] Y. Zou, J. Kan, Y. Wang, *The J. Phys. Chem. C* **2011**, *115*, 20747.
[333] B. Zhao, R. Z. Liu, X. H. Cai, Z. Jiao, M. H. Wu, X. T. Ling, B. Lu, Y. Jiang, *J. Appl. Electrochem.* **2014**, *44*, 53.
[334] H. W. Zhang, L. Zhou, C. Z. Yu, *RSC Adv.* **2014**, *4*, 495.
[335] C. Wu, H. Zhang, Y. X. Wu, Q. C. Zhuang, L. L. Tian, X. X. Zhang, *Electrochim. Acta* **2014**, *134*, 18.
[336] X. Zhu, X. Y. Song, X. L. Ma, G. Q. Ning, *ACS Appl. Mater. Interfaces* **2014**, *6*, 7189.
[337] B. Jang, O. B. Chae, S. K. Park, J. Ha, S. M. Oh, H. B. Na, Y. Piao, *J. Mater. Chem. A* **2013**, *1*, 15442.
[338] S. Liu, R. Wang, M. Liu, J. Luo, X. Jin, J. Sun, L. Gao, *J. Mater. Chem. A* **2014**, *2*, 4598.
[339] H. L. Fei, Z. W. Peng, L. Li, Y. Yang, W. Lu, E. L. G. Samuel, X. J. Fan, J. M. Tour, *Nano Res.* **2014**, *7*, 502.
[340] Y. Yang, X. J. Fan, G. Casillas, Z. W. Peng, G. D. Ruan, G. Wang, M. J. Yacaman, J. M. Tour, *ACS Nano* **2014**, *8*, 3939.
[341] M. Zhang, B. Qu, D. Lei, Y. Chen, X. Yu, L. Chen, Q. Li, Y. Wang, T. Wang, *J. Mater. Chem.* **2012**, *22*, 3868.
[342] D. Chen, W. Wei, R. Wang, J. Zhu, L. Guo, *New J. Chem.* **2012**, *36*, 1589.
[343] L. Tian, Q. Zhuang, J. Li, C. Wu, Y. Shi, S. Sun, *Electrochim. Acta* **2012**, *65*, 153.
[344] J. Lin, A. R. O. Raji, K. W. Nan, Z. W. Peng, Z. Yan, E. L. G. Samuel, D. Natelson, J. M. Tour, *Adv. Funct. Mater.* **2014**, *24*, 2044.
[345] O. Vargas, A. Caballero, J. Morales, *Electrochim. Acta* **2014**, *130*, 551.
[346] W. B. Yue, S. S. Tao, J. M. Fu, Z. Q. Gao, Y. Ren, *Carbon* **2013**, *65*, 97.
[347] G. X. Zhao, T. Wen, J. Zhang, J. X. Li, H. L. Dong, X. K. Wang, Y. G. Guo, W. P. Hu, *J. Mater. Chem. A* **2014**, *2*, 944.
[348] Q. Yang, Q. Liang, J. Liu, S. Q. Liang, S. S. Tang, P. J. Lu, Y. K. Lu, *Mater. Lett.* **2014**, *127*, 32.
[349] Z. X. Huang, Y. Wang, Y. G. Zhu, Y. M. Shi, J. I. Wong, H. Y. Yang, *Nanoscale* **2014**, *6*, 9839.
[350] S. H. Choi, Y. C. Kang, *ChemSusChem* **2014**, *7*, 523.
[351] C. L. Liu, Y. Wang, C. Zhang, X. S. Li, W. S. Dong, *Mater. Chem. Phys* **2014**, *143*, 1111.
[352] P. J. Lu, M. Lei, J. Liu, *CrystEngComm* **2014**, *16*, 6745.
[353] Y. Sun, X. Hu, W. Luo, Y. Huang, *J. Mater. Chem.* **2011**, *21*, 17229.
[354] W. Song, J. Xie, S. Liu, G. Cao, T. Zhu, X. Zhao, *New J. Chem.* **2012**, *36*, 2236.
[355] J. Xie, W. T. Song, G. S. Cao, T. J. Zhu, X. B. Zhao, S. C. Zhang, *RSC Adv.* **2014**, *4*, 7703.
[356] J. J. Zhang, J. W. Liang, Y. C. Zhu, D. H. Wei, L. Fan, Y. T. Qian, *J. Mater. Chem. A* **2014**, *2*, 2728.
[357] Y. Q. Cao, L. Zhang, D. L. Tao, D. X. Huo, K. P. Su, *Electrochim. Acta* **2014**, *132*, 483.
[358] H. Kim, H.-D. Lim, J. Kim, K. Kang, *J. Mater. Chem. A* **2014**, *2*, 33.
[359] V. H. Nguyen, H. B. Gu, *J. Appl. Electrochem.* **2014**, *44*, 1153.
[360] J. L. Yang, J. J. Wang, D. N. Wang, X. F. Li, D. S. Geng, G. X. Liang, M. Gauthier, R. Y. Li, X. L. Sun, *J. Power Sources* **2012**, *208*, 340.
[361] H. B. Liu, C. Miao, Y. Meng, Q. Xu, X. H. Zhang, Z. Y. Tang, *Electrochim. Acta* **2014**, *135*, 311.

[362] X. L. Li, T. T. Li, Y. L. Zhang, X. L. Zhang, H. Y. Li, J. M. Huang, *Electrochim. Acta* **2014**, *139*, 69.
[363] H. L. Fei, Z. W. Peng, Y. Yang, L. Li, A. R. O. Raji, E. L. G. Samuel, J. M. Tour, *Chem. Commun.* **2014**, *50*, 7117.
[364] R. W. Mo, Z. Y. Lei, D. Rooney, K. N. Sun, *Electrochim. Acta* **2014**, *130*, 594.
[365] X. J. Zhu, J. Hu, W. Y. Wu, W. C. Zeng, H. L. Dai, Y. X. Du, Z. Liu, L. Li, H. X. Ji, Y. W. Zhu, *J. Mater. Chem. A* **2014**, *2*, 7812.
[366] W. C. Wang, Y. Wang, Y. H. Gao, Y. P. Zhao, *J. Supercrit. Fluids* **2014**, *85*, 95.
[367] B. Wang, B. H. Xu, T. F. Liu, P. Liu, C. F. Guo, S. Wang, Q. M. Wang, Z. G. Xiong, D. L. Wang, X. S. Zhao, *Nanoscale* **2014**, *6*, 986.
[368] J. Hassoun, F. Bonaccorso, M. Agostini, M. Angelucci, M. G. Betti, R. Cingolani, M. Gemmi, C. Mariani, S. Panero, V. Pellegrini, B. Scrosati, *Nano Lett.* **2014**, *14*, 4901.
[369] G. Wu, R. Ran, B. T. Zhao, Y. J. Sha, C. Su, Y. K. Zhou, Z. P. Shao, *J. Energy Chem.* **2014**, *23*, 363.
[370] T. F. Liu, L. Zhao, J. S. Zhu, B. Wang, C. F. Guo, D. L. Wang, *J. Mater. Chem. A* **2014**, *2*, 2822.
[371] W. B. Luo, S. L. Chou, Y. C. Zhai, H. K. Liu, *J. Mater. Chem. A* **2014**, *2*, 4927.
[372] Y. Shi, S. L. Chou, J. Z. Wang, D. Wexler, H. J. Li, H. K. Liu, Y. P. Wu, *J. Mater. Chem.* **2012**, *22*, 16465.
[373] a) X. Li, T. Li, Y. Zhang, X. Zhang, H. Li, J. Huang, *Electrochim. Acta* **2014**, *139*, 69; b) W. Wei, W. Lv, M. B. Wu, F. Y. Su, Y. B. He, B. H. Li, F. Y. Kang, Q. H. Yang, *Carbon* **2013**, *57*, 530.
[374] L. H. Hu, F. Y. Wu, C. T. Lin, A. N. Khlobystov, L. J. Li, *Nat. Commun.* **2013**, *4*, 1687.
[375] J. Zong, X. J. Liu, *Electrochim. Acta* **2014**, *116*, 9.
[376] K. Wang, Y. Wang, C. Wang, Y. Xia, *Electrochim. Acta* **2014**, *146*, 8.
[377] Y. Jiang, R. Z. Liu, W. W. Xu, Z. Jiao, M. H. Wu, Y. L. Chu, L. Su, H. Cao, M. Hou, B. Zhao, *J. Mater. Res.* **2013**, *28*, 2584.
[378] C. C. Xu, L. Li, F. Y. Qiu, C. H. An, Y. A. Xu, Y. Wang, Y. J. Wang, L. F. Jiao, H. T. Yuan, *J. Energy Chem.* **2014**, *23*, 397.
[379] S. Wi, J. Kim, S. Nam, J. Kang, S. Lee, H. Woo, M. Lee, C. H. Sonu, T. Moon, B. Park, *Curr. Appl. Phy.* **2014**, *14*, 725.
[380] B. Cheng, X. D. Zhang, X. H. Ma, J. W. Wen, Y. Yu, C. H. Chen, *J. Power Sources* **2014**, *265*, 104.
[381] X. J. Zhu, Z. Yan, W. Y. Wu, W. C. Zeng, Y. X. Du, Y. Zhong, H. D. Zhai, H. X. Ji, Y. W. Zhu, *Sci. Rep.*, **2014**, *4*, 5768.
[382] M. S. Choi, H. S. Kim, Y. M. Lee, B. S. Jin, *J. Mater. Chem. A* **2014**, *2*, 7873.
[383] X. Sun, Y. Xu, M. Jia, P. Ding, Y. Liu, K. Chen, *J. Mater. Chem. A* **2013**, *1*, 2501.
[384] J. X. Wang, X. H. Li, Z. X. Wang, B. Huang, Z. G. Wang, H. J. Guo, *J. Power Sources* **2014**, *251*, 325.
[385] H. K. Roh, H. K. Kim, K. C. Roh, K. B. Kim, *RSC Adv.* **2014**, *4*, 31672.
[386] B. H. Lin, Q. Yin, H. R. Hu, F. J. Lu, H. Xia, *J. Solid State Chem.* **2014**, *209*, 23.
[387] S. Aziz, J. Q. Zhao, C. Cain, Y. Wang, *J. Mater. Sci. Technol.* **2014**, *30*, 427.
[388] K. V. Sreelakshmi, S. Sasi, A. Balakrishnan, N. Sivakumar, A. S. Nair, S. V. Nair, K. R. V. Subramanian, *Energy Technol.* **2014**, *2*, 257.
[389] B. W. Ju, X. Y. Wang, C. Wu, X. K. Yang, H. B. Shu, Y. S. Bai, W. C. Wen, X. Yi, *J. Alloys Compd.* **2014**, *584*, 454.
[390] S. J. R. Prabakar, Y. H. Hwang, B. Lee, K. S. Sohn, M. Pyo, *J. Electrochem. Soc.* **2013**, *160*, A832.
[391] J. R. He, Y. F. Chen, P. J. Li, Z. G. Wang, F. Qi, J. B. Liu, *RSC Adv.* **2014**, *4*, 2568.
[392] Z. J. He, Z. X. Wang, H. J. Guo, X. H. Li, X. W. Wu, P. Yue, J. X. Wang, *Mater. Lett.* **2013**, *91*, 261.
[393] B. H. Song, M. O. Lai, Z. W. Liu, H. W. Liu, L. Lu, *J. Mater. Chem. A* **2013**, *1*, 9954.
[394] J. Liu, H. Xia, D. Xue, L. Lu, *J. Am. Chem. Soc.* **2009**, *131*, 12086.
[395] Y. Yang, L. Li, H. L. Fei, Z. W. Peng, G. D. Ruan, J. M. Tour, *ACS Appl. Mater. Interfaces* **2014**, *6*, 9590.
[396] S. H. Choi, Y. C. Kang, *Chem. Eur. J.* **2014**, *20*, 6294.
[397] Q. He, D. L. Zhao, Y. Y. Zhu, J. X. Zhang, in *Eighth Chin. Natl. Conf. Funct. Mater. Appl.*, Vol. Adv. Mater. Res. Harbin Cihna,*873* (Eds: G. M. Zhao, L. Chen, Y. Tang, B. Long, Z. Nie, L. He, H. Chen), **2014**, 575.
[398] D. Chen, R. Yi, S. R. Chen, T. Xu, M. L. Gordin, D. P. Lv, D. H. Wang, *Mater. Sci. Eng., B* **2014**, *185*, 7.
[399] D. Z. Chen, H. Y. Quan, S. L. Luo, X. B. Luo, F. Deng, H. L. Jiang, *Phys. E* **2014**, *56*, 231.
[400] Z.-F. Li, H. Zhang, Q. Liu, Y. Liu, L. Stanciu, J. Xie, *ACS Appl. Mater. Interfaces* **2014**, *6*, 18894.
[401] D. Pham-Cong, K. Ahn, S. W. Hong, S. Y. Jeong, J. H. Choi, C. H. Doh, J. S. Jin, E. D. Jeong, C. R. Cho, *Curr. Appl. Phy.* **2014**, *14*, 215.
[402] a) S. T. Li, Z. Wei, Y. F. Tang, K. Qian, Y. M. Li, S. D. Ji, H. J. Luo, Y. F. Gao, P. Jin, *Sci. Adv. Mater.* **2014**, *6*, 1293; b) V. S. R. Channu, D. Ravichandran, B. Rambabu, R. Holze, *Appl. Surf. Sci.* **2014**, *305*, 596.
[403] J. Xu, Z. L. Li, X. Y. Zhang, S. N. Huang, S. S. Jiang, Q. Y. Zhu, H. J. Sun, G. S. Zakharova, *Int. J. Nanotechnol.* **2014**, *11*, 808.
[404] Z. F. Li, H. Y. Zhang, Q. Liu, Y. D. Liu, L. Stanciu, J. Xie, *ACS Appl. Mater. Interfaces* **2014**, *6*, 18894.
[405] H. Zhu, X. Z. Wu, L. Zan, Y. X. Zhang, *ACS Appl. Mater. Interfaces* **2014**, *6*, 11724.
[406] H. X. Gong, Y. C. Zhu, L. L. Wang, D. H. Wei, J. W. Liang, Y. T. Qian, *J. Power Sources* **2014**, *246*, 192.